Complex Coacervate Core Micelles in Solution and at Interfaces

Promotor:	Prof. dr. M. A. Cohen Stuart, hoogleraar fysische chemie, met bijzondere aandacht voor de kolloïdchemie
Copromotor:	Dr. A. de Keizer, universitair docent bij de leerstoelgroep Fysische Chemie en Kolloïdkunde

Samenstelling promotiecommissie

Prof. dr. M. Ballauff	Universität Bayreuth, Deutschland
Prof. dr. J. Feijen	Universiteit Twente, Enschede, Nederland
Prof. dr. E.J.H. Sudhölter	Wageningen Universiteit, Nederland
Prof. dr. C.G. de Kruif	NIZO food research, Ede, Nederland

Complex Coacervate Core Micelles in Solution and at Interfaces

Stefan van der Burgh

Proefschrift
ter verkrijging van de graad van doctor
op gezag van de rector magnificus
van Wageningen Universiteit,
prof. dr. ir. L. Speelman,
in het openbaar te verdedigen
op maandag 26 april 2004
des namiddags te vier uur in de Aula.

ISBN 9085040191

Contents

Stellingen

1. Een polyelectroliet met titreerbare groepen zal als gevolg van complexering een verandering ondergaan in de effectieve pK en doorgaans ook in de ladingsdichtheid.
   Dit Proefschrift, hoofdstuk 3

2. Micellen met complexcoacervaatkern zijn een veelbelovend systeem voor de preventie van eiwitadsorptie en bacterie-adhesie aan diverse oppervlakken.
   Dit Proefschrift, hoofdstuk 6

3. De methode voor quaternisatie van polyvinylpyridine zoals beschreven door Kawaguchi en Satoh levert voor lage substitutiegraden zeer waarschijnlijk een polydispersiteit in substitutiegraad op.
   D. Kawaguchi en M. Satoh, Macromolecules, 1999, 32, 7828-7835

4. Bij het bestuderen van polyelectroliet-multilagen is reflectometrie onontbeerlijk.
   D. Kovacevic et al., Langmuir, 2002, 18, 5607-5612
   Productinfo nanostrata Inc. (www.nanostrata.com)

5. Het verkeersveiligheidsbeleid van de Nederlandse overheid werkt contraproductief en dient voornamelijk de staatskas.

6. Een overheid dient er naar te streven zo min mogelijk mensen in dienst te hebben.

7. De mythe dat economische groei en zorg voor het milieu met elkaar in tegenspraak zijn is niet wetenschappelijk onderbouwd.
   Bjorn Blomberg, The Skeptical Environmentalist

Stellingen behorende bij het proefschrift
"Complex coacervate core micelles in solution and at interfaces"
S. van der Burgh, Wageningen, 26 april 2004

CHAPTER 1

Introduction

This thesis deals with the behavior and properties of complex coacervate core micelles. These micelles may form spontaneously upon mixing aqueous solutions of charged polymers and oppositely charged diblock-copolymers. In this chapter, a general introduction to the subject is given after which we formulate the aims of the research and give an outline of this thesis.

1.1. Polymers in everyday life

Polymeric molecules or macromolecules are important in many aspects of everyday life. In living organisms, polymers are relevant in many processes, such as the storage of information in DNA and RNA and the storage of energy in carbohydrate polymers such as starch in plants and glycogen in humans and animals. Another carbohydrate polymer, cellulose, is a key component in the strengthening of plant cells. Proteins are a special class of rather complicated polymers, that play a role in almost all vital biological functions. Also in industrial processes, products, and medical applications, polymeric molecules are very relevant. On a macro-scale, polymers can form materials such as e.g. plastics, cloth, and contact lenses. In technology, living organisms, and medical applications, the relevance of polymers is however not often found on a macro scale, but on a microscale or even nanoscale. Examples are colloidal stabilization of inks and paints, or adsorption of polymers on the inner surface of dialysis tubes, thereby reducing fouling of the tubes by serum proteins, as the polymers prevent adsorption of proteins.

Although many polymers can dissolve, and can be considered as 'free' molecules in this state, their relevance in biology and industry mostly arises from their *interaction* with other (macro)molecules or with interfaces.

There are several ways to classify polymers. One option is to discriminate between biological polymers, such as starch, cellulose, and proteins on the one hand, and synthetic polymers, prepared by chemical reactions in a laboratory or industrial plant, on the other hand. Another possibility is to classify polymers in terms of their primary structure, i.e. the sequence of monomers in the chain. A chain of identical monomers is called a homopolymer. When two of such chains with different chemical composition are linked end-to-end, the resulting molecule is called a diblock-copolymer. More exotic architectures are also possible, such as, e.g., tri-block-copolymers and branched polymers. In this thesis, we will only deal with homopolymers and diblock-copolymers.

The behavior of a polymer in a given liquid medium is determined by various character-

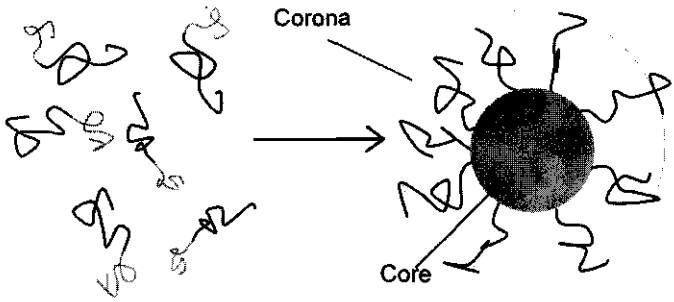

FIGURE 1.1. Spontaneous formation of polymeric micelles from an aqueous solution of amphiphilic diblock-copolymers.

istics, such as chain length, solubility, and presence of charges. An example is an aqueous solution containing hydrophobic and hydrophilic polymers, such as, respectively, polystyrene and polyacrylamide. The hydrophobic polymers will form a precipitate on the bottom of the flask, whereas the hydrophilic polymers will be molecularly dispersed in solution, due to the favorable interactions between water molecules and hydrophilic groups of the polymer. If we now have a diblock-copolymer, that consists of end-to-end linked hydrophobic and hydrophilic chains, particles may be formed as shown in Figure 1.1. This behavior is a consequence of the dual nature or amphiphilicity of this diblock-copolymer and the particles are called micelles. In a way, such diblock-copolymers are the polymeric equivalents of the well known amphiphiles, usually called surfactants or soaps. In Figure 1.1, the black blocks are hydrophilic and the gray blocks are hydrophobic. The hydrophobic parts of the diblock-copolymer try to minimize their contact area with the solvent, and form a dense core. The hydrophilic parts form the corona of the micelles and are thus 'grafted' with one end at the core-corona interface. In order to have as much contact with the water molecules as possible, the corona chains stretch away from the core-corona interface into the solvent.

In this thesis, binary mixtures of synthetically prepared, oppositely charged (diblock-co)polymers have been studied. In such mixtures, an insoluble phase often forms in the case of mixtures of *homopolymers*. Such an insoluble phase (which contains both polymers in high concentrations) is commonly called a "complex coacervate". When at least one of the homopolymers is replaced by a diblock-copolymer consisting of a charged block and a neutral hydrophilic block, a new kind of objects may be formed, which we shall call complex coacervate core micelles (CCCM's). Under appropriate conditions, these small colloidal objects form spontaneously due to the attraction between positively and negatively charged polymers that form the core. The dimensions of this core are to a large extent determined by the neutral, water-soluble blocks that

are linked to one of the charged polymers.
The central themes of this thesis are the behavior and properties of these complex coacervate core micelles. Apart from a characterization of these objects in solution, their interaction with surfaces has been studied. In order to fully comprehend all aspects of complex coacervate core micelles, one needs insight into properties of polyelectrolytes in aqueous solution, complex coacervation, and polymeric micelles. In the next sections, these aspects will be discussed separately.

1.2. Polyelectrolytes in solution

Polyelectrolytes are chain molecules that consist of (linearly) linked charged, or chargeable, groups. Polyelectrolytes that have a constant charge density are called quenched, whereas polyelectrolytes with pH dependent charge densities are called annealed or weak polyelectrolytes. In this thesis, complex coacervation systems have been studied where at least one of the components has annealed charges. We will first consider the behavior of monomeric acids and bases. The dissociation behavior of these annealed, *monomeric* groups is given by

$$\begin{aligned} AH \quad &\underset{\rightleftarrows}{K_A} \quad A^- + H^+ \\ B + H_2O \quad &\underset{\rightleftarrows}{K_B} \quad BH^+ + OH^- \end{aligned} \tag{1.1}$$

where A denotes an acidic monomer and B denotes a basic monomer, and K_A and K_B are the equilibrium constants of the acidic and basic reaction, respectively defined as $K_A = [A^-][H^+]/[AH]$ and $K_B = [BH^+][OH^-]/[B]$. By introducing α as the fraction of charged monomers, defined as

$$\begin{aligned} \alpha_A &= \frac{[A^-]}{[A^-] + [AH]} \\ \alpha_B &= \frac{[BH^+]}{[BH^+] + [B]} \end{aligned} \tag{1.2}$$

and pK and pH, defined as the negative logarithms of the equilibrium constants and the proton concentration, respectively, we can write

$$\begin{aligned} pH &= pK_A + log\left(\frac{\alpha_A}{1-\alpha_A}\right) \qquad (a) \\ pH &= pK_w - pK'_B - log\left(\frac{\alpha_B}{1-\alpha_B}\right) \qquad (b) \end{aligned} \tag{1.3}$$

for the acid and base monomers, respectively. Here pK_w is the logarithm of the self-dissociation constant of water, that is about (using conventional units) 14 at room

temperature. Let us now consider the case when these annealed groups are chemically

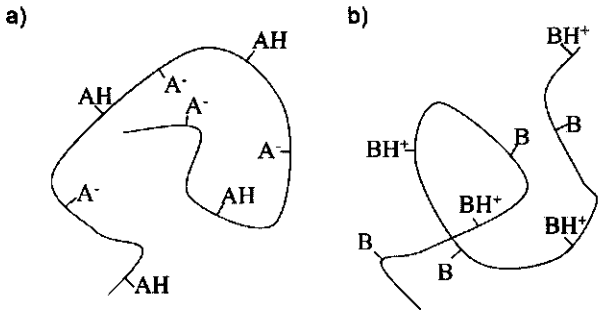

FIGURE 1.2. Annealed polyacid (a) and polybase (b) in bulk solution, both with $\alpha = 0.5$.

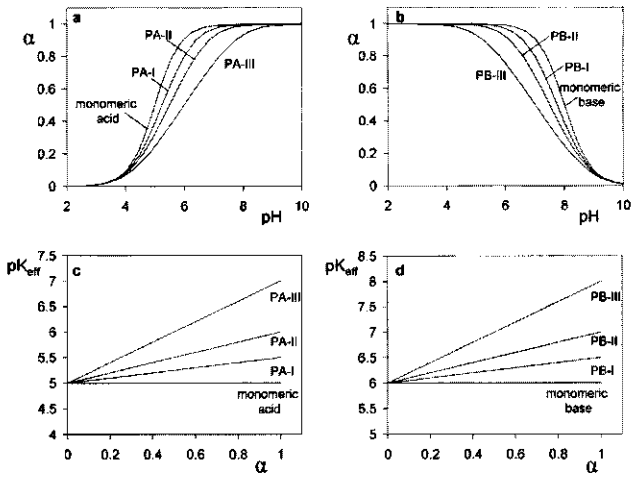

FIGURE 1.3. Dissociation behavior of monomeric and polymeric acid (plane a) and monomeric and polymeric base (b). The pK_{eff} vs. α data are given in planes (c) and (d) where $pK_{eff} = pK_0 + \Delta pK$, as in Equation 1.4. The value of $\partial pK/\partial\alpha$ is 0.5 for PA-I and PB-I, 1.0 for PA-II and PB-II, and 2.0 for PA-III and PB-III.

linked in chain molecules, as is schematically sketched in Figure 1.2 where α_A and α_B are both equal to 0.5. The chemical linking will not change the intrinsic values of the equilibrium constants K_A and K_B. Note that the distance between neighboring groups in such a polyelectrolyte molecule is in the order of several tenths of a nanometer. The repulsion between charges of equal sign is thus strongly felt and more thermodynamic work is required for further dissociation than for the first charges that appear on the polyelectrolyte chains. All in all, the equilibrium constants are no longer constants,

due to this electrostatic intrachain repulsion. However, by adding correction terms Δ p$K_A(\alpha_A)$ and Δp$K_B(\alpha_B)$ to Equation 1.3, its applicability can also include annealed polyelectrolytes:

$$pH = pK_A^0 + \Delta pK_A(\alpha_A) + log\left(\frac{\alpha_A}{1-\alpha_A}\right) \qquad (a)$$
$$pH = pK_w - pK_B^0 - \Delta pK_B(\alpha_B) - log\left(\frac{\alpha_B}{1-\alpha_B}\right) \qquad (b) \qquad (1.4)$$

Often, Δp$K(\alpha)$ turns out to be a linear function of α[1]. Moreover, the concentration of salt in the solution is very influential on the intrachain repulsion: the salt ions screen the charges. Due to this effect ∂p$K(\alpha)/\partial\alpha$ is a function of salt concentration. With increasing salt concentration in the solution, the intrachain repulsion will decrease, and ∂p$K(\alpha)/\partial\alpha$ will be lowered. With increasing salt concentration in solution, the typical polyelectrolyte character will thus be less pronounced. In Figure 1.3a and 1.3b, we have sketched α vs pH for a monomeric acid and base, and for polyelectrolytes with various ∂p$K(\alpha)/\partial\alpha$. In Figure 1.3c and 1.3d, we show the corresponding pK_{eff}(= p$K_0 + \Delta$pK) vs. α for the same cases. We see that for the polyelectrolytes, the curves are stretched out over more pH-units as compared to their monomeric counterparts. For example, to obtain $\alpha = 0.7$, for a monomeric acid, a pH value of 5 is enough, whereas for PA-III, p$H = 7$ is required.

1.3. Complex Coacervation

Complex coacervation is the phase separation that may occur upon mixing aqueous solutions of oppositely charged macromolecules. The dense coacervate phase is rich in polyelectrolytes, and the other phase consists mostly of water and small ions. The driving force for complex coacervation consists of at least two important contributions, which both are related to the (poly)electrolyte character of the molecules. In bulk solution, a polyelectrolyte chain is surrounded by a 'cloud' of oppositely charged small ions which remain in the vicinity of the chain. This cloud of ions is called the electrical double layer. Firstly, upon complexation, the small ions are released from the polyelectrolyte double layers. This leads to an increase in the entropy of the system. Secondly, the electrostatic energy of the polyelectrolytes is decreased, as the screening of the charges is done much more efficiently in a dense complex coacervate, due to the smaller distances between oppositely charged groups, compared to the distance between polyelectrolyte groups and counterions in bulk solution. The two driving forces are opposed by a decrease in polyelectrolyte configurational and translational entropy, as the polyelectrolyte molecules are now restricted to the polymer rich phase and may lose some conformational entropy. In Figure 1.4, a schematic view of complex coacervation

is presented. Complex coacervation can often be suppressed by addition of salt or by decreasing the charge densities of the polyelectrolytes. In the case of complex coacervation between annealed species, changes in pH may also oppose complex coacervation. Complex coacervation has been extensively studied by Bungenberg de Jong[2] and complex coacervation theory was pioneered by Voorn and Overbeek[3]. Their model was a very simple one as they assumed that the free energy was that of a neutral polymer/solvent mixture plus that of a dilute electrolyte solution according to the Debye-Hückel theory. They elaborated the general theory for the simple case where the molecular weights of the oppositely charged chains and their charge densities were equal and low, and where the oppositely charged molecules were present in stoichiometric amounts. In addition,

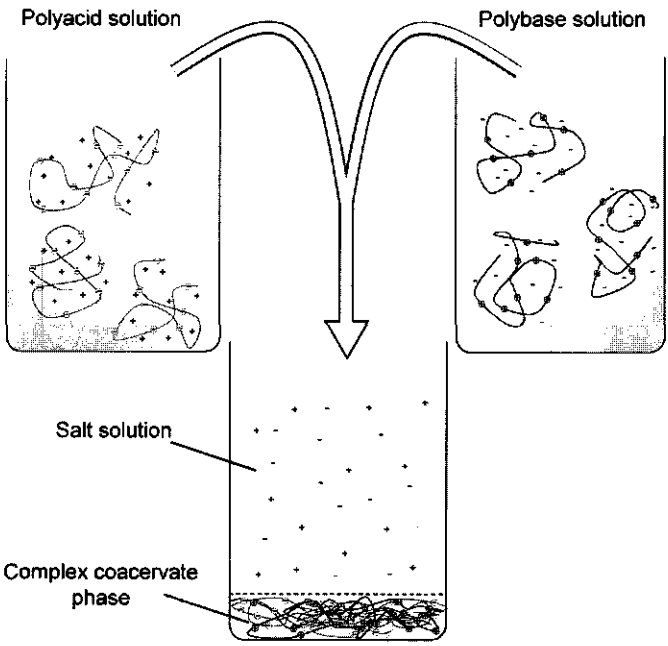

FIGURE 1.4. Schematic view of complex coacervation. In the separate solutions, the polyelectrolyte chains form electrical double layers with their counterions. After complexation, the counterions are randomly distributed over the system.

they modeled the charges of the polyelectrolytes as quenched, which is a serious oversimplification with respect to real-life systems. The polymer rich phase is very dense, so that the oppositely charged groups are packed very closely and efficiently screen each other efficiently. This affects the proton transfer equilibria as can be understood from the following argument.

Consider an annealed polyelectrolyte chain with a given charge density that is transferred from a low ionic strength bulk solution to a concentrated coacervate phase. Due to the dense packing in the coacervate phase, the electrostatic suppression of charging that was strongly felt in bulk solution, will decrease strongly, or even become an enhancement. This affects Δ pK_A and ΔpK_B, and as we learn from Equation 1.4, α and pH will have to adjust to changes in Δ pK. Therefore, pH measurements during complex coacervation experiments will be discussed extensively in this thesis, as such data contain valuable information. From the above, we can infer that with increasing salt concentration in the bulk solution, all these changes become smaller, e.g. ΔpK will approach zero, the pK changes that the polyelectrolyte chains undergo upon complexation will decrease, and changes in bulk pH will also be minimized. As follows from the consideration of driving forces, complex coacervation can often be entirely suppressed if the salt concentration reaches a critical value. If the ionic strength in the solutions containing the polyelectrolytes is too high, no complexation will take place upon mixing. Upon addition of salt, the coacervate phase will redissolve into separate polyelectrolyte chains *. In Figure 1.5, we give a stability diagram taken from reference[4], where the

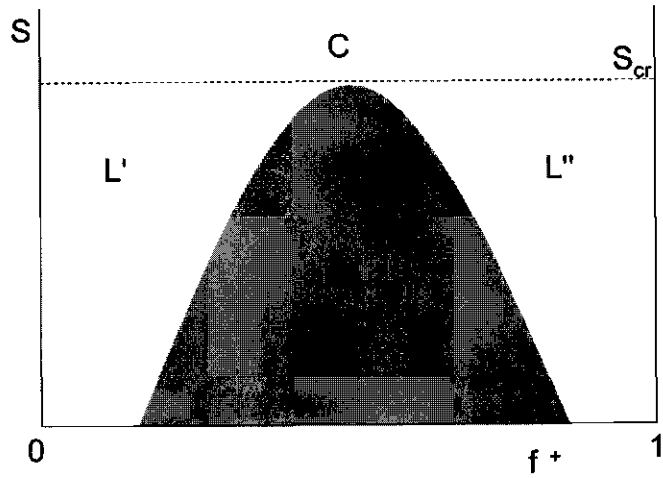

FIGURE 1.5. Complex coacervation stability diagram.

ionic strength (S) is plotted vs. composition. The composition is expressed as the number of basic groups over the total number of acid and basic groups, i.e.

$$f^{+} = \frac{[B]_t}{[B]_t + [A]_t} \tag{1.5}$$

*We note, however, that not all salts are equally effective in this respect. Valency and ion specific effects are very pronounced, and some complexes cannot be redissolved with common electrolytes.

where $[B]_t$ and $[A]_t$ are the overall concentrations of polybase and polyacid, respectively, expressed in terms of monomeric groups. The dark gray area (L) in Figure 1.5 is the 'instability region', where the complexes form a separate (coacervate) phase, as was sketched in Figure 1.4. Outside the gray region, the complex particles formed are soluble, because they are (colloidally) stabilized by their excess charge[5]. The charge sign depends on the composition; at low f^+, the particles are anionically stabilized (L'), at high f^+ the particles are cationically stabilized (L"). Above a critical salt concentration, complexation no longer takes place (region C). Typical values for this critical ionic strength are in the order of, say, 0.2 to 1 M[4, 6].

1.4. Polymeric micelles

When we dissolve amphiphilic diblock-copolymers in water at concentrations above the so-called critical micelle concentration (CMC), the molecules self-assemble spontaneously into colloidal objects, consisting of a dense hydrophobic core and an extended hydrophilic corona, as was sketched in Figure 1.1. The corona ensures the solubility of these objects in water. A very important design parameter of these diblock-copolymers is the length, in particular the length ratio, of the blocks. Let us consider two extreme block length ratios, namely (i) where the length of the corona block is negligible with respect to the core block and (ii) the reverse. In the first case, so-called 'crew-cut' micelles will be formed with a relatively thin corona, so that the overall radius is dominated by the core. In the latter case, starlike micelles are formed, where the radius of the core is very small compared to the overall radius of the micelles. It has been shown by Borisov and Zhulina[7] that the internal structure of a micelle is sensitive to the block lengths of the core- and corona-blocks. In Figure 1.6, we sketch how the internal structure of

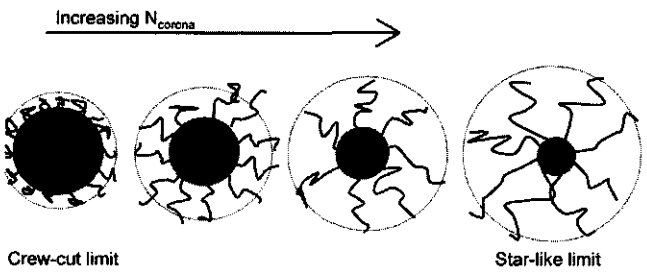

FIGURE 1.6. Effect of N_{corona} on micellar structure and aggregation number

the micelles changes upon increasing the corona block length (N_{corona}), while the core block length (N_{core}) is constant. The aggregation number, P, is defined as the number

of diblock-copolymers per micelle, and is given by

$$P = \frac{\frac{4}{3}\pi R_{core}^3 \phi}{N_{core} V_{core}} \tag{1.6}$$

where V_{core} is the volume of a core monomer and ϕ is the volume fraction of polymers in the core. At the left hand side of Figure 1.6 where $N_{corona} << N_{core}$, crew-cut micelles are formed. At the right hand side of Figure 1.6 where $N_{corona} >> N_{core}$, starlike micelles are formed. The changes in internal structure of the micelles result from an increase of N_{corona}. The grafting density of the corona blocks on the core/corona interface is given as $\sigma = P/4\pi R_{core}^2$. As can be understood from Figure 1.6, longer corona chains require more space on the core/corona interface, so that σ must decrease. From Equation 1.6 and the definition of σ, it follows that $\sigma \propto R_{core}$. So, as σ decreases upon increasing N_{corona}, the radius of the core, and thus P, must decrease also. For both the crew-cut limit and the starlike limit, theoretical scaling relationships were derived by Borisov and Zhulina[7]. They showed that for starlike micelles the following scaling relationship is valid

$$P \propto (N_{core}\gamma)^{4/5} \left(ln \frac{H_{corona}}{R_{core}} \right)^{-6/5} \tag{1.7}$$

where γ is the surface tension of the core-solvent interface, and H_{corona} is the thickness of the corona, given by

$$H_{corona} \propto N_{corona}^{3/5} \upsilon^{1/5} P^{1/5} \tag{1.8}$$

where υ is the excluded volume parameter for the corona chains and N_{corona} is the degree of polymerization of the corona chains (the excluded volume parameter υ is derived from the Flory-Huggins parameter χ by $\upsilon = 1 - 2\chi$, where χ is defined as the contact free energy change associated with the transfer of a segment from pure polymer to pure solvent[8, 9]. When $\chi > 0.5 (\upsilon < 0)$, there is attraction between the polymer segments; conversely, when $\chi < 0.5 (\upsilon > 0)$ there is repulsion between the polymer segments, i.e. they prefer contact with the solvent). Equation 1.7 is only valid under good solvent-conditions for the corona chains, i.e. $\upsilon_{corona} > 0 (\chi < 0.5)$. For crew-cut micelles the following scaling relationship was found[7]:

$$P \propto N_{core}^2 \gamma^{7/11} N_{corona}^{-18/11} \upsilon^{-6/11} \tag{1.9}$$

again for good solvent conditions. From equations 1.7-1.9 we learn (i) that for $N_{corona} << N_{core}$, P will decrease with increasing N_{corona} for the crew-cut micelles and (ii) that P becomes virtually independent of N_{corona} for the star like limit. The latter conclusion was verified experimentally by Willner and coworkers[10] by small angle neutron scattering experiments. An increase of N_{core} will give an increase of P for both the star like and crew-cut limits. However, no specific cross-over values for N_{corona}/N_{core} were given by Borisov and Zhulina[7] for the crew-cut and starlike limits. Another theoretical analysis of the self-assembly of diblock-copolymers in a selective

solvent was performed by Nagarajan and Ganesh[11], who found that in a good solvent for the corona blocks $P \propto N_{corona}^{-0.51}$. They did, however, not distinguish regimes in terms of micellar structure, such as crew-cut or starlike micelles.

1.5. Complex coacervate core micelles

1.5.1. Preparation and experiments

We will now take a closer look at complex coacervate core micelles, thereby using relevant information from sections 1.2 - 1.4. In Figure 1.7, we present a sketch of a complex coacervate core micelle (CCCM). The core of these objects is basically the same coacervate phase as was shown in Figure 1.4, where it resulted from the mixing of two homopolymers. In the CCCM, however, this phase is restricted to smaller sizes, due to the hydrophilic corona chains. The CCCM's are two-components objects, so that the mixing ratio of the components is a very relevant parameter. Experimentally, we have addressed the mixing ratio by titrations in a light scattering cell, equipped with a small combined electrode for pH measurements. In these titrations, one of the (diblock-co)polymers is titrated with a concentrated solution of the other component, so that volume changes are negligible. Both solutions start out with equal ionic strength and initial pH, so that the ionic strength is constant and changes in pH can be attributed to interaction between the components. This setup was also used in other experiments to titrate (micellar) solutions with concentrated salt solutions, or with acid or base. After each dosage, light scattering intensity and pH were recorded. Also, the intensity autocorrelation function was recorded, which represents the fluctuations arising from the Brownian motion of particles in a liquid. Such data yielded a diffusion coefficient, that can be converted by the Stokes-Einstein equation[12] into a particle radius, at least for spherical particles.

1.5.2. Aggregation diagram

In this section, we analyze the aggregation mechanism of the CCCM's. Let us start with a dilute solution of anionic diblock-copolymers, and then change the composition f^+ of the mixture (at constant overall concentration), e.g., by gradually adding cationic homopolymer. This is schematically pictured in Figure 1.8. In doing so, we may at one point form micelles as shown in Figure 1.7. This point is expected at a composition where the positive and negative polyelectrolyte charges approximately balance each other. Outside this point, which we will call the preferred micellar composition (PMC), no micelles will be formed. However, there is still interaction between the polymers[13], leading to soluble complex particles (SCP). These SCP are usually small; their size is mainly determined by that of the minority component. At low f^+, the minority component is the cationic homopolymer, and negatively charged SCP^- are formed. Vice versa, at high f^+, the charge sign is cationic and SCP^+ are formed.

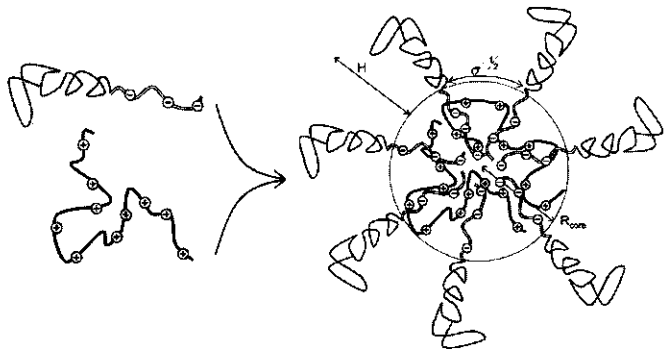

FIGURE 1.7. Complex coacervation core micelle. The radius of the core is indicated by R_{core}, the thickness of the corona is given as H_{corona}, and the distance between the chains on the core-solvent interface is given as the reciprocal square root of the grafting density, σ.

In Figure 1.8, we show schematically the speciation as a function of f^+ for each of various kinds of particles: free diblock-copolymer (dbp) and homopolymer (hp) in (a), $SCP^{+,-}$ in (b), and micelles in (c). In Figure 1.8a, we see that the concentration of free diblock-copolymers decreases with increasing f^+, as the molecules are consumed during the formation of SCP. At the critical excess anionic charge (CEAC), the concentration of free diblock-copolymers has become zero and the concentration of SCP^- is at a maximum. Now, upon further addition of homopolymers, the SCP^- are consumed during the formation of CCCM's until the preferred micellar composition (PMC) is reached. Now, beyond the PMC, the micelles disintegrate upon overdosing the cationic homopolymers and SCP^+ are formed. Beyond the critical excess cationic charge (CECC) the homopolymer concentration increases and the concentration of micelles is again zero. Micelles are thus only found between the CEAC and CECC, with a maximum in micellar concentration at the PMC. In section 1.5.1 we mentioned that during a homopolymer/diblock-copolymer titration experiment, the light scattering intensity is monitored. From the concentration profiles in Figure 1.8, and some insight in light scattering theory, a light scattering intensity vs. f^+ diagram can be constructed. Generally, light scattering intensity is expressed in terms of the Rayleigh ratio ΔR[14].

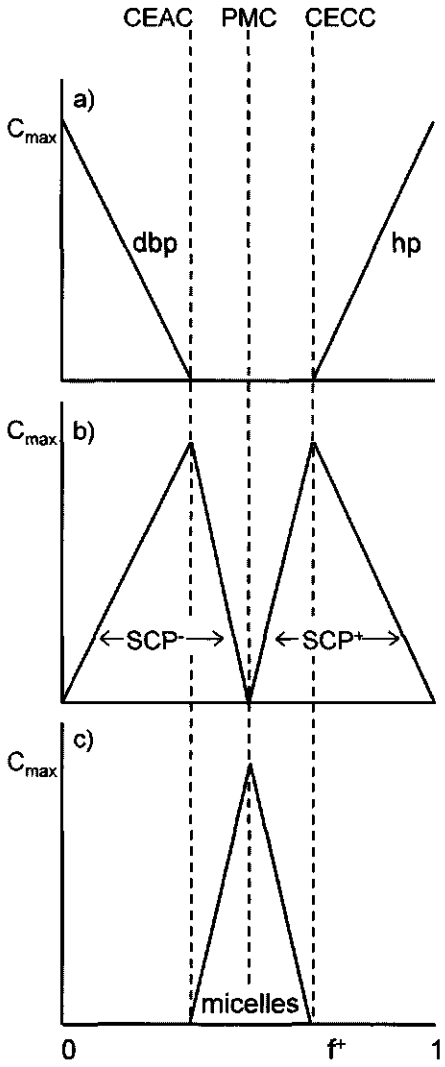

FIGURE 1.8. Speciation of a mixture of cationic homopolymer(hp) and anionic diblock-copolymer(dbp), as a function of composition into free molecules (a), soluble complex particles ($SCP^{+,-}$), (b), and CCCM's (c) at constant overall concentration. The critical excess anionic charge (CEAC), critical excess cationic charge (CECC), and PMC are indicated by dotted vertical lines.

The general expression for this quantity is given by Equation 1.10a[14]

$$\Delta R = KCM_w P(q)S(q) \qquad (a)$$

$$\Delta R \propto (I_{sample} - I_{solvent})Y \qquad (b)$$

$$I \propto \sum CM(\frac{\partial n}{\partial c})^2 \qquad (c) \tag{1.10}$$

where K is the optical constant given by $4\pi^2 n_{sol}^2(\partial n/\partial c)^2/(N_{AV}\lambda_0^4)$ with n_{sol} the solvent refractive index, N_{AV} Avogadro's number, and λ_0 is the wavelength of the laser, C is the weight concentration of scattering objects, M_w is their molar mass, $P(q)$ is the particle form factor and $S(q)$ is the interparticle structure factor. Equation 1.10b gives the relationship between I_{sample}, $I_{solvent}$, and ΔR. The term Y in Equation 1.10b is an experimental calibration factor. Equation 1.10a was simplified to Equation 1.10c by making the following simplifications: (a) $K \propto (\partial n/\partial c)^2$, (b) given the small size of the objects compared to the scattering wave vector, $P(q)$ is unity, and (c) given the low concentrations, $S(q)$ is unity, and (d) we assume that $I_{sample} >> I_{solvent}$. From these simplifications it follows that the scattered intensity is thus simply proportional to the weight concentration of objects and their molar mass. In Equation 1.10c, W_i is the weight fraction of species i. As the molar masses are expected to be very different for the various particles, namely $M_{micelles} > M_{SCP} > M_{hp,dbp}$, we expect a maximum in light scattering intensity between the CEAC and the CECC, located at the PMC. The scattering of dbp and hp is negligible at this scale. The light scattering intensity will increase linearly with f^+ below the CEAC, as the concentration of SCP^- is linear with f^+. In Figure 1.9, we show a schematic light scattering diagram. From the speciation profiles as shown in Figure 1.7, we can also make some predictions about the pH changes that may occur during a titration experiment. When f^+ is below the PMC, there are free anionic groups in the system and when f^+ is above the PMC, there are free cationic groups in the system. Around the PMC the concentration of free annealed groups is at a minimum. One characteristic of free, annealed groups is that they can act as a pH-buffer. Above, we reasoned that the pH of the solution will change as a result of complexation. When the system is far away from the PMC, these pH changes will be suppressed due the buffering effect of free annealed groups. Around the PMC the number of free groups is at a minimum, so that also the buffering capacity goes through a minimum, and a maximum in $\partial p\mathrm{H}/\partial f^+$ is expected.

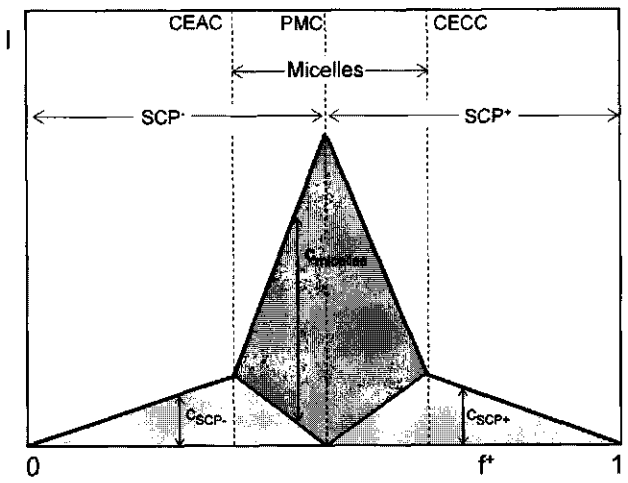

FIGURE 1.9. Aggregation diagram for CCCM's. On the vertical axis, the light scattering intensity is plotted, on the horizontal axis f^+ is plotted.

1.6. Aims of this investigation

Complex coacervation between homopolymers has been recognized as a useful tool in e.g. surface modification[15], protein purification[16], drug delivery[17], and gene delivery[18]. The complex coacervation core micelles are a novel system to obtain soluble complexes without excess charge, as the complex domain is restricted to the micellar cores. This absence of excess charge opens perspectives in drug delivery, because large *charged* objects do not diffuse easily through cell membranes. The CCCM's are also novel in the field of self-assembly, as their self-assembly does not arise from amphiphilicity, but from bringing together two components, that have excellent water solubility. Yet, when brought together under the right conditions, they spontaneously form reversible, salt-sensitive objects. The salt reversibility was demonstrated elegantly by Harada and Kataoka[19], who encapsulated enzymes in the micelles and cycled the ionic strength in the solution above and below the critical ionic strength. The activity of the enzymes turned out to be correlated to these cycles, as the enzymes were active above the critical ionic strength, and inactive below. At the start of our investigation, little was known about the effects of various experimental parameters, such as e.g. ionic strength, pH, mixing ratio, block lengths (and ratio) of the diblock-copolymer, and chain length of the homopolymer, on behavior and properties of the CCCM's. The earliest reports on CCCM's as a new class of electrostatically driven association colloids are by Kabanov et al.[20] and Kataoka et al.[21]. It was found by Cohen Stuart et al.[13], that the micelles exist only in a small region of composition. In general, the

shape of the micelles is spherical, and typical dimensions are in the order of several tens of nanometers[21-24]. Recently, a number of studies devoted to the use of these micelles as drug-delivery systems has been published[25, 26]. However, structural studies to gain fundamental insight on e.g. the effect of block lengths, pH, and ionic strength were not found in literature. The main aim of this thesis is therefore to get insight in fundamental physical aspects of these micelles, such as the aggregation mechanism, reversibility, effect of pH and ionic strength, and colloidal stability. In addition, more applied aspects have been studied, such as the use of CCCM's as stabilizers of colloidal particles, as solubilizers of insoluble complex coacervate, and as adsorbates on various surfaces.

1.7. Outline of this thesis

The first part of this thesis deals with the characterization of the micelles in bulk solution; this part is described in chapters 2, 3, and 4. The second part deals with applied aspects of the micelles and is presented in chapters 5 and 6.

In *chapter 2*, the effect of varying the diblock-copolymer block lengths and homopolymer molecular weight are described. It was found that a minimum block length ratio in the diblock-copolymer is a prerequisite to avoid precipitation. With constant block length for the core block, and increasing block length of the corona block, a decrease in aggregation number was found. The overall micellar (hydrodynamic) radius, however, increases slightly. It was also found that the micellar radius is sensitive to the molecular weight of the homopolymers. If the homopolymer molecular weight is increased beyond a critical value, the micellar radius increases slightly. At the critical homopolymer molecular weight, a micelle contains one single homopolymer chain. For these critical micelles, molecular weight and aggregation numbers could be calculated from the composition of the system at the PMC. A second method to interpret the data is the so-called light scattering mass analysis (LSMA) method that is introduced in this chapter. A comparison is made between the LSMA method and other interpretations of the experimental data. From analytical expressions for corona stretching, we estimated aggregation numbers, and from the molar volume of the core components, the core density could also be estimated.

In *chapter 3*, the roles of ionic strength and pH have been studied using potentiometric titrations and dynamic light scattering titrations. In the dynamic light scattering titrations, either the composition of the system was varied by titrating a solution of diblock-copolymer with oppositely charged homopolymer, or the composition was fixed and the pH was varied by adding strong base or acid. By varying the composition of the system, starting from pure diblock-copolymer at pH = 7, micelles

were formed when the number of cationic and anionic polyelectrolyte groups was roughly equal. We call this composition the preferred micellar composition (PMC). Upon complexation the bulk pH changes slightly, because the polyelectrolytes undergo changes in charge density and pK value. The bulk pH responds to these changes by adjusting to the new values of pK and charge densities. It will be shown that with increasing bulk ionic strength, more sodium ions are taken up in the complex.

In *chapter 4*, small angle neutron scattering (SANS) data are presented. We used the approach by Pedersen for modelling small angle scattering profiles of block-copolymer micelles[27, 28]. The aggregation numbers that were found are compared with the LSMA method. From the data, the micellar core densities were also estimated.

In *chapter 5*, a three-component system is described, consisting of charged diblock-copolymer, and two oppositely charged homopolymers. The experimental technique is again light scattering titration. In this system particles are formed that are much larger than the original micelles. We argue that these particles form a new kind of colloids, comparable to a micro-emulsion.

In *chapter 6*, we show by means of reflectometry that CCCM's can adsorb on anionic and hydrophobic surfaces. It turns out that, with respect to the composition of the system, the adsorbed mass is at a maximum for a micellar system, i.e. the micelles adsorb significantly more than the separate components. From an analysis of the adsorption kinetics, and the adsorbed amounts as a function of composition, we deduce that the micelles unfold upon adsorption. We also show that the micelles can act as anti-fouling agents, as they can protect silica and polystyrene surfaces from protein adsorption. The micelles are also able to stabilize colloidal silica particles. However, to achieve this, a minimum corona chain length was required. The thickness of the adsorbed micellar layer agrees with the hydrodynamic radius of the micelles in bulk solution.

1.8. References

1. M. Borkovec, B. Jönsson, and G.J.M. Koper, *Ionization Processes and Proton Binding in Polyprotic Systems: Small Molecules, Proteins, Interfaces, and Polyelectrolytes.* Surface and Colloid Science, ed. E. Matijevic. Vol. 16. 2001, Kluwer Academic, Plenum Press: New York. p. 19-339.
2. H.G. Bungenberg de Jong, in *Colloid Science II*, H.R. Kruyt, Editor. 1949, Elsevier, Amsterdam. p. 335-384.
3. J.Th.G. Overbeek and M.J. Voorn, Journal of Cellular and Comparative Physiology, 1957. **49**: p. 7-26.

4. D. Kovacevic, S. van der Burgh, A. de Keizer, and M. A. Cohen Stuart, Langmuir, 2002. **18**: p. 5607-5612.
5. D. J. Burgess, *Complex Coacervation: Microcapsule Formation*, in Macromolecular Complexes in Chemistry and Biology, P. Dubin, et al., Editors. 1994, Springer-Verlag: Berlin. p. 285-300.
6. S.T. Dubas and J.B. Schlenoff, Macromolecules, 2001. **34**: p. 3736-3740.
7. O.V. Borisov and E.B. Zhulina, Macromolecules, 2002. **35**: p. 4472-4480.
8. P.J. Flory, *Principles of Polymer Chemistry.* 1953, Ithaca NY: Cornell Univ. Press.
9. G.J. Fleer, M.A. Cohen Stuart, J.M.H.M. Scheutjens, T.Cosgrove, and B.Vincent, *Polymers at Interfaces.* 1993, London: Chapman Hall. 502.
10. L. Willner, A. Poppe, J. Allgaier, M. Monkenbusch, P. Linder, and D. Richter, Europhysics Letters, 2000. **51**: p. 628-634.
11. R. Nagarajan and K. Ganesh, Journal of Chemical Physics, 1989. **90**: p. 5843-5855.
12. R.S. Stock and W.H. Ray, Journal Polymer Science, Polymer Physics Edition, 1985. **23**: p. 1393-1447.
13. M.A. Cohen Stuart, N.A.M. Besseling, and R.G. Fokkink, Langmuir, 1998. **14**: p. 6946-6849.
14. B. J. de Gans, S. Wiegand, E.R. Zubarev, and S.I. Stupp, Journal of Physical Chemistry B, 2002. **106**: p. 9730-9736.
15. T. W. Graul and J. B. Schlenoff, Analytical Chemistry, 1999. **71**: p. 4007-4013.
16. J.Y. Shieh and C. E. Glatz, *Precipitation of Proteins with Polyelectrolytes: Role of Polymer Molecular Weight,* in *Macromolecular Complexes in Chemistry and Biology,* P. Dubin, et al., Editors. 1994, Springer Verlag: Berlin. p. 273-284.
17. P. van de Wetering, J.-Y. Cherng, H. Talsma, D.J.A. Crommelin, and W.E. Hennink, Journal of Controlled Release, 1998. **53**: p. 145-153.
18. A.V. Kabanov, P.L. Felgner, and L.W. Seymour, eds. *Interpolyelectrolyte Complexes for Gene Delivery: Polymer Aspects of Transfection Activity.* Self-Assembling Complexes for Gene Delivery - from Laboratory to Clinical Trial. 1998, John Wiley and Sons: Chichester. p. 197-218.
19. A. Harada and K. Kataoka, Journal of American Chemical Society, 1999. **121**: p. 9241-9242.
20. A.V. Kabanov, T. K. Bronich, V.A. Kabanov, K. Yu, and A. Eisenberg, Macromolecules, 1996. **29**: p. 6797-6802.
21. K. Kataoka, H. Togawa, A. Harada, K. Yagusi, T. Matsumoto, and S. Katayose, Macromolecules, 1996. **29**: p. 8556-8557.
22. A. Harada and K. Kataoka, Langmuir, 1999. **15**: p. 4208-4212.
23. A. Harada and K. Kataoka, Macromolecules, 1998. **31**: p. 288-294.
24. A. Harada and K. Kataoka, Macromolecules, 1995. **28**: p. 5294-5299.

25. L.W. Seymour, K. Kataoka, and A.V. Kabanov, *Cationic Block Copolymers as Self-Assembling Vectors for Gene Delivery.*, in *Self-Assembling Complexes for Gene Delivery,* A.V. Kabanov, L.W. Seymour, and P. Felgner, Editors. 1998, John Wiley and Sons: Chichester. p. 219-239.
26. K. Kataoka and A.V. Kabanov, *Polymeric Micelles in Biology and Pharmaceutics.* Colloids and Surfaces B: Biointerfaces, ed. K. Kataoka and A.V. Kabanov. 1999, Amsterdam: Elsevier. p. 339.
27. J.S. Pedersen and M.C. Gerstenberg, Macromolecules, 1996. **29**: p. 1363-1365.
28. J. S. Pedersen, Journal of Chemical Physics, 2001. **114**: p. 2839-2846.

CHAPTER 2

Colloidal Stability and Aggregation Mechanism

ABSTRACT

Complex coacervate core micelles were prepared with various polyelectrolytes and oppositely charged diblock-copolymers. The diblock-copolymers consist of a charged block and a water-soluble neutral block. Our experimental technique was dynamic light scattering in combination with titrations. With these titrations, the mixing ratio between the components was varied. At mixing ratios where the excess charge of the polyelectrolyte mixture is approximately zero, micelles may be formed. Whether or not stable micelles are formed, depends on the block lengths of the diblock-copolymers and the molecular weight of the homopolymers. In addition, the chemical nature of the corona blocks and type of ionic groups of the polyelectrolytes also influence the stability. A corona block that is three times longer than the core block is a prerequisite for stable micelles. If this ratio is increased further, the molecular weight of the homopolymers as well as the type of the ionic groups starts to play a major role. With very asymmetric block length ratios, where the corona block is much longer than the core block, no micelles are formed if the core block is very short. If the neutral block is too short, the polymeric mixture forms a macroscopic precipitate. With a constant core block length, the aggregation number decreases with increasing corona block length, as is predicted by scaling models for polymeric micelles with a neutral corona. We support our experimental data with simple models for curved polymer brushes and scaling models for polymeric micelles with neutral corona blocks.

*Published in Langmuir, 2004, **20**, pp 1073 - 1084*

2.1. Introduction

Complex coacervate core micelles (CCCM's) are two-component self-assembling colloids. The components are a double hydrophilic diblock-copolymer with one polyelectrolyte block and a water-soluble neutral block, and an oppositely charged homopolymer. The two polyelectrolyte blocks prefer to phase separate, forming a complex coacervate that is restricted in its growth by crowding of the neutral blocks on the surface of the complex coacervate core. In Figure 1.7, a schematic picture of a CCCm was presented.

A first study on this type of micelles was performed by Harada and Kataoka[1]. They used a slightly different micellar topology than presented in Figure 1.7, namely both oppositely charged polyelectrolyte blocks (poly(L-lysine) and poly(α, β- Aspartic acid)) were connected to a neutral PEG (poly ethylene glycol) block. Monodisperse micelles with 15 nm hydrodynamic radius were formed. The stoichiometric micelles were electroneutral. The micelles carried no excess charge, as values for the ζ-potential at stoichiometric conditions were very small. Kabanov et al.[2] used a quenched polyelectrolyte, PVP (Poly *N*-ethyl-4-vinylpyridinium bromide) and an annealed ionic block in the diblock-copolymer. They showed that micelles disintegrate above 0.35 M NaCl. The micelles were stable over a wide pH range.

Spherical morphology of the micelles was demonstrated by performing dynamic light scattering experiments at different angles[3]. Cohen Stuart et al.[4] showed that upon mixing poly acrylic acid and poly(dimethylaminoethylmethacrylate) -copoly(glycerylmethacrylate) solutions a transient phase separation may occur that rearranges into micelles after a certain relaxation time. These relaxation times were extremely salt-sensitive, a variation as wide as 10^4 was observed in a salt range up to 0.3 M NaCl. The threshold ionic strength for micellar disintegration was 0.5 M NaCl, which is in line with the value found by Kabanov et al.[2].

Two further reports by Harada and Kataoka[5, 6] deal in detail with the core-shell architecture of the micelles using dynamic and static light scattering. Their system was PEG-Pasp (Poly(EthyleneGlycol)-Poly(Aspartic acid)) and chicken egg white lysozyme. The PEG block length was 273 units. Micelles were stable over a wide range of mixing ratios, going from 1.0 to 2.67, expressed as the number of aspartic acid groups over the total number of lysine and arginine groups in the lysozyme. From the static light scattering experiments, molecular weights in the range from 1 - 2 * 10^6 gram/mole were found, increasing with increasing mixing ratio. The calculated aggregation numbers show a decrease of lysozyme units per micelle (56-40) and an increase of PEG-Pasp molecules per micelle (62-122) as a function of the mixing ratio. This was accompanied by an increase in micellar size, going from 23.6 to 32.9 nm hydrodynamic radius. They deduced from the molecular weights of the micelles and

the macroscopic loading ratios that the micellar core was constant ($\sim$ 7 nm) over the whole mixing range, so that the increase in micellar radius would arise from increased corona chain stretching. The corona thickness was found to be halfway theoretical estimates on fully stretched chains and random coil conformation. This is in line with theoretical and experimental work on polymers grafted on a curved surface in a good solvent[7]. They conclude that the thermodynamic penalty of corona stretching plays only a minor role in the mechanism of micelle formation, compared to the electrostatics in the core.

Harada and Kataoka[8] also demonstrate chain length recognition in the micellar core. Their system consists of two diblock-copolymers with analogous neutral blocks (PEG) of equal molecular weight (5 K) and oppositely charged ionic blocks (Poly(aspartic acid) and poly(L-lysine)). Samples were prepared with chain lengths 18 and 78 for the ionic blocks. Micellization was only possible between matched block lengths. Three component mixtures, i.e. block lengths 18 and 78 of polycation mixed with block length 78 of polyanion showed that the 18 units species did not participate in the micellization.

With complex coacervate core micelles, there are many experimental parameters that can be varied, *e.g.* block lengths, molecular weight of the homopolymer, pH, ionic strength, mixing ratio, overall concentration, and chemical composition of the (diblock-co)polymers. Most of these parameters influence the interaction between the oppositely charged blocks and thus the aggregation mechanism.

Complex coacervate core micelles are formed when the cationic and anionic charges of the diblock-copolymer and homopolymer are present in roughly equal amounts[4]. We call this composition the preferred micellar composition (PMC). At compositions (far) away from the PMC no micelles are formed. Although interaction may take place, the structure of the aggregates is probably very loose[4], because aggregation into larger, dense objects is hampered by the excess charge of the aggregates. The PMC cannot be predicted straightforwardly from bulk charge densities, since the charge densities in the core differ from those in the bulk solution. The complex coacervate, with a high concentration of cationic and anionic groups is not the same environment as the bulk solution, so that the dissociation behavior of the chargeable groups is different from that in bulk solution. The linear charge densities increase for both polyelectrolytes. In Chapter 3 of this thesis, we take a closer look at changes in pH and pK that annealed polyelectrolytes undergo upon complexation.

2.2. Micellar free energy balance

The driving force for phase separation in complex coacervation has an entropic and an energetic part leading to a gain in free energy contribution, $F_{complex}$. The entropic part

is associated with the release of the counter ions from the polyelectrolyte double layers. The energetic part is of an electrostatic nature. In bulk solution, the distance between a polyelectrolyte charge and its counter ions is a compromise between the maximalization of the entropy of the counter ions and minimization of the electrostatic energy. The entropy of the counter ions favours a homogeneous distribution throughout the system. The electrostatic energy favours close contact between the opposite charges.
In a complex coacervate, the counter ions have been replaced by polyions of equal charge sign. The distance between the polyions is again a compromise between maximalization of the entropy of the polyions and minimization of the energy. Since the entropy loss of polyions is very small compared to that of small ions, the average distance between the oppositely charged groups can be much smaller. Therefore, the electrostatic energy will be much lower in the complex coacervate.
An early theoretical study on complex coacervation was performed by Voorn and Overbeek[9] for low charge density polyelectrolytes. Another theoretical study was performed by Odijk[10] who calculated phase transitions due to attraction between weakly charged polyelectrolyte chains and highly charged rod like macromolecules. In these theories, a macroscopic phase separation is predicted at charge stoichiometric conditions. One phase is rich in polyelectrolytes and the other phase consists mostly of water and small ions. In the case of complex coacervate core micelles, this phase separation is restricted to colloidal dimensions.
The equilibrium aggregation number (P) results from a complex interplay between different forces. We express P as the number of diblock-copolymers per micelle. The surface free energy favours micellar growth to minimize the contact area between solvent and coacervate cores. In itself, $F_{surface}$ is an unfavorable contribution. With increasing P, the contribution of $F_{surface}$ becomes less unfavorable, since the surface area per unit core material decreases with increasing P. The penalty that underlies micellization is the stretching of core and corona blocks that favour low values for P. These contributions will be named F_{core} and F_{corona}. The micellar free energy is thus given by

$$F_{micelle} = F_{surface} + F_{core} + F_{corona} + F_{complex} \tag{2.1}$$

If $F_{micelle}$ is expressed per diblock-copolymer, the equilibrium aggregation number can be found by two conditions: $\partial F_{micelle}/\partial P = 0$ and $F_{micelle} < 0$. If we assume that $F_{complex}$ is independent of P, which seems a logical assumption for large P, and we neglect F_{core} for strongly asymmetric diblock-copolymers[11] then P is only determined by $F_{corona}$and $F_{surface}$. The effect of block length variation can be studied qualitatively in analogy to hydrophobically associating systems, for which scaling relationships have been derived. According to scaling theories for micelles formed by strongly asymmetric diblock-copolymers with a neutral-hydrophobic architecture[11, 12], two limiting cases can be distinguished, depending on the chain lengths N of the participating blocks: (i)

star-like micelles where $N_{corona} >> N_{core}$, so that the radius of the core is very small compared to the overall dimensions of the micelles and (ii) the so called 'crew-cut' micelles where $N_{core} >> N_{corona}$, so that the micellar radius is dominated by the core. See also Figure 1.6. For the star-like micelles and crew-cut micelles, the scaling relation ships are given by Equations 1.7 - 1.9. As was found by Willner et al.[13] in a SANS study on amphiphilic diblock-copolymers with constant N_{core} and varying N_{corona}, the decrease of core radius with decreasing P (and thus increasing N_{corona}) was overcompensated by the increase in corona thickness, so that $R_{micel} = R_{core} + H_{corona}$ increases with increasing N_{corona}. The self-assembly of diblock-copolymers in a selective solvent has been addressed theoretically by Nagarajan and Ganesh[14], who found also found that P decreases for a constant N_{core} and increasing N_{corona}, they found $P \sim N_{corona}^{-0.51}$. In the dilute regime, where intermicellar interactions are negligible, the block lengths of the core blocks (N_{core}) and corona blocks (N_{corona}) thus govern the micellar physics, such as aggregation number and radius. Note that Equations 1.7 - 1.9 only consider $\partial F_{micelle}/\partial P = 0$ and that the condition $F_{micelle} < 0$ is not taken explicitly into consideration. The block lengths also govern stability of the micellar system. For very asymmetric block length ratios, it is clear that stable micelles are not to be expected. On the one hand, if $N_{core} << N_{corona}$ the entropy and energy gain associated with the complexation is insufficient to balance the stretching of the corona blocks so that no micelles are formed. On the other hand, if $N_{core} >> N_{corona}$, there is not sufficient stop-mechanism from the crowding of (short) corona chains on the core surface, and we expect a macroscopic complex coacervate phase or precipitate. Note that such a precipitate is not the same as the liquid/liquid like phase separation as presented in Figure 1.4. Due to the presence of the water-soluble neutral block, the formation of a homogeneous liquid phase is hindered. For intermediate block length ratios, the balance between stability and instability is much more subtle. For the build up of osmotic pressure in the corona, the minimum requirement is that $\sigma^{-1/2} < R_g$ where σ is the grafting density of corona chains on the core surface and R_g is the unperturbed dimension of a corona block.

2.3. Further analysis of aggregation mechanism

The aggregation diagram of CCCM's as shown in Figure 1.9 was discussed in Section 1.5.2. In this section we will show that there is even more information to be found from a light scattering intensity (I) vs f plot. In Figure 2.1, we again show the aggregation diagram. Newly introduced are the slopes $\partial I/\partial f$, indicated as a, and the light scattering intensity at the CEAC and PMC, indicated as I_{CEAC} and I_{PMC}. It is important to realize that at the points where the value or sign of $\partial I/\partial f$ changes, there is exclusively one type of particle in the system, i.e. the composition of the particles directly reflects the macroscopic composition of the system, f. In Table 2.1, this is summarized.

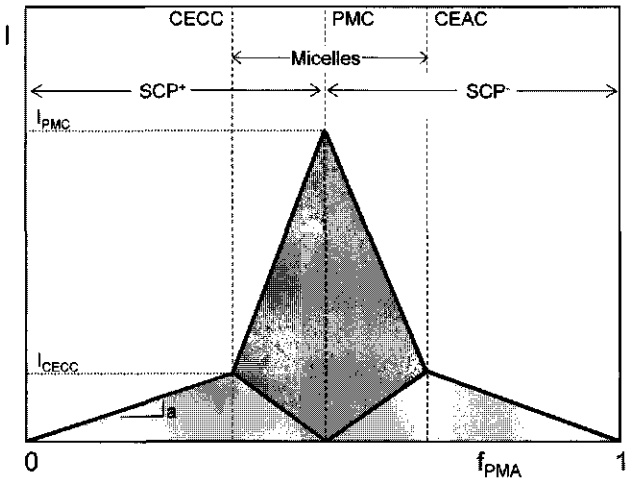

FIGURE 2.1. Aggregation diagram of the CCCM's.

Particle	CEAC	PMC	CECC
SCP^-	Maximum	Zero	Zero
CCCM	Zero	Maximum	Zero
SCP^+	Zero	Zero	Maximum

TABLE 2.1. Concentrations of SCP^-, CCCM, and SCP^+ at the CEAC, PMC, and CECC.

So, at the CEAC, only SCP^- are found with composition f_{SCP^-}. Let us assume that the SCP^- prefer to minimize their aggregation number, due to their excess charge. This means, that in the case of the homopolymers as the minor component, the SCP^- consist of one homopolymer that is fully saturated by oppositely charged blocks from the diblock-copolymer. The number of diblock-copolymers per SCP^- (thus per homopolymer chain), P_{SCP}, follows from the chain length of the homopolymer N_{hp}, the block length of the core block from the diblock-copolymer N_{core}, and f_{CEAC}:

$$P_{SCP} = \frac{N_{hp}}{N_{core}}\left(\frac{1}{f_{CEAC}} - 1\right) \tag{2.2}$$

From Equation 2.2, the molar mass of a SCP^- follows straightforwardly as $M_{SCP} = M_{hp} + P_{SCP}M_{dbp}$, where the subscripts *hp* and *dbp* denote homopolymer and diblock-copolymer respectively. From Equation 2.2, we know the molar mass of the particles at the CEAC, and from the experiment, we know the polymer concentration and light scattering intensity. In Equation 1.10, we stated that $I \propto CM$. This relationship is valid throughout the aggregation diagram, so that the molar masses of SCP and CCCM

can be determined relative to one another by

$$\frac{M_{CCCM}}{M_{SCP}} = \frac{I_{PMC}/C_{PMC}}{I_{CEAC}/C_{CEAC}} \tag{2.3}$$

We showed that the absolute value of M_{SCP} can be calculated by making *one* assumption: each SCP^- carries only one homopolymer. The data for the right hand side of Equation 2.3 follow from the experiment, so that the molar mass of a CCCM can now be calculated exactly. From the molar mass of the CCCM, the number of diblock-copolymers per micelle, P, can be calculated. We call this method the light scattering mass analysis (LSMA) and we will apply this method in the Results and Discussion section. Note that the above explained exercise is also valid for titrating a cationic diblock-copolymer solution with anionic homopolymer by reversal of the terminology with respect to the charge signs.

The value of I at the CEAC is thus a measure for the molar mass of the SCP^-. By performing a series of light scattering titration experiments with varying chain length for the homopolymer, we expect that I_{CEAC} is a function of N_{hp}. One could also say that the slope $\partial I/\partial f$ is a function of N_{hp}.

From the molar mass of a CCCM, it's aggregation number (P) can be calculated, expressed as the number of diblock-copolymers per micelle. From the molar volumes of the core components, and upon assuming a polymer volume density, the core radius can be calculated by

$$R_{core} = \left(\frac{3V_{dry}}{4\pi\phi}\right)^{1/3} \tag{2.4}$$

where V_{dry} is the dry volume of the core components, and ϕ is the polymer volume fraction in the core. From the core radius, and aggregation number, the grafting density of corona chains at the core/corona interface follows as

$$\sigma = \frac{P}{4\pi R_{core}^2} \tag{2.5}$$

The corona thickness follows from σ, R_{core}, the corona chain length N_{corona}, and the excluded volume parameter υ which characterizes the binary interactions between polymer segments ($\upsilon = 1 - 2\chi$ within Flory-Huggins theory). The following two equations were taken from Wijmans and Zhulina[7]. Firstly, the thickness of a polymeric brush on a flat surface in good solvent is given by:

$$H_{flat} = \left(\frac{8}{\pi}\right)^{1/3} l N_{corona} \upsilon^{1/3} \left(l^2\sigma\right)^{1/3} \tag{2.6}$$

where l is the monomer length. For spherical particles the brush height will depend on the relative reciprocal curvature $\omega = R_{core}/H_{flat}$ and H_{corona} follows from

$$\left(\frac{H_{corona}}{H_{flat}}\right)^3 \left(1 + \frac{3H_{corona}}{4\omega H_{flat}} + 0.2\left(\frac{H}{\omega H_{flat}}\right)^2\right) = 1 \tag{2.7}$$

The theoretical micellar radius is now given by $R_{micel} = R_{core} + H_{corona}$.

2.4. Materials and methods

2.4.1. Chemicals

The chemical structure and composition of the (diblock-co)polymers used in this study are given in Figure 2.2 and Table 2.2. The poly(dimethylaminoethylmethacrylate) (PAMA) homopolymer and PAMA-*co*-poly(glycerylmethacrylate) (PAMA-PGMA) diblock-copolymers were synthesized in the group of Dr. Arnold in Halle, Germany. Chain length of the PAMA homopolymer was 126. The synthesis routes are given by Hoogeveen[14]. The poly(acrylic acid)-*co*-poly(acryl amide) (PAA-PAM) samples were a kind gift from Dr. M. Destarac from Rhodia, Aubervilliers, France. Their synthesis routes are reported by Taton et al.[15]. The PAA and poly(*N*-ethyl-4-vinylpyridiniumbromide) (PVP) homopolymers were obtained from Polymer Source Inc., Canada and were used as received. The PMA polymethacrylic acid (PMA) homopolymer series was obtained from Polymer Standards Service and used as received. The polydispersities of all polymers were low, typically around 1.05-1.1. All other chemicals (salts, basic and acidic solutions) were of analytical grade.

Sample	$N_{PAMA,PAA}$	$N_{PGMA,PAM}$	M (gram/mol)
$PAMA_5PGMA_{95}$	5	95	20000
$PAMA_{12}PGMA_{118}$	12	118	20000
$PAMA_{35}PGMA_{105}$	35	105	20000
$PAMA_{63}PGMA_{64}$	63	64	20000
$PAMA_{90}PGMA_{30}$	90	30	20000
$PAA_{14}PAM_{14}$	14	14	2000
$PAA_{14}PAM_{69}$	14	14	6000
$PAA_{14}PAM_{139}$	14	14	11000
$PAA_{42}PAM_{42}$	42	42	6000
$PAA_{42}PAM_{97}$	42	97	10000
$PAA_{42}PAM_{208}$	42	208	18000
$PAA_{42}PAM_{417}$	42	417	33000

TABLE 2.2. Block lengths of the diblock-co-polymers used in this study

2.4.2. Equipment

Dynamic Light Scattering (DLS) was performed with an ALV light scattering instrument equipped with a 400 mW argon ion laser tuned at a wavelength of 514 nm. Temperature was controlled by a Haake C35 thermostat, providing cell accuracy $\pm$ 0.1 K. In order to analyse the measured autocorrelation functions the method of cumulants

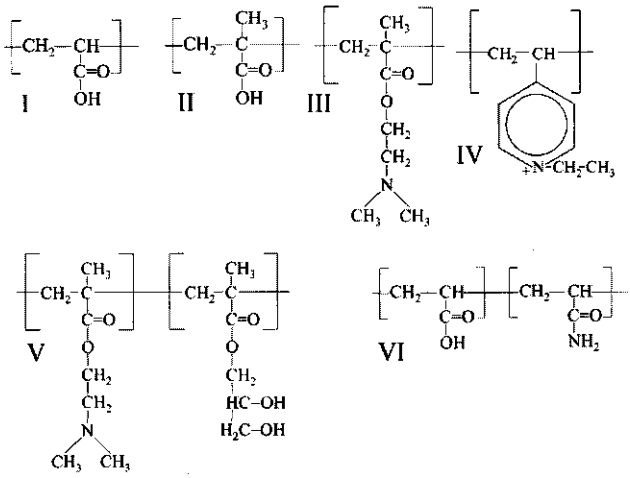

FIGURE 2.2. Chemical structure of the (diblock-co)polymers used in this study. I: PAA (Poly-(Acrylic acid)). II: PMA (Poly-(Methacrylic acid)). III: PAMA (Poly-(Dimethylamino ethylmethacrylate)). IV: PVP (poly(*N*-ethyl-4-vinylpyridiniumbromide))). V: PAMA-PGMA (PAMA-*co*-Poly(Glycerylmethacrylate). VI: PAA-PAM (PAA-*co*-Poly(Acrylamide)).

was used[16]. In this method, it is assumed that the scattering particles are spherical and that only the translational diffusion coefficient contributes to the decay of the autocorrelation function. The average diffusion coefficient and corresponding hydrodynamic radius of the particles were calculated using the Stokes-Einstein relation for spherical particles. Titrations were carried out using a Schott-Geräte computer controlled titration set-up to control sequential addition of titrant and cell stirring. The millivolt values were recorded with a combined Ag/AgCl glass electrode. These values were converted into pH values after calibration of the electrode.

During the mole fraction titrations, one of the (diblock-co)polymers is titrated with a concentrated solution of the other component. Typical concentrations of the titrated species are in the order of several millimoles per litre, expressed in terms of monomers. After every dosage pH and 90° laser light scattering intensity (I) were recorded, and - if possible - the hydrodynamic radius of the particles (R_h). Variations in pH, R_h and I are studied as a function of the mole fraction of added species f_X. We express f_X as

$$f_x = \frac{[X]_0}{[X]_0 + [Y]_0} \tag{2.8}$$

where X is the added species and Y is the titrated, oppositely charged, species. In Equation 2.8, concentrations are always expressed as overall concentrations of chargeable groups in the system. The initial pH values and ionic strength of both solutions

were corrected with either base or acid to match at a pH value around 7. At this starting pH, bulk pH is almost constant upon titration PAA with PAMA or vice versa[17]. Because of the matched bulk conditions, changes in pH can be attributed to interactions between the oppositely charged species and do not result from volumetric effects. However, slight differences ($\pm$ 0.2 units) in starting pH remain, as due to the low polymer concentrations, a more close matching was not possible.

2.5. Results and discussion

2.5.1. Colloidal stability. The effect of diblock-copolymer architecture

A mixture of oppositely charged polyelectrolytes at charge stoichiometric composition will lead to a macroscopic phase separation. This phase separation can be restricted to colloidal dimensions by chemically linking one of the polyelectrolytes to a water-soluble neutral block. Stable micelles are only formed if the lengths of the neutral and ionic block of the diblock-copolymer are appropriate. In Table 2.3, the effect of variation in neutral/ionic block length ratios with a more or less constant total block length of the diblock-copolymer is given. From the results in Table 2.3, it follows that the very asymmetric block length ratios are ill-suited to form stable CCCM. Also, the 1:1 block length ratio leads to a macroscopic phase separation. Either the GMA monomers are not sufficiently hydrophilic or the overall block length is too short.With the $PAMA_{35}PGMA_{105}$ sample, micelles were formed within a wide range of M_w for the PAA and PMA homopolymers. With the $PAMA_{12}PGMA_{118}$ sample, however, the interaction is also sensitive to the molecular weight of the PAA samples. It was already shown theoretically by Voorn and Overbeek[9] that higher degrees of polymerisation favour phase separation. Apparently, there is also a critical minimum molecular weight for the homopolymers. With the $PAMA_{12}PGMA_{118}$sample, this critical molecular weight is somewhere between 12 and 154 K. With the $PAMA_{35}PGMA_{105}$ sample, the critical homopolymer molecular weight is below 10 K for PMA. In Table 2.4, we present an overview of the micellization properties of PAA-PAM samples. The block length variation that was available in these samples was given in Table 2.2. The results in Table 2.4 show similar behaviour with respect to block length ratios as in Table 2.3. Depending on the total block length of the diblock-co-polymer, when the corona-core block length ratio is roughly 1:1 precipitation may occur. If $N_{corona} > N_{core}$, stable micelles can be formed. With the PAA-PAM samples, we also show a difference in interaction between annealed (PAMA) and quenched (PVP) polycations. The degrees of polymerisation for the shortest PVP and PAMA are not too far apart. Micellization was not possible, however, with PAMA. Apparently, the driving force for aggregation is stronger with PVP samples.

From the results in Tables 2.3 and 2.4, we conclude that four parameters in block-co-polymer design determine the micellization qualities of a system. (i.) the block length

Sample	homopolymer (M_w(K),N)	mixture at the PMC (R_h)
$PAMA_5PGMA_{95}$	PAA(136,1900)	no micelles
$PAMA_{12}PGMA_{118}$	PAA(12,170)	no micelles[a]
$PAMA_{12}PGMA_{118}$	PAA(154,2100)	micelles (30 nm)
$PAMA_{35}PGMA_{105}$	PAA(various), PMA(10-600, 115-7000)	micelles (18-40 nm)[b]
$PAMA_{63}PGMA_{64}$	PAA(12,170)	precipitation[a]
$PAMA_{90}PGMA_{30}$	PAA(136,1900)	precipitation

TABLE 2.3. The effect of block length ratio variation at constant total Mw ($\approx$ 20K) for the PAMA-PGMA diblock-copolymer with PAA and PMA homopolymers. Ionic strength was 100 mM $NaNO_3$, pH was 7. Micellar radii were determined with dynamic light scattering. [(a)] Data were used from Cohen Stuart et al.[4]. [(b)] In some cases precipitation took place, but it was not a general phenomenon.

Sample	homopolymer (M_w(K),N)	mixture at the PMC (R_h)
$PAA_{14}PAM_{14}$	PAMA(20,126)	precipitation[a]
$PAA_{14}PAM_{69,139}$	PAMA(20,126)	no micelles[a]
$PAA_{14}PAM_{69,139}$	PVP(29-690,140-3200)	micelles (12-21 nm)[b]
$PAA_{42}PAM_{42}$	PAMA(20,126)[a],PVP(various)[b]	micelles/precipitation
$PAA_{42}PAM_{97,208,417}$	PAMA(20,126)[a] PVP(various)[b]	micelles[c]

TABLE 2.4. Micellization properties of PAA-PAM diblock-copolymer samples. Hydrodynamic radii were determined with Dynamic Light Scattering. The pH was around 7 for all experiments. [a] Ionic strength was 30 mM $NaNO_3$. [b] Ionic strength was 50 mM Na_2HPO_4/NaH_2PO_4 buffer. [c] The micelles were stable with PVP in very high concentrations (20 - 60 gram/litre)[18]

ratio, (ii.) the total block length of the diblock-co-polymer. (iii.) the chemical structure of the corona monomers and (iv.) the molecular weight and type of ionic groups of the homopolymer.

It shows for both series that if the corona-core block length ratio exceeds 3:1 precipitation can be avoided completely. If we compare the $PAA_{14}PAM_{14}$ and $PAA_{42}PAM_{42}$ samples from the PAA-PAM series, stable micelles are possible with the $PAA_{42}PAM_{42}$ sample whereas the $PAA_{14}PAM_{14}$ sample leads to a precipitate. The PAM corona blocks are much more hydrophilic than the PGMA blocks. Compare the $PAMA_{64}PGMA_{65}$ sample with the $PAA_{42}PAM_{42}$ sample. Although the total length of the $PAMA_{64}PGMA_{65}$ exceeds the $PAA_{42}PAM_{42}$ length, micellization was not possible. We attribute this difference to the different solvability of PAM compared to PGMA. As can be understood from the chemical composition of PAM and PGMA in Figure 2.2, PAM is more hydrophilic then PGMA. Therefore, the PAM corona chains will be highly swollen, thereby forming a thick corona, that is an excellent steric barrier against corona-corona

interpenetration. The PGMA chains, however, will adopt a less swollen conformation, so that the corona is relatively thin. As the PGMA chains prefer a lower degree of solvation, corona-corona interpenetration is facilitated, leading to colloidal instability. From our data, we can conclude that the role of the corona blocks is thus highly important. However, this was not found by Harada and Kataoka[5, 6] who state that the entropic penalty of corona stretching plays only a minor role in the micellization process. As their system was diblock-copolymer + oppositely charged enzymes, it apparantly behaves different than our system, and this may be related to the higher degree of ordering of an enzmye/block-copolymer system.

2.5.2. Morphology - Variation of Corona Block Length

Results of light scattering titrations of $PAA_{42}PAM_{42}$, $PAA_{42}PAM_{97}$, $PAA_{42}PAM_{208}$, and $PAA_{42}PAM_{417}$ with PAMA homopolymer are shown in Figure 2.3. Firstly, we will determine the PMC from these data. At the PMC, there is no excess polyelectrolyte charge, so that the PAMA homopolymers and PAA-PAM diblock-copolymers can form neutral micelles. Outside the PMC, excess polyelectrolyte charge hinders the aggregation into micellar objects. Therefore, we expect a peak in the light scattering intensity data at the PMC as we suggested in Figure 2.1. In Figure 2.3a, however, instead of a single peak we see a broad area with several peaks for the $PAA_{42}PAM_{42}$, $PAA_{42}PAM_{97}$, and $PAA_{42}PAM_{208}$ series, and a more or less constant intensity plateau for $PAA_{42}PAM_{417}$. These peaks show the presence of the micelles, that are absent at low and high f_{PAMA}. The exact position of the PMC in these peak areas can be determined from the pH data. If the system is at non-stoichiometric composition, there are free, non-complexed, polyelectrolyte groups in the solution. These free groups will act as a pH buffer, so that the effect of changes in charge density and pK of the polyelectrolytes on the bulk pH are suppressed. As the system is approaching the PMC, the concentration of these free groups will decrease, so that the buffering capacity decreases and pH changes are more pronounced. At the PMC, the concentration of buffering groups will be at a minimum, so that a maximum in $|\partial pH/\partial f_{PMA}|$ is expected to correspond with the PMC. If the PAMA is overdosed, the micelles disintegrate. All curves in Figure 2.3b curves exhibit a maximum in $|\partial pH/\partial f_{PMA}|$ at $f_{PMA} \approx 0.47$. Apparently, the PAMA and PAA blocks form a (neutral) complex with a nearly 1:1 composition. From the pH data we conclude that the PMC is at $f_{PAMA} \approx 0.47$ for all series. In addition, at $f_{PAMA} = 0.47$, agreements between theoretical and experimental cumulant functions were much better than around the right hand side of the intensity peaks. Thus, also from the intensity data, we conclude that the PMC is at $f_{PAMA} = 0.47$ for all series. The length of the neutral PAM block does not influence the position of the PMC, as both the intensity peaks and the typical changes in the pH curves occur at the same f_{PAMA} values for all PAA-PAM samples. The value of f_{PMC} suggests that the charge

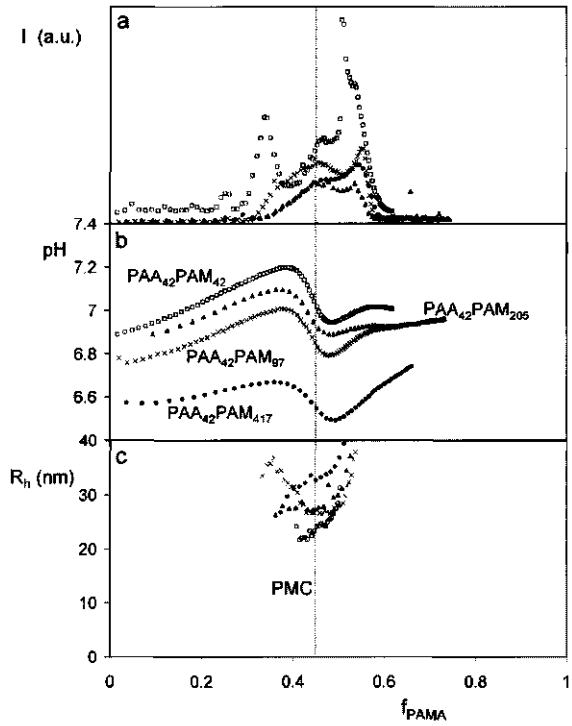

FIGURE 2.3. Mole fraction titrations of $PAA_{42}PAM_{42}$ (□), $PAA_{42}PAM_{97}$ (×), $PAA_{42}PAM_{208}$ (▲) and $PAA_{42}PAM_{417}$ (•) with PAMA solution. (a) Light scattering intensity (arbitray units), (b) pH data, (c) micellar radii. Experimental conditions: concentration of PAA monomeric units was 2.7 mM/litre. Ionic strength was 30 mM $NaNO_3$. The PMC is indicated by the dotted vertical line through all three figures at $f_{PAMA} = 0.47$. high intensities with $PAA_{42}PAM_{42}$ at $f_{PAMA} \approx 0.5$ were caused by a macroscopic phase separation. At $f_{PAMA} \approx 0.6$, the solution was again optically clear to the naked eye.

neutralization process is mostly a matching of the polyelectrolyte charges.

In Figure 2.3c, the micellar radii are given. It is seen that micelles only form around the PMC, and are in the order of 25 - 35 nm, depending on the block lengths of the PAA-PAM. A little beyond the PMC, an increase of the micellar radii is seen, that coincides with a second peak in the scattered intensity. We attribute this second peak to swelling of the micelles just before they disintegrate, as the peak is directly followed by a rapid decrease of the scattered intensity to the level of a molecular solution. The very high scattered intensities of the second peak of the $PAA_{42}PAM_{42}$ sample were caused by a macroscopic phase separation. Apparently, the very short (3K) PAM hairs cannot provide an effective steric barrier at all compositions. In addition, note that the shape

of the I vs f_{PAMA} curve does not follow the simplified pattern of Figure 2.1 with the $PAA_{42}PAM_{42}$ sample, whereas all other curves are much more in line with Figure 2.1. At this moment, we have no explanation for the peak of the $PAA_{42}PAM_{42}$ sample, that appears around $f_{PAMA} \approx 0.35$. Although an intensity peak is seen, no particles were detected by the dynamic light scattering. All in all, this sample is not the best choice to form CCCM's.

We stress that Figures 1.8 and 2.1 present a simplified view on the various effects that play a role in the aggregation mechanism of the CCCM's. In these Figures, we assume a constant micellar composition and zero excess charge on the individual micelles between the CECC and CEAC, implying that all excess charge is carried by the SCP. Yet, variations in R_h around the PMC are clearly seen in Figure 2.3c. It is conceivable that the excess charge that exists in the micellar window on the left and right hand side of the PMC, also affects the micelles and thus their core density, radius and aggregation number. Yet, the variations are small, and therefore we think that Figures 1.8 and 2.1 do justice to the aggregation mechanism to a large extent. In addition, when the experimental cumulant function is closest to single-exponential, the diffusion coefficient (and thus the radius) that is calculated is the most reliable. When this is not the case, with our specific software, the diffusion coefficient is always underestimated, so that the radius is overestimated. Therefore, the radii in Figure 2.3c are the most reliable close to, or just at, the PMC. So, the monotonous increase of R_h around the PMC for the $PAA_{42}PAM_{42}$, $PAA_{42}PAM_{208}$, and $PAA_{42}PAM_{417}$ and the minimum in R_h for $PAA_{42}PAM_{208}$ as seen in Figure 2.3c may be caused by a combination of subtle changes in P, and experimental error in the determination of R_h.

It is of interest to explain the up-down-up behaviour that is seen in the pH data in Figure 2.3b. At pH = 6.7, both PAA and PAMA have about 75 percent charged groups in bulk solution. The experiment starts out with PAA as the major component, so that all PAMA that is initially added will be 'consumed' by the PAA. Hereby, PAMA increases its charge density to a larger extent than PAA, which leads to a net proton uptake. Upon further addition of PAMA, the micellar region is reached, where the excess polyelectrolyte charge is minimal. In order to match the charge densities, PAA has to increase its charge density, which is seen in a proton release, and thus a lowering of the bulk pH. Upon overdosing the PAMA, the micelles disintegrate, which leads to an increase of the pH. This pH increase is the result of the polyelectrolytes again taking on their bulk charge densities. charged groups in bulk solution.

A cross section of the light scattering intensity, I, and R_h versus N_{corona} of the PAM block at the PMC is presented in Figure 2.4. The intensities are normalized for the weight concentration. With increasing corona block length, an increase in hydrodynamic micellar radius is seen. The intensity, however, decreases strongly with increasing block length. From Equations 1.7 and 1.9 it follows that at a constant value for

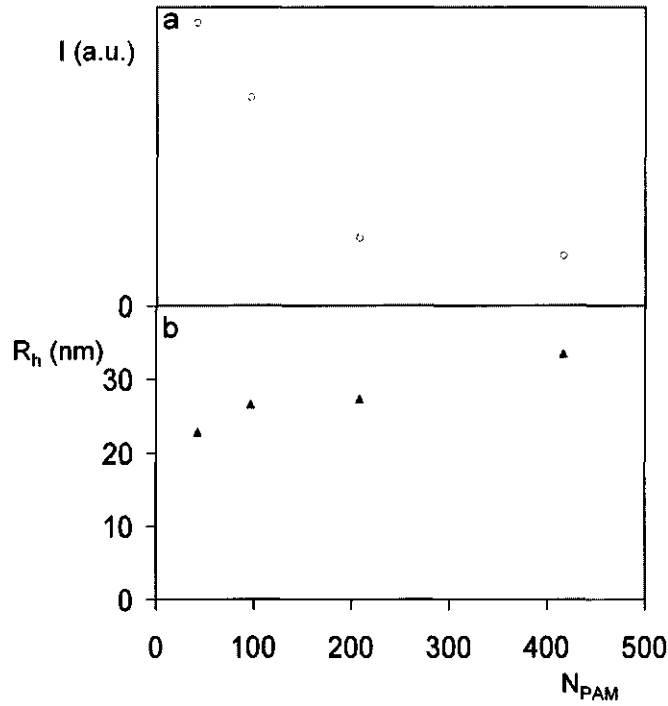

FIGURE 2.4. Cross section of light scattering intensities (a) and micellar radii (b) at the PMC. On the horizontal axis is the chain length of the PAM block of the $PAA_{42}PAM_{42-417}$ samples. The intensity data are corrected for overall weight concentration of the polymers in solution. The lines are a guide to the eye.

N_{core}, P decreases with increasing N_{corona}. From the reciprocal relationship between I and M_{PAM}, it is possible to compare the scaling exponent in Equation 1.9 with our experimental data.

The $\partial n/\partial c$ value of chargeable species is dependent on their charge density. Because we have $f_{PAMA} \approx 0.5$ at the PMC, we assume fully charged polyelectrolyte groups in the core, so that the $\partial n/\partial c$ values are 0.27[19], 0.21[20], and 0.185[21] (ml/g) for PAA, PAMA and PAM respectively. It was shown by Harada and Kataoka[6], that the $\partial n/\partial c$ of CCCM's is the sum of the $\partial n/\partial c$ values of the separate components, so that:

$$(\frac{\partial n}{\partial c}) = W_A(\frac{\partial n}{\partial c})_A + W_B(\frac{\partial n}{\partial c})_B + W_C(\frac{\partial n}{\partial c})_C + ... \tag{2.9}$$

where W_i is the weight fraction of species i in the system. The $\partial n/\partial c$ values that were calculated with Equation 2.9 were used in Equation 1.10c. The scaling relationship for M_w can be translated into a scaling relationship for P, the number of diblock-copolymers per micelle, by correcting for the specific mass of the 'building blocks' (M_{bb})

of the micelles. The mass of such a building block is the total mass of the PAA-PAM molecule and its oppositely charged PAMA groups. In Table 2.5, the values for $\partial n/\partial c$ and M_{bb} are given. From these data, P was calculated as

$$P \propto M_{bb}^{-1} I(\frac{\partial n}{\partial c}) \tag{2.10}$$

Note that Equation 2.10 does not calculate *absolute* P values, but only calculates the relative variations in P. In Table 2.5, the P values that were calculated with the LSMA method are given. Only with the $PAA_{42}PAM_{42}$ sample, the LSMA method could not be applied, as a clear CEAC is not visible in the experimental I data in Figure 2.3a.

Sample	M_{bb}(K)	$\partial n/\partial c$	P(LSMA)
$PAA_{42}PAM_{42}$	12.2	0.219	-
$PAA_{42}PAM_{97}$	16.2	0.210	70
$PAA_{42}PAM_{208}$	24.2	0.202	17
$PAA_{42}PAM_{417}$	39.2	0.195	11

TABLE 2.5. Values of M_{bb}, $\partial n/\partial c$, and P(LSMA) for the PAA-PAM series

From the P values as determined with the LSMA method, it was possible to calculate micellar radii as a function of the volume fraction of polymers in the core, using Equations 2.4 - 2.7. When doing so, the micellar radii were overall 30 percent lower than shown in Figure 5c, even with very low values for ϕ. We attribute this to the 'fuzziness' of the I vs f_{PAMA} curves in Figure 2.3a, where especially the CEAC and the corresponding I values, cannot be determined unambiguously.

In Figure 2.5, P and N_{corona} are plotted on logarithmic scales, as determined from the experimental data with Equation 1.10 and the LSMA method. These experimental data are compared with the scaling laws for the crew-cut limit from Equation 1.9, and the -0.51 scaling exponent, that was derived by Nagarajan and Ganesh for a diblock-copolymer micelle where the corona block is in a good solvent[14]. The scaling exponents for the experimental data were -0.96 for the data determined with Equation 1.10 and -1.28 for the LSMA method. The theoretical scaling exponent for the crew-cut micelles determined by Borisov and Zhulina is -18/11 (= -1.64). The sensitivity of P to variations in N_{corona} for both experimental data sets turns out to be less than the theoretical case for the crew-cut micelles and more than the scaling exponent from the Nagarajan and Ganesh model. There may be several reasons for this discrepancy. Firstly, the theoretical scaling exponents are valid for A-B diblock-copolymers with high selectivity towards water, with e.g. a polystyrene core block, such as PS-PAM or PS-PEO diblock-copolymers. With our system, the selectivity is less since the diblock-copolymer as well as the homopolymer are hydrophilic. The differences in chemical composition are not as

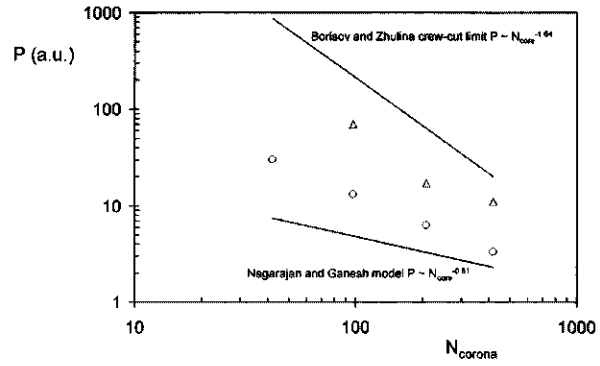

FIGURE 2.5. Aggregation numbers vs corona block length. The data points were determined with the LSMA method (△) and Equation 2.10 (○). The data points that were determined with Equation 2.10 are not on an absolute scale, and only be interpreted as the relative dependence of P on N_{corona}. The solid lines are the scaling laws by Borisov and Zhulina (Equation 1.7) and Nagarajan and Ganesh[14].

extreme in their affinity towards water (see Figure 2.2) compared to the hydrophobically associating systems. This may affect the energy balance and aggregation mechanism and thus the scaling exponent. Secondly, the Nagarajan and Ganesh model is valid for a rather wide range of corona block lengths ($30 < N_{corona} < 700$), whereas the Borisov and Zhulina model represents a *limiting* case.

It is, however, surprising that one single scaling exponent is sufficient to describe the experimental scaling relationship between P and N_{corona}. One would expect the $PAA_{42}PAM_{42}$ micelles, with 42 core units and 42 corona units, to be in the crew-cut regime, whereas the $PAA_{42}PAM_{417}$ micelles, with 42 core units and 417 corona units, are expected to take on a more starlike morphology. In the starlike limit, P becomes virtually independent of N_{corona}, as was shown experimentally by the data of Willner et al.[13].

2.5.3. Variation of homopolymer molecular weight

The results of light scattering titrations of $PAMA_{35}PGMA_{105}$ with PMA 113 K and 600 K are shown in Figure 2.6. The pH data, light scattering intensity (I), and hydrodynamic radii are plotted in Figure 2.6 a, b and c respectively. All data are plotted as a function of f_{PMA}. The initial pH values of both the PMA 113 K and 600 K solutions and the $PAMA_{35}PGMA_{105}$ solutions were matched at pH = 6.8. In Figure 2.6c, the pH slightly deviates from the starting value, with a maximum pH-value around 7.1. If we compare the pH data for 113 K and 600 K, we see that they are quite similar. Apparently, both 113 K and 600 K PMA consume the same amount protons from the bulk solution upon complexation.

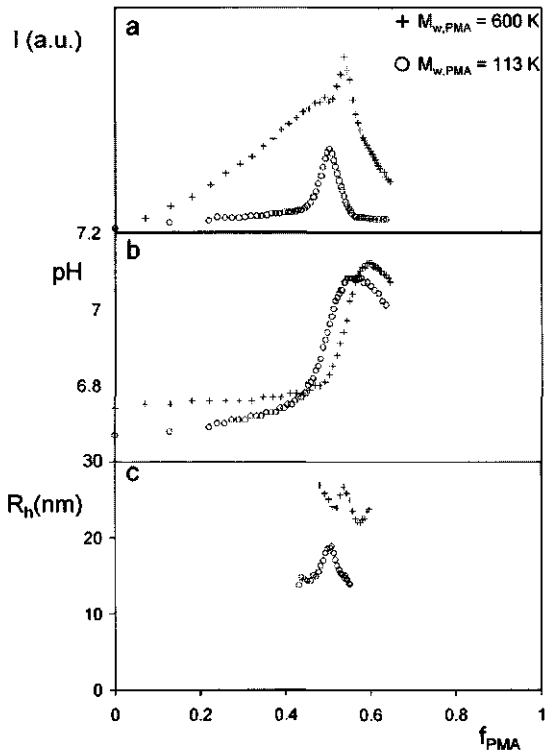

FIGURE 2.6. Mole fraction titrations of $PAMA_{35}PGMA_{105}$ with two molecular weights of PMA (113 K and 600 K, corresponding to chain lengths 1300 and 6900 respectively). a: light scattering intensity. b: pH data. c: Micellar radii. Experimental conditions: concentration of PAMA monomeric units was 1.7 mM/liter. Ionic strength was 100 mM NaCl.

We explain this pH increase from charge density adjustments of the polyelectrolytes. Due to the polymeric nature of PMA and PAMA, their charge densities in bulk solution are determined by the screening of the charged groups. In the complex coacervate, the screening differs from the screening in bulk solution. Since a pH increase is seen, we conclude that PAMA is increasing its charge density to a somewhat larger extent than PMA.

At the PMC, the concentration of buffering groups will be at a minimum, so that a maximum in $|\partial pH/\partial f_{PMA}|$ is expected to correspond with the PMC. Both the 113 K and 600 K pH curves exhibit a maximum in $|\partial pH/\partial f_{PMA}|$ at $f_{PMA} \approx 0.5$. From the pH data we conclude that the PMC is at $f_{PMA} \approx 0.5$ for both 113 and 600 K PMA.

For the light scattering intensity data, we expect a maximum at the PMC. This is confirmed by Figure 2.6a. At the PMC, there is no excess polyelectrolyte charge, so that the PMA chains and PAMA blocks can form neutral complex coacervate nanophases, that are restricted in their growth by the PGMA blocks. If we now look at the I data, we see a maximum at $f_{PMA} \approx 0.5$ for both curves. This point coincides with the PMC that was determined from the pH data. Apparently, the PAMA and PMA groups form a complex with approximate composition 1:1 at pH $\approx$ 7. Note that these I curves resemble those of Figure 2.1 rather better than the data in Figure 2.3a.

The similarity in the pH curves at different M_{PMA} suggests that the interaction between PAMA and PMA is the same on a quantitative basis. In the I and R_h curves, however, pronounced differences are seen. With the 113 K experiment, the I curves resemble Figure 2.1 to a large extent, whereas with the 600 K experiment, a CEAC is hardly seen, and the experiment shows a more or less constant $|\partial I/\partial f_{PMA}|$ until the PMC is reached. We attribute these differences to a different aggregation mechanism, that is sensitive to the molecular weight of the homopolymers.

The hydrodynamic radii that are seen in Figure 2.6c for the 113 K PMA experiment are around 18 nm, whereas the hydrodynamic radii for the 600 K PMA experiment are around 25 nm. The reason for the difference in R_h will de discussed later. Apart from these differences, R_h goes through a maximum for both experiments. Yet, the variations are small but systematic. In our point of view, these variations proof the hypothesis that the micelles also carry some of the excess charge that is present around the PMC. The micellar aggregation number, and possibly core density, are thus not constant between the CEAC and the CECC. The double minimum that is seen with the 600 K experiment can be explained as follows. Above, we reasoned that P may not be constant around the PMC, as just outside the PMC, the micelles may also carry some of the excess charge that is present in the polymer mixture. Therefore, P is expected to decrease somewhat when the composition of the system is moved away from the PMC. This causes the maximum in R_h at the PMC. When the system is moved away from the PMC even further, the particles will become less well-defined and more polydisperse, leading to an overestimation of R_h, so that the apparent particle radius again increases (see also methods section).

For the experiments shown in Figure 2.6 (diblock-co-polymer in titration cell), with the homopolymers as the minor component below the PMC, we assumed that the SCP^+ that are formed below the PMC, contain one homopolymer per object, and their composition can then be calculated from Equation 1.2. The molar mass of the SCP^+ is proportional to the molecular weight of the homopolymers, i.e. $M_{SCP} \propto M_{PMA}$. The weight normalized scattered intensity at the CECC is thus a measure for M_{SCP}, as $I \propto CM$. In Figure 2.7, I_{CECC}/C is plotted vs N_{PMA}. The data points are rather well described by a straight line, confirming that $M_{SCP} \propto M_{PMA}$.

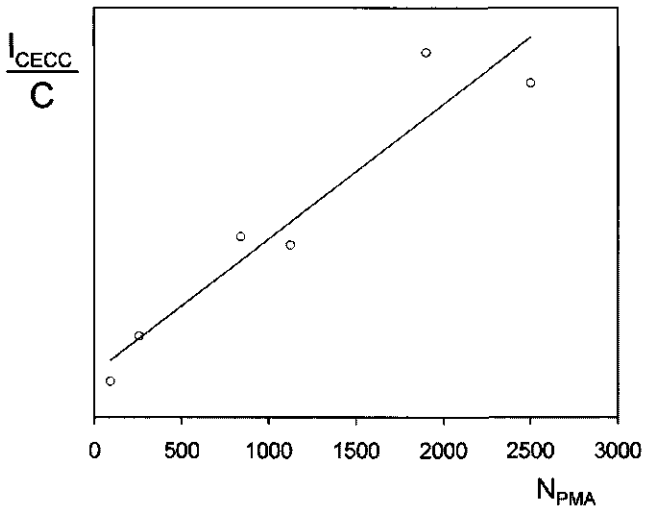

FIGURE 2.7. Master curve of all I_{CEAC}/C values vs N_{PMA}. The vertical axis is on an arbitrary scale. The solid line is a linear fit through the data points.

In Figure 2.8, we present data from light scattering titrations for two different PVP samples (M_w = 30 K and 309 K) with $PAA_{14}PAM_{69}$ in 50 mM Na_2HPO_4/NaH_2PO_4 buffer. Data are plotted as a function of f_{PAA}. In contrast to the experiments of Figure 2.3, we started out with the homopolymer in the titration cell and the di-block-co-polymer was added in small doses. In the $PAA_{14}PAM_{69}$/PVP system, the charged groups on the PVP are of a quenched nature, i.e. they are not pH sensitive. So, only PAA can adjust its charge density upon complexation. However, as the solution was buffered there was no effect on bulk pH, so that in contrast to Figure 2.3c, it was not possible to determine a PMC from the pH curves.

If we now consider the intensity curves in Figure 2.8a, we see again that the I values are higher with the longer homopolymer chains, similar to the data presented in Figure 2.6b. In analogy to Figure 2.6a, the curves show a pronounced maximum around the symmetric composition of the system ($f \sim 0.5$).

The shape of the I curves is somewhat different from Figure 2.6b. The difference between I_{PMC} and I_{CECC} is less on an absolute scale, which is also seen by the noise, which is a bit more prominent. We attribute this lower I to the smaller radii of the system PVP/$PAA_{14}PAM_{69}$. The radii of both 30 K and 309 K are plotted in Figure 10b and are in the order of 12 - 14 nm, whereas in Figure 8a the radii are in the order of 18 - 25 nm. The lower intensities can be attributed to this difference in size, since $I \propto R^6$. Small differences in $\partial n/\partial c$ between the two systems may also play a role.

With respect to chain length difference, the I curves exhibit a behaviour similar to

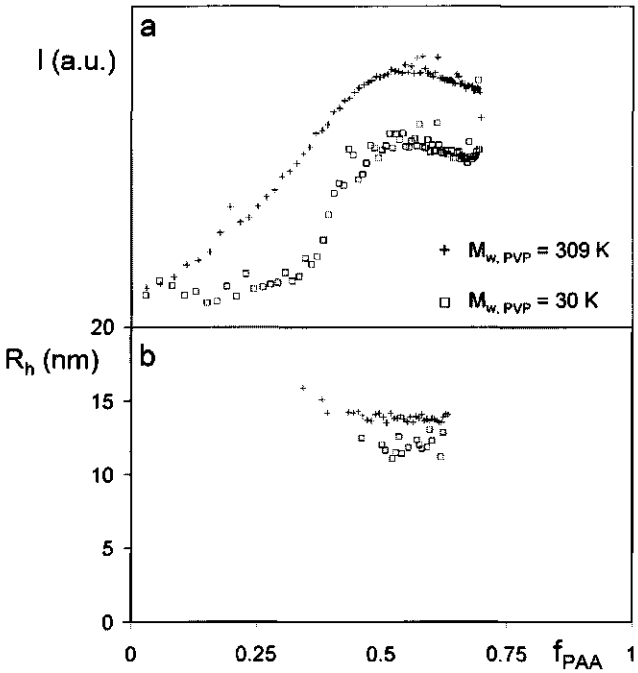

FIGURE 2.8. Mole fraction titrations of two different molecular weight PVP solutions (indicated in the figure) with $PAA_{14}PAM_{69}$ solution. a: light scattering intensity. b: micellar radii. Experimental conditions: concentration of PVP monomeric units was 2 mM/litre. Ionic strength was 50 mM Na_2HPO_4/NaH_2PO_4 buffer set at pH 7. In contrast to the experiment shown in Figure 8, the homopolymer was in the titration cell. Diblock-co-polymer solution was titrated to vary f_{PAA}.

Figure 2.6a. The non-stoichiometric objects that are formed with the short PVP chains have a low M_w and contribute little to I. Only around the PMC, when these small objects aggregate into micelles, the intensity increases significantly. The 309 K experiment shows a steady $\partial I/\partial f$, suggesting a M_w value of the SCP that is not too different from the stoichiometric micelles. Apparently, also in the 309 K experiment, single homopolymer chain micelles were formed in analogy to the 600 K PMA experiment. Also with this system, we see a difference in R_h between the two PVP chain lengths, the micelles with longer PVP being larger (15 vs 12 nm).

Also for the $PVP/PAA_{14}PAM_{69}$ system experiments were performed with a wide range of M_w for the homopolymers. The M_w values of the total series were 29, 130, 301, and 690 K for PVP. In Figure 2.8, we also see a difference in $\partial I/\partial f$ for different values of M_{PVP}. With these data, an interpretation of the $\partial I/\partial f$values is not possible, as the diblock-co-polymer is the minor component at low f, and not the homopolymer.

Due to the reversal of the major and minor components, no simple scaling relationship between M_{SCP} and M_{PVP} can be derived.

In Figure 2.9, R_h at the PMC is plotted semilogarithmically versus the chain length

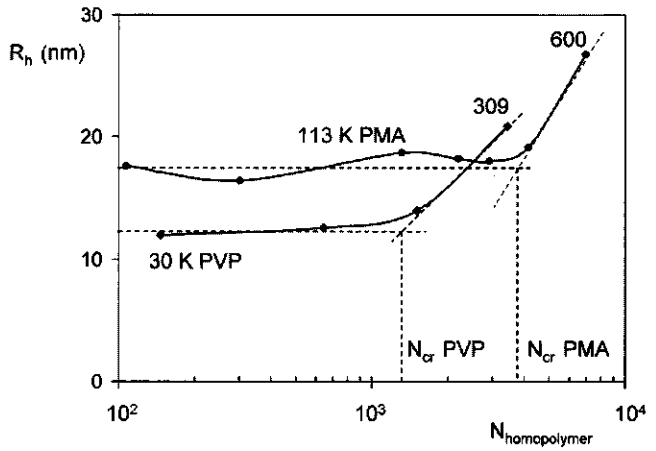

FIGURE 2.9. Hydrodynamic micellar radii obtained by varying homopolymer molecular weights. $PAA_{14}PAM_{69}$/PVP system (♦); $PAMA_{35}PGMA_{105}$/PMA system (•). The values for N_{cr} were determined by taking the intersection point between the linear line sections (constant values with $N_{homopolymer} < N_{cr}$ and the increase with $N_{homopolymer} > N_{cr}$ as indicated in the figure (indicated by the dotted lines)).

of the homopolymers for both systems. A more or less constant size is observed up to a given chain length N_{cr} with both systems. For the $PAA_{14}PAM_{69}$/PVP system, N_{cr} ≈1300 monomers (260 K). For the $PAMA_{35}PGMA_{105}PMA$ system, $N_{cr} \approx 4000$ monomers (300 K). The micellar radii are 12.8 and 18.0 nm respectively. Beyond N_{cr}, the micellar size increases. We explain the change in micellar size as follows: up to N_{cr}, there is a constant amount of PVP or PMA monomers in the core, independent of $N_{homopolymer}$. This amount is determined by the density and volume of the core which is, in turn, regulated by the balance between osmotic pressure of the corona and interfacial tension of the core-solvent interface. It can be distributed over many short chains, fewer long chains or one very long chain with degree of polymerisation N_{cr}. However, if the homopolymer chain length is increased further, the core can no longer accommodate the entire chain; its volume must increase so that the micellar radius changes. This change in radius may imply a morphological change. The diffusion coefficient of the micelles is converted into a radius using a spherical model (Stokes-Einstein). Since the shape of the objects is unknown, one should be careful to think of the measured radii of the larger objects as 'real' sizes. Although it is not possible with our experimental technique to determine the nature of this morphology, one may think of a spherical

morphology with core blocks that are strongly stretched or a cylindrical form.
If the spherical micelles with homopolymer chain length N_{cr} do indeed contain one single homopolymer chain, both the aggregation number (P) and molecular weight M_w of the micelles can be calculated. From the PMC, the core composition is known if we assume that it is equal to the macroscopic loading ratio of the chargeable groups. The aggregation number now follows from f at the PMC, the homopolymer chain length (N_{hp}) and the block length of the core block (N_{core}):

$$P = \frac{f_{PMC}}{1 - f_{PMC}} \frac{N_{hp}}{N_{core}} \tag{2.11}$$

The molar mass of the micelles follows from P and the molar masses of the homopolymer (M_{hp}) and the diblock-co-polymer (M_{db}):

$$M_{micelle} = M_{hp} + M_{db}P \tag{2.12}$$

In Table 2.6 P, M_w and R_h of the micelles with homopolymer chain length N_{cr} are given together with the values that were determined using the LSMA method. The molecular weights and the values of P are in the same range as reported by Harada and Kataoka[5,6]. The specific molar volumes of the core components that were used in Equation 2.4 were found in literature[21, 22].

System	N_{cr}	P(LSMA)	M_w(LSMA)	P(CHP)	M_w(CHP)	$R_{h,exp}$ (nm)
$PAMA_{35}PGMA_{105}$	4000	171	$4.4*10^6$	114	$2.6*10^6$	18.0
$PAA_{14}PAM_{69}$	1300	107	$9.8*10^5$	92	$7.3*10^5$	12.6

TABLE 2.6. Values for N_{cr}, P, M_w, and R_h for both systems, determined by the LSMA method and the critical homopolymer chain length (CHP). The LSMA values were averaged over 7 experiments with the $PAMA_{35}PGMA_{105}$/PMA series and standard deviation was around 10 percent.

In Figure 2.10, we use these estimates to plot the total radius of the micelles $R_{total} = R_{core} + H$ and R_{core} versus ϕ. In the calculations, we used a segment length for the grafted chains of 0.3 nm. For υ, we used 1 which corresponds to good-solvent conditions (athermal limit). The calculated micellar radii are not very sensitive to ϕ, because the core radius and corona radius have an opposite contribution to the overall radius. At low ϕ, there is a large core with a thin corona; at high ϕ, there is a small core with a thick corona. Harada and Kataoka[5] also calculated core radii from their experimental data. They arrived at approximately 7 nm, which is in the same order as our date in Figure 2.10, where we arrive at 7 nm core radius for the $PAA_{14}PAM_{69}$/PVP sample and 10 nm for the $PAMA_{35}PGMA_{105}$/PMA sample. We compare these values with a rough estimate of the contour length of the core blocks, which is given by N_{core} times the segment length, and thus gives 5.6 nm for the PAA block and 14 nm for the PAMA block. Apparently, the core blocks are in a rather stretched conformation, as the core

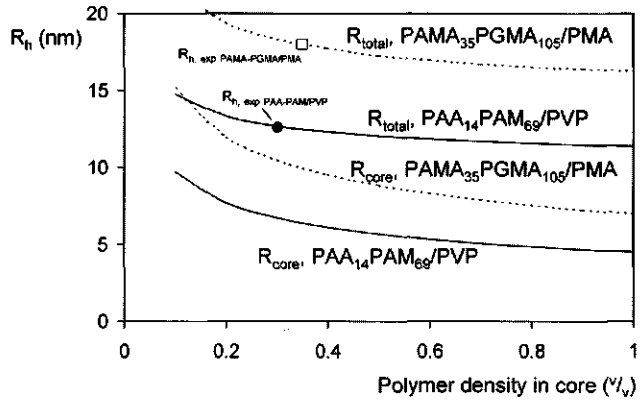

FIGURE 2.10. Theoretical radii of $PAA_{14}PAM_{69}$/PVP (dashed lines) and $PAMA_{35}PGMA_{105}$/PMA (solid lines) with critical hompolymer molecular weight. The upper lines represent the overall radius of the micelles, the bottom lines represent the core radii. The data are presented vs polymer volume fraction in the core. Calculations parameters were $l = 0.4$ and $\upsilon = 1$. The experimental values are indicated in the figure by (•) for the $PAA_{14}PAM_{69}$/PVP (18.0 nm) system and (□) for the $PAMA_{35}PGMA_{105}$/PMA system (12.6 nm).

radii are the same order of magnitude as the contour lengths of the core blocks. For both systems, the calculated values agree well with the experimental values in the whole range of ϕ. From the calculated values, we arrive at $\phi \approx 0.3$ for both systems. We

System	R_h (exp)	$R_h(\phi = 0.3)$(nm)	$\phi(R_h(\text{exp}))$
$PAMA_{35}PGMA_{105}$/PMA	18.0	20.7	1
$PAA_{14}PAM_{69}$/PVP	12.6	13.9	0.9

TABLE 2.7. Micellar radii calculated for the P values that were found with the LSMA method. The values in the third column were calculated with the ϕ value that was found from Figure 2.10. The ϕ values in the most right-hand side column were obtained by satisfying $R_{core} + H_{corona} = R_h(\text{exp})$ in a fit procedure.

calculated micellar radii for the P values that were found with the LSMA method using Equations 2.4 - 2.7. Results are given in Table 2.7. As the P values that were found with the LSMA method are higher than those found from the critical homopolymer chain length, somewhat higher ϕ values are needed to fit the theoretical micellar radius to the experimental data. Yet, variations in ϕ only slightly affect the calculated radii as was demonstrated in Figure 2.10. In Table 2.8, an overview of all experimental radii, deduced P values and molar masses is given.

diblock-copolymer	homopolymer	R_h (exp)	P (LSMA)	M_w (LSMA)	P (CHP)	M_w (CHP)
$PAMA_{35}PGMA_{105}$	PMA	18	171	$4.4*10^6$	114	$2.6*10^6$
$PAA_{42}PAM_{42}$	PAMA	22.9				
$PAA_{42}PAM_{97}$	PAMA	26.6	70	$1.2*10^5$		
$PAA_{42}PAM_{208}$	PAMA	27.3	17	$4.2*10^5$		
$PAA_{42}PAM_{417}$	PAMA	33.6	11	$4.3*10^5$		
$PAA_{14}PAM_{69}$	PVP	12.6	107	$9.8*10^5$	92	$7.3*10^5$

TABLE 2.8. Overview of hydrodynamic radii R_h, aggregation numbers P, and molar masses M_w of micellar systems studied in this chapter, as determined with the LSMA method and from the critical homopolymer chain length

2.6. Conclusions

We conclude that the block length ratio and the total length of the diblock-co-polymer as well as the molecular weight of the homopolymer determine the colloidal stability of a complex coacervation core system. A block length ratio $N_{corona}/N_{core} > 3$ is a minimum requirement to completely avoid precipitation. If this ratio is increased, the homopolymers start to play a major role in the aggregation process. With the 12:118 $PAMA_{12}PGMA_{118}$ sample, 12 K PAA is not able to form micelles, whereas 154 K PAA leads to stable micelles. With the 14 units core blocks in the PAA-PAM series, the annealed polyelectrolyte PAMA is not able to form micelles. Either no aggregation takes place, as is the case with $N_{corona} = 69$ and 139, with the very short corona block (14 units) aggregation does take place, but on a macroscopic level. However, the PAA-PAM samples with $N_{corona} = 69$ and 139 do form stable micelles with the quenched polyelectrolyte PVP. The chemical composition of the corona blocks, and thus, its solubility is very important. With the very hydrophilic PAM corona blocks, micelles could be formed with a 1:1 block length ratio. This ratio was not sufficient with the PAMA-PGMA samples, although the total block length of the latter sample was larger. From our light scattering titration experiments, we have shown that micelles exist in a small window with respect to the mixing ratio of the two components. Around pH 7, the charge density adjustments of the polyelectrolytes almost balance each other, so that the effect on bulk pH is minimal. The composition of the system at the PMC is symmetric, i.e. there is a 1:1 loading ratio of PAMA and PAA or PMA monomers in the system. We assume that, at the PMC, the composition of the micellar cores reflects the overall composition in the titration cell. The position of the PMC is not influenced by the architecture of the diblock-co-polymer. Outside the PMC, particles of low aggregation number are formed, since the excess polyelectrolyte charge hinders the formation of micelles. If the diblock-co-polymer is the major component outside the PMC, the molar mass of these particles is governed by the molecular weight of the

homopolymer. Typical micellar hydrodynamic radii were in the order of 12 - 30 nm radius. This micellar radius depends on the block lengths of the diblock-co-polymer and on the molecular weight of the homopolymer. We have shown that when the chain length of the homopolymer is increased beyond N_{cr}, larger objects are found. These objects may be cylindrical or 'stretched spheres'. The critical chain lengths for the homopolymers were 4000 for the PAMA-PGMA/PMA system and 1300 for the PAA-PAM/PVP system. From these chain lengths and the mixing ratios, values for P were calculated, these were in the order of several tens up to well over a hundred. A simple core-shell model that calculates the the core radius and the extension of the corona blocks agreed rather well with the experimental radii. Variations in N_{corona} with a constant N_{core} lead to lower values for P with increasing N_{corona}. The overall radius of the micelles, however, increases with N_{corona}. The qualitative relationship between P and N_{corona} is in agreement with scaling models for polymeric micelles with neutral corona blocks.

2.7. References

1. A. Harada and K. Kataoka, Macromolecules, 1995. 28: p. 5294-5299.
2. A.V. Kabanov, T. K. Bronich, V.A. Kabanov, K. Yu, and A. Eisenberg, Macromolecules, 1996. 29(21): p. 6797-6802.
3. K. Kataoka, H. Togawa, A. Harada, K. Yagusi, T. Matsumoto, and S. Katayose, Macromolecules, 1996. 29: p. 8556-8557.
4. M.A. Cohen Stuart, N.A.M. Besseling, and R.G. Fokkink, Langmuir, 1998. 14: p. 6946-6949.
5. A. Harada and K. Kataoka, Langmuir, 1999. 15: p. 4208-4212.
6. A. Harada and K. Kataoka, Macromolecules, 1998. 31: p. 288-294.
7. C. M. Wijmans and E.B. Zhulina, Macromolecules, 1993. 26: p. 7214-7224.
8. A. Harada and K. Kataoka, Science, 1999. 283: p. 65-67.
9. J.Th.G. Overbeek and M.J. Voorn, Journal of cellular and Comparative Physiology, 1957. 49: p. 7-26.
10. T. Odijk, Macromolecules, 1980. 13: p. 1542-1546.
11. O.V. Borisov and E.B. Zhulina, Macromolecules, 2002. 35: p. 4472-4480.
12. A. Halperin and S. Alexander, Macromolecules, 1989. 22: p. 2403-2412.
13. L. Willner, A. Poppe, J. Allgaier, M. Monkenbusch, P. Linder, and D. Richter, Europhysics Letters, 2000. 51: p. 628-634.
14. N. Hoogeveen, M.A. Cohen Stuart, and G. J. Fleer, Macromolecular Chemical Physics, 1996. 197: p. 2553-2564.
15. D. Taton, A. Z. Wilczewska, and M. Destarac, Macromolecular Rapid Communication, 2001. 22: p. 1497-1503.
16. R.S. Stock and W.H. Ray, 1985. 23: p. 1393-1447.

17. Submitted to Macromolecules, This Thesis, Chapter 3.
18. Submitted to Langmuir, This Thesis, Chapter 5.
19. E. P. K. Currie, A.B. Sieval, M. Avena, H. Zuilhof, E.J.R. Sudhölter, and M.A. Cohen Stuart, Langmuir, 1999. 15: p. 7116-7118.
20. N. G. Hoogeveen, M.A. Cohen Stuart, and G. J. Fleer, Journal of Colloid and Interface Science, 1996. 182: p. 146-157.
21. J. Brandrup and E.H Immergut, Polymer Handbook. 3rd. ed, ed. J. Brandrup and E.H. Immergut. 1989: John Wiley and Sons, Chichester.
22. W. Groenewegen, S.U. Egelhaaf, A. Lapp, and J.R.C. van der Maarel, Macromolecules, 2000. 33: p. 3283-3293.

CHAPTER 3

Charge Neutralization and Protonation Equilibria

ABSTRACT

The formation of complex coacervation core micelles from PAMA-PGMA (poly(dimethylamino-ethylmethacrylate-copoly(glycerylmethacrylate)) and PAA (poly(acrylic acid)) has been studied using potentiometric titrations and dynamic light scattering. Mixing ratio, pH and ionic strength have been explored in a wide range of the experimental parameter window. Upon varying the pH of aqueous PAMA-PGMA/PAA mixtures of different composition, particles were detected between pH = 4 and pH = 9. The width of this micellar window was wide if the molar ratio between PAMA and PAA monomers was close to unity and smaller with low fractions of PAA. All mixtures exhibited a maximum light scattering intensity as a function of pH. However, if the ratio was close to unity, a macroscopic phase separation occurred around the maximum light scattering intensity. With the other samples, colloidal particles were formed that were around 20 nm radius. By varying the ratio of the components around pH = 6.7, the polymeric mixture spontaneously formed micelles when the PAA groups made up roughly half of the total concentration of ionic groups. Upon overdosing the PAA, the micelles disintegrated. The hydrodynamic radius of the micelles varied between 15 and 20 nm. An evaluation of the charge balance in the titrations showed that not only protons but also sodium ions are present in the complex. With increasing ionic strength, more sodium ions reside in the complex. In addition, the position of the preferred micellar composition was a function of the ionic strength.

Submitted to Macromolecules, 2004

3.1. Introduction

The role of ionic strength on complex coacervation[1] and complex coacervate multilayers[2] is generally recognized. One common conclusion is that increase of ionic strength will suppress the formation of multilayers[3] or a complex coacervate phase[4]. More subtle effects of ionic strength variations were reported by Kovacevic et al.[3,5] and Dautzenberg[6]. Both reports describe a so-called 'glass-transition' in the polyelectrolyte multilayer[3,5] or complex coacervate particle[6].

The effect of ionic strength on complex coacervate core micelles (CCCM) has not yet been addressed systematically as only the disintegration of micelles above a certain critical ionic strength (0.15 - 0.5 M) was reported by Kabanov et al.[7], Cohen Stuart et al.[8], and Harada and Kataoka[9], similar to the suppression of multilayering or complex coacervation.

In this Chapter, we analyze the charge neutralization of CCCM's where the core consists of annealed polyelectrolytes. The CCCM's were prepared from an anionic homopolymer, poly(acrylic acid) (PAA) and an oppositely charged diblock-copolymer, poly(dimethylamino-ethylmethacrylate)-copoly(glycerylmethacrylate) (PAMA-PGMA). We have either varied the pH at constant polyelectrolyte mixing ratio, or varied the mixing ratio at constant starting pH and varying ionic strength or polymer concentration. The experiments at equal starting pH were performed at 5, 10, 50, and 100 mM $NaNO_3$ and varying overall polymer concentration.

The dissociation behavior, and thus the charge density, of weak polyelectrolytes is described by Equation 1.4. If the environment of a weak polyelectrolyte is changed, such that the electrostatic screening is altered, the pK and α will adjust to this new environment. The transfer of a polyelectrolyte chain from bulk solution to a coacervate phase may be considered as a significant change in screening conditions. Upon such a transfer, the equilibrium in proton distribution between polyelectrolytes and bulk solution will shift and, as a result, the bulk pH changes.

In the mole fraction titrations, a wide range of composition (f_{PAA}) (f_{PAA} is defined by Equation 1.5) has been covered, starting with pure PAMA-PGMA ($f_{PAA} = 0$) to a surplus of PAA ($f_{PAA} = 0.8$). We expect to find a composition somewhere between $f_{PAA} = 0$ and $f_{PAA} = 1$ where (almost) all polymer goes into micelles, the so-called preferred micellar composition (PMC). If the charge neutralization is exclusively a matching of the charges on the polyelectrolyte chains, the following condition should be satisfied at the PMC:

$$f_{PAA}\alpha_A = (1 - f_{PAA})\alpha_B \tag{3.1}$$

where α_A and α_B are the charge densities of polyacid and polybase respectively in the core of the CCCM. A first guess is that micelles will form when the total number of dissociated cationic groups equals the number of dissociated anionic groups, i.e. when

$f_{PAA} = 0.5$.

Alternatively, we have performed proton titrations of the polyelectrolyte mixtures where the OH^- consumption was monitored from p$H = 4$ to p$H = 9$. From the data obtained in such an experiment, the degree of protonation of PAA/PAMA mixtures can be calculated as a function of pH. However, one cannot distinguish between deprotonation of an associated PAA or protonated PAMA group. Therefore, we present the data from these experiments in terms of the overall degree of protonation of the mixtures (Ω_{mix}), which is defined as

$$\Omega_{mix} = f_{PAA}(1 - \alpha_A) + (1 - f_{PAA})\alpha_B \tag{3.2}$$

where α_i is the charge density of the polyelectrolyte groups in the complex. By substituting Equation 3.1 into Equation 3.2, we simply find that $\Omega_{mix} = f_{PAA}$ will give a neutral complex if the charge neutralization is based on polyelectrolyte charge-matching only. See Figure 3.1 for a sketch. In this Chapter the charge neutralization process of the micellar core at various salt concentrations was studied. If, at the PMC, $\Omega_{mix} \neq f_{PAA}$, we must conclude that besides polyelectrolyte groups, small ions also reside in the complex. This is not unlikely, because the formation and behavior of polyelectrolyte multilayers of PAA and PAMA appears to be very sensitive to the type of small ions that is used as a background electrolyte[5], suggesting specific interactions between the polyelectrolytes and small ions.

3.2. Materials and methods

3.2.1. Chemicals and equipment

The chemical structure and composition of the PAMA-PGMA diblock-copolymer and PAA homopolymer were given in Figure 2.2 and Table 2.2. Block lengths were 35 and 105 for the PAMA and PGMA in the diblock-copolymer respectively. Chain length of the PAMA homopolymer was 126. The PAA homopolymer was obtained from Polymer Source Inc., Canada and was used as received ($M_w = 60$ K). The polydispersities of all polymers were low, typically around 1.05 - 1.1. All other chemicals, such as e.g. distilled water and $NaNO_3$ were of analytical grade. The light scattering titration setup was described in Chapter 2.

3.2.2. Calculation of protonation curves

During the titrations, the ionic strength (S) was calculated as

$$S = \frac{2V_e c_e + |V_a c_a - V_{ti} c_{ti}| + V_{ti} c_{ti} + V_a c_a}{2V_{total}} \tag{3.3}$$

where the volume and concentration are denoted by V and c and the subscripts e, a, and ti denote salt, acid, and titrant respectively and V_{total} is the total volume in the

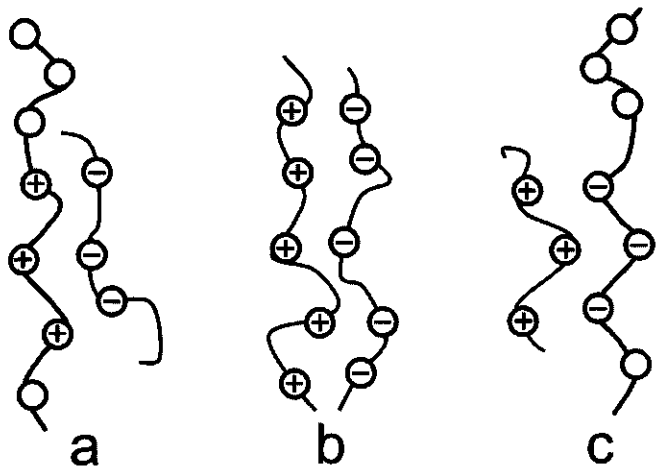

FIGURE 3.1. In this figure we demonstrate that $\Omega_{mix} = f_{PAA,PMC}$ has to be satisfied in order to have a charge neutral complex. Empty circles in the polybase chain denote non-protonated monomers, whereas the empty circles in the polyacid chain denote protonated monomers. The degree of protonation of a polyacid/polybase mixture, Ω_{mix}, is defined in Equation 3.2. Electroneutrality can be obtained by satisfying $\Omega_{mix} = f_{PAA}$. This condition is valid for the entire f_{PAA} range, as shown in a ($f_{PAA} < 0.5$), b ($f_{PAA} = 0.5$) and c ($f_{PAA} > 0.5$).

cell. In their contribution to the ionic strength, polyelectrolyte species were treated as monomers. From the ionic strength we calculated f_d (the ionic activity coefficient) using the Davies equation:

$$-log(f_d) = 0.51\left(\frac{\sqrt{S}}{1+\sqrt{S}} - 0.3S\right) \tag{3.4}$$

Finally, the proton and hydroxide concentrations at any given point during the titration can be calculated from the activity, using:

$$\begin{aligned} \left[H^+\right]_i &= 10^{[-pH_i - log(f_d)_i]} \\ \left[OH^-\right]_i &= 10^{[pH_i - pK_w - log(f_d)_i]} \end{aligned} \tag{3.5}$$

The consumption of hydroxide ions by the sample can be calculated by subtracting a theoretical blank from $V_{ti}c_{ti}$. This theoretical blank represents the amount of OH^- that would be needed to obtain the same pH increase as for a solution containing only water and small ions. The theoretical blank is calculated by

$$B_{blank} = \left(\left[H^+\right]_i - \left[OH^-\right]_i\right)V_i - \left(\left[H^+\right]_0 - \left[OH^-\right]_0\right)V_0 \tag{3.6}$$

The consumption of hydroxide ions per mole of substrate is now given by

$$M_{OH,i} = \frac{(V_{ti}c_{ti} - B_{blank})}{V_i [N]_i} \tag{3.7}$$

where $[N]_i$ is the molar concentration of ionizable units in the solution. From M_{OH}, charge densities can be calculated by taking the $\alpha = 0$ or $\alpha = 1$ limit, and relating the hydroxide consumption to the number of titratable groups in the system. We also applied Equations 3.3 - 3.7 on mixtures of PAA and PAMA-PGMA, where is not possible to interpret the hydroxide consumption in terms of a charge density, as we cannot distinguish between (de)protonation of PAA or PAMA. We therefore use the overall degree of protonation, Ω_{exp}, as was defined in Equation 3.2.

3.3. Results and discussion

3.3.1. Protonation of PAA and PAMA in bulk solution at various ionic strengths

In Figure 3.2, the charge densities of PAA and PAMA in 5, 10, 50, and 100 mM $NaNO_3$ are presented as a function of pH. The screening effect of salt shows up as the higher charge densities at a given pH at higher salt concentrations. This clearly represents a polyelectrolyte character. This polyelectrolyte character is also seen in the 'stretching' of the curves over more pH units with decreasing ionic strength. With both polyelectrolytes, an increase of the ionic strength decreases the stretching of the curves. The curves differ in steepness, *i.e.* $\partial\alpha/\partial pH$ has different values for PAA and PAMA. We attribute this to the difference in chemical structure of the polyelectrolytes. For PAA the charged group is very close to the backbone, whereas with PAMA, the charged groups are located at the end of a long side group (see Figure 2.2). Hence, the distances between charges are smaller for PAA than for PAMA and there is much more nearest neighbor interaction for PAA, leading to more stretched out α-curves[11]. In Figure 3.3, we show $pK_i + \Delta\ pK(\alpha_i)$ vs α for PAMA and PAA. In this Figure, we see that $\partial\ pK/\partial\alpha$ is rather sensitive to the ionic strength for PAMA. Moreover, $\Delta pK(\alpha_B) \approx 0$ for the 100 mM $NaNO_3$ experiment for the entire α-range. The PAA chains show pronounced intra chain repulsion for all $NaNO_3$ concentrations. In addition, it appears that $pK^0_{A,B}$ is a function of the ionic strength, as the intercepts on the vertical axis shift upwards with increasing ionic strength. This effect was also found by Borkovec et al.[10], who explained this in the framework of the Debye Hückel theory. Note that Figure 3.3 resembles the sketches in Figure 1.3c and 1.3d to a large extent.

In Table 3.1 we give the values for pK^0 of both polyelectrolytes at 5, 10, 50 and 100 mM $NaNO_3$. These pK^0 values were determined with Equation 1.4, by linear extrapolation of the linear part of the curves to $\alpha = 0$. The values of PAA are in the same order as with literature data, *e.g.* a value of 4.75 was found by Martell and Smith[11]. Also the

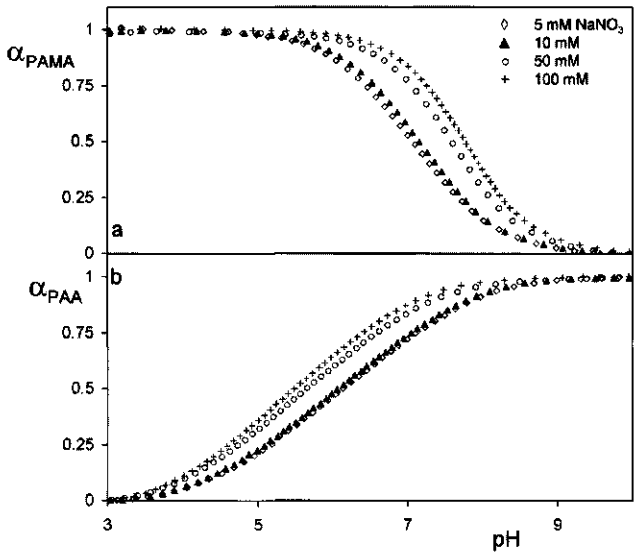

FIGURE 3.2. Charge density of PAMA (a) and PAA (b) vs. pH for various [$NaNO_3$] as determined by proton titrations. Polymer concentrations were around 20 mM, expressed as ionizable units. The data were calculated from the raw potentiometric data using Equations 3.3 - 3.7.

values of pK_B^0 agree with literature, as a value of p$K_A^0 = 7.3$ (i.e. pK_B = pK_w - pK_A = 6.7) was found for PAMA by An and Thomas[12], which is in line with the data from Hoogeveen et al. [13], who found a pK_A value of 7 - 7.5.

[$NaNO_3$] (mM)	pK^0 PAA	pK^0 PAMA
5	5.14	6.63
10	5.08	6.59
50	4.79	6.30
100	4.70	6.17

TABLE 3.1. pK_0 values for PAA and PAMA determined from Figure 3.3 and Equation 1.4

3.3.2. Micellar stability upon pH variations

In Figure 3.4 results are shown from light scattering titrations at various fixed f_{PAA} and initial pH = 2.6 in 50 mM $NaNO_3$. The pH was increased by titrating the solutions with 0.1 M NaOH solution. In Figure 3.4a, the light scattering intensity (I)

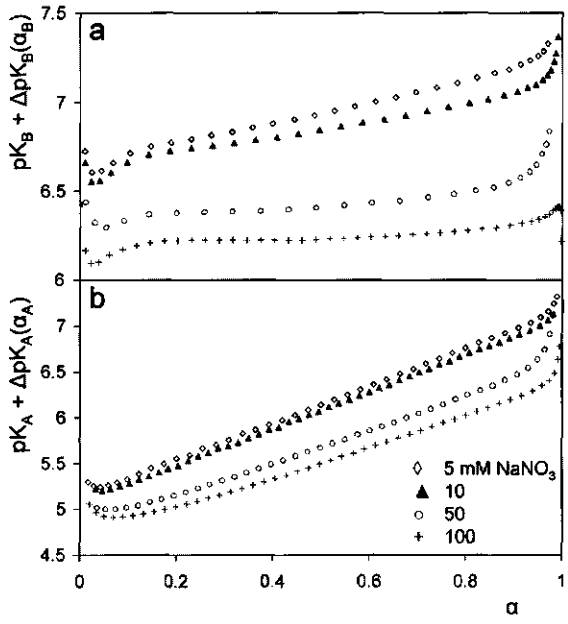

FIGURE 3.3. Dependence of $pK_i + \Delta pK(\alpha_i)$ on a for PAMA (a) and PAA (b) in 5, 10, 50 and 100 mM $NaNO_3$. Note that these data are the same as in Figure 3.2, but presented in a different fashion.

is plotted as a function of pH. We see that for all experiments, I has a maximum value I_{max} at pH_{max}. We assume that at pH_{max}, there is no excess polyelectrolyte charge and the state of the system is comparable to the PMC.

With increasing f_{PAA}, a shift of pH_{max} towards lower pH values as well as an increase of I_{max} is seen. At low pH, PAA is barely charged, whereas PAMA is highly charged, which requires a high value for f_{PAA} to satisfy Equation 3.1. The peaks for $f_{PAA} = 0.49$ and 0.62 are very high compared to the other experiments. This is due to flocculation (macroscopic phase separation) of the polymer mixtures. With the experiments at $f_{PAA} = 0.23$, 0.32, and 0.43, the solutions remained clear to the eye throughout the entire pH region. Most likely, with a longer (or more soluble) corona block, also the $f_{PAA} = 0.49$ and $f_{PAA} = 0.62$ mixtures the colloidal stability would improve.

In Figure 3.4b, the particle size R_h is plotted as a function of pH. For the $f_{PAA} = 0.23$ and 0.32 experiments, the micellar window is very small, 1 or 1.5 pH units, and is found around I_{max}. For $f_{PAA} = 0.49$ and 0.62, *no micelles* were detected around pH_{max}, but a macroscopic phase separation was seen. Apparently, at these compositions, the PGMA 'hairs' on the core surface are not able to stabilize the complex coacervate in the form of colloidal particles. At pH values below these phase separating regions,

particles are seen also for $f_{PAA} = 0.49$ and 0.62. Colloidal stability throughout the entire pH region was obtained at $f_{PAA} = 0.43$.

For all experiments, the micelles fall apart at p$H > 9.5$, as is seen from the low values for I, that are in the order of scattering expected for molecular solutions. Between pH = 8 and 8.5 the micellar radii coincide for all experiments at $R_h \approx 16$ nm, except for the $f_{PAA} = 0.23$ experiment, where $R_h = 19.8$ nm. In Table 3.2, we give an overview of the pH_{max} values as well as the radii at I_{max}.

For pH values below and above pH_{max}, the particles are somewhat larger than

f_{PAA}	pH_{max}	R_h at pH_{max}
0.23	8.75	19.8
0.32	8.68	19.52
0.43	8.57	16.4
0.49	7.59	flocculation
0.62	6.70	flocculation

TABLE 3.2. Values of pH_{max} and R_h in Figure 3.4

in the peak area (except for $f_{PAA} = 0.49$ and 0.62 where no micelles were formed around pH_{max}). It seems likely that, at low pH, the objects carry some excess cationic charge. The particles that are present at low pH ($f_{PAA} = 0.43$, 0.49 and 0.62) are thus probably loose and polydisperse, with low aggregation numbers, as this excess charge prevents aggregation into dense objects. As the excess cationic charge is decreased by deprotonation, the objects rearrange into micelles ($f_{PAA} =$ 0.23, 0.32, and 0.43), or even flocculate ($f_{PAA} = 0.49$ and 0.62), as seen in Figure 3.4. By increasing the pH beyond pH_{max}, the sign of the excess charge is changed from positive to negative, leading to an increase in radius due to swelling, while the scattering intensity decreases. Again, we have objects of low aggregation number that eventually disintegrate completely when the pH is increased beyond 9.5.

In Figure 3.5a, hydroxide consumption of the complexes (M_{OH}), expressed as mole OH- per mole polyelectrolyte groups is presented, for the experiments shown in Figure 3.4. The data were obtained by conventional acid-base titrations and processed using Equations 3.3 - 3.7. We attribute the upswings in that are seen in all curves at high pH in Figure 3.5a to CO_2 in the samples. With our specific experimental setup, CO_2 could not be avoided during the experiments, since 'bubbling' the samples with either N_2 or argon would greatly disturb the light scattering experiments and no gas-tight cap was available for the titration cell. In Figure 4a, we have seen that there is no more interaction between the species at p$H > 9.5$, given the low scattering in that pH region. In the protonation curves of the polyelectrolytes in Figure 3.2 we have seen that $\Omega = 0$ ($\Omega_{PAA} = 1 - \alpha_{PAA}$) for both polyelectrolytes in bulk solution at pH

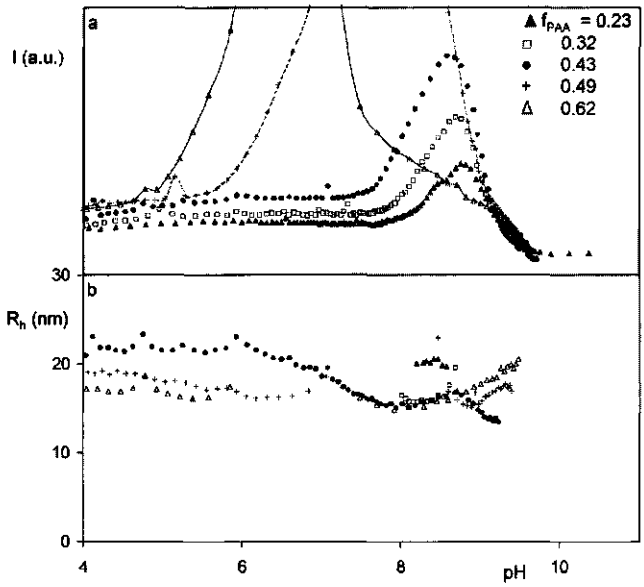

FIGURE 3.4. 90° laser light scattering intensity (a) and micellar radius (b) for various premixed samples of PAA and PAMA-PGMA in 50 mM $NaNO_3$. Total concentration of ionizable groups ([PAA] + [PAMA]) was around 20 mM for all experiments which is corresponds to approximately 10 g/l. The experiment was carried out by adjusting the solutions to p$H \approx 2.6$ and titrating them with 0.1 M NaOH solution. The very high peaks with $f_{PAA} = 0.49$ and 0.63 result from flocculation. In order to clearly see the other three curves, we decided not to show the entire peaks for $f_{PAA} = 0.49$ and 0.63. The other experiments were clear to the eye throughout the entire pH region.

values higher than 9. This means that, after the micelles have disintegrated around pH 9.5, we expect no further hydroxide consumption, as the free polyelectrolytes are fully deprotonated and we expect the M_{OH} curves to level off. However, large upswings due to CO_2 uptake overlap with the micellar disintegration process. We have made an attempt to extrapolate the M_{OH} data to plateau values as indicated in Figure 3.5a by the dotted lines.

From these hydroxide consumption data, the degrees of protonation of the micellar mixtures can be estimated by taking either the $\Omega = 1$ or $\Omega = 0$ limit, where Ω is given by Equation 3.2. At the high pH limit, the polymers are free in solution, as can be concluded from the very low scattering intensities in Figure 3.4a. In Figure 3.2, we see that both PAA and PAMA are fully deprotonated in bulk solution at p$H > 9.5$. From that we assume that $\Omega_{exp} = 0$ for all samples and pH values higher than 9.5. The degree of protonation of the mixtures thus follows from $\Omega_{exp,i} = M_{pH=9.5} - M_{OH,i}$. It is of particular interest to study the difference between the experimentally determined

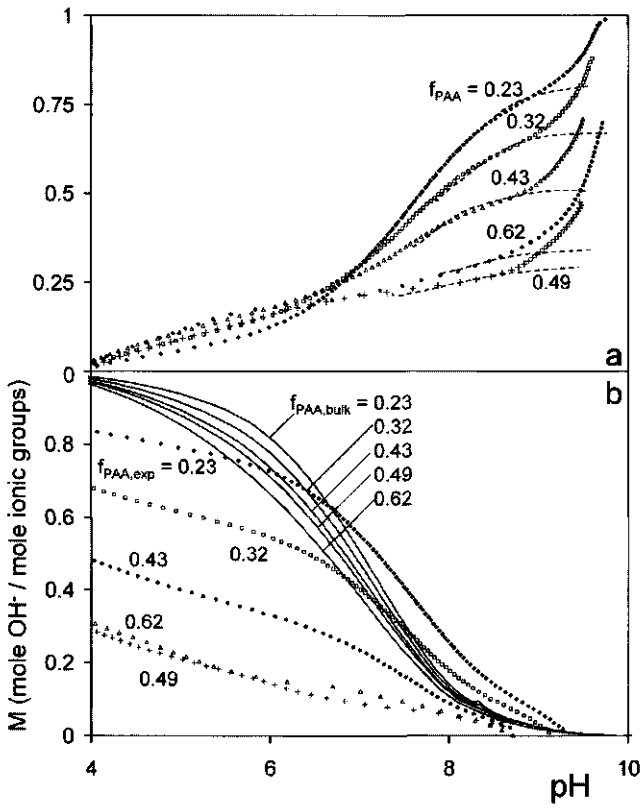

FIGURE 3.5. Hydroxide consumption and protonation data for the experiments shown in Figure 3.4. Hydroxide consumption of the PAA/PAMA-PGMA mixtures (a) and degree of protonation of the mixtures (b). The subscripts PAA,exp and $PAA,bulk$ denote the experimental and theoretical data, respectively. The curves in (a) were calculated using equations 3.3 - 3.7. The dotted lines in (a) indicate plateau values that we extrapolated to correct for CO_2 contamination as discussed in the text. The concentration of ionic groups in the solutions was around 20 mM. The solid curves in (b) were calculated with Equation 3.1. The position of the experimental data in (b) may not be exact as was discussed in the text.

degree of protonation of the micelles, Ω_{exp}, and the hypothetical Ω_{bulk}. The overall degree of protonation of a hypothetical, non-interacting PAA/PAMA mixture in bulk solution, Ω_{bulk}, is defined by Equation 3.2, where we take the bulk charge densities as shown in Figure 3.2. We will take this 'theoretical' Ω_{bulk} as a reference to the experimental Ω_{exp} values for the PAA/PAMA-PGMA mixtures that followed from the experiments. In Figure 3.5b, Ω_{exp} and Ω_{bulk} are plotted as a function of pH. Ω_{bulk} = 1 for both PAA and PAMA for pH < 4. The Ω_{bulk} values fully develop from 0 to 1,

whereas the Ω_{exp} values cover a smaller window of protonation within the experimental pH range.

In the Ω_{exp} values, at the lower pH limit, we see an increasing deviation from a fully protonated state with increasing f_{PAA}. This can be explained from interaction between the polyelectrolytes. Apparently, at low pH, the polyelectrolytes have already formed complexes. In their highly protonated bulk states at low pH, PAA is uncharged and PAMA is fully charged, so that in order to form a complex at low pH, protons have to be expelled into the bulk solution. Given the low light scattering intensities at low pH for all experiments, the complexation has not yet developed to its maximum extent. Above, we reasoned that $\Omega_{mix} = f_{PAA}$ has to be satisfied in order to have a neutral complex. We conclude from Figure 3.5b that at I_{max}, $\Omega_{exp} << f_{PAA}$, for most experiments. It is quite conceivable that not only protons, but also sodium ions play a role in the neutralization and screening of charges in the complex. The vast amounts of sodium ions that are suggested by the differences between Ω_{exp} and f_{PAA} at the I_{max} positions, however, must arise from the uncertainties in our M_{OH} data. Such amounts of sodium ions in the complex would not do justice to one of the main contributions to the driving force for complex coacervation, namely the release of small ions from the polyelectrolyte double layers.

Despite the problems with interpretation of the data at high pH and thus the absolute values of Ω_{exp}, a clear difference is seen in hydroxide consumption between the experiments with different f_{PAA}. We attribute these differences to internal titration between the two polyelectrolytes.

In Figure 3.6, we present an overview of pH_{max} as a function of f_{PAA}. Together with these experimental points, we show calculated values from the bulk protonation curves from Figure 3.2 and Equation 3.2, where $\alpha_{A,B}$ was taken as the charge density in bulk solution. From the 50 mM $NaNO_3$ data, we calculated the pH_{max} values for the hypothetical case that the charge densities of the polyelectrolytes are the same in the bulk and in the micellar cores, thereby assuming that pH_{max} represents the situation where Equation 3.1 is satisfied, *i.e.* no excess polyelectrolyte charge. We see from the experimental data that pH_{max} decreases with increasing f_{PAA}. This relationship can be attributed to the polybase/polyacid mixture that will shift its PMC to higher pH values with decreasing f_{PAA}.

The experimental pH_{max} values, however, do not overlap with the hypothetical PMC's. The reason for that can be found in the changes in both the pK values and the charge densities of the polyelectrolytes upon complexation. In bulk solution, the degree of dissocation of a polyacid or polybase is given by Equation 1.4. The $\Delta p\mathrm{K}_i(\alpha_i)$ in Equation 1.4 term arises from intrachain electrostatic repulsion, and is therefore a function of α_i. With increasing ionic strength, $\Delta p\mathrm{K}/\Delta\alpha$ will decrease, as the charges on the chains are screened much more effectively. These changes will also occur upon

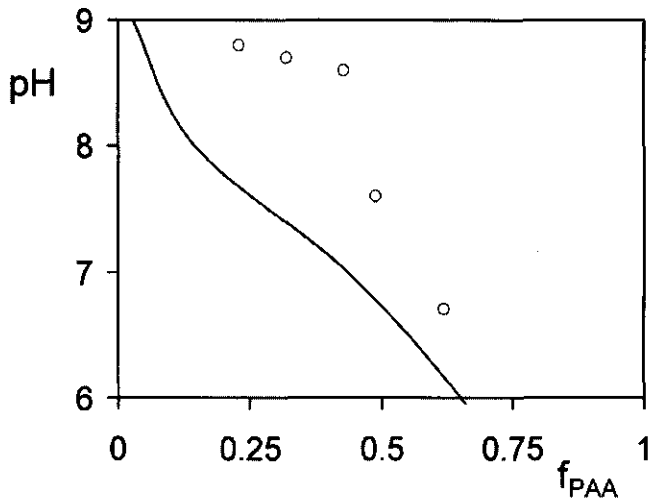

FIGURE 3.6. Experimental pH_{max} points, expressed as pH_{max} vs. f_{PAA}, obtained from Figure 3.4b (o).The solid curve on the left hand side is calculated from the protonation curves in Figure 3.2 and represents Equation 3.1 ($\alpha_{PAA} f_{PAA} = \alpha_{PAMA}(1 - f_{PAA})$).

transferring an annealed polyelectrolyte chain from bulk solution to a coacervate phase. The discrepance between theoretical and experimental PMC in Figure 3.6 are explained from changes in $\Delta pK_i(\alpha_i)$ and α_i that occur upon complexation.

For the $f_{PAA} = 0.43$ sample, we checked the reversibility of the micelles with respect to pH. After the experiment was performed as presented in Figure 3.4, the mixture was 'back-titrated' with 0.1 M HCl to p$H \approx 3$. The data are presented in Figure 3.7. The I values, presented in Figure 3.7a, are lower for the 'back titration'. Not only is the peak intensity lower, over the whole pH range also all other intensities are lower for the reversed titration. The hydrodynamic radii of the micelles are presented in Figure 3.7b. For the experiment that started from acidic conditions, the micellar window covers the entire pH range, whereas for a reversal of the titration the micellar window is much smaller. In addition, in the reverse experiment, the micelles are somewhat smaller (14 nm vs. 16 nm). Apparently, the system is not fully reversible with respect to pH, as the back titration yields slightly different values for both I and R_h. This may partially be caused by the increase of ionic strength due to the addition of NaOH and HCl solutions.

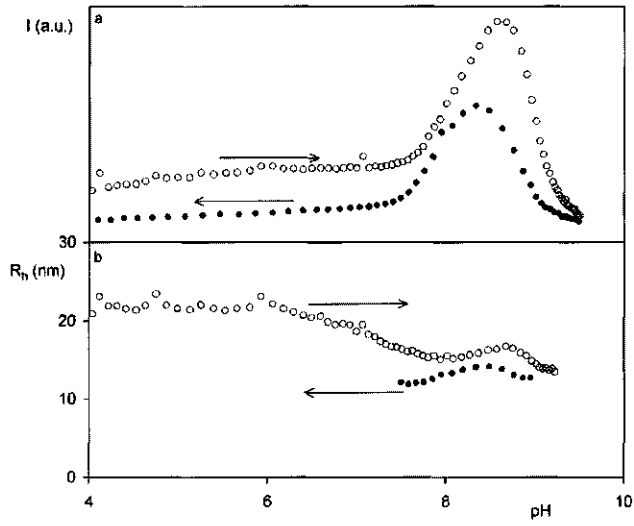

FIGURE 3.7. Reversibility of the micelles with respect to pH for $f_{PAA} = 0.43$. The open symbols are the same data as presented in Figure 3.4. The closed symbols were obtained by a back-titration with 0.1 M HCl solution, starting at pH = 9.5. The light scattering intensity is plotted in (a) and the micellar radii are plotted in (b). The arrows in the figure indicate the direction of titration for the two series.

3.4. The effect of ionic strength in mole fraction titrations

In Figure 3.8 the maximum pH change vs. the initial pH values of solutions of PAMA and PAA homopolymer solution is shown. These data were obtained by titrating the PAMA solutions with the PAA solutions. Always, both solutions had the same initial starting pH. At lower starting values for the pH, we see that the pH decreases slightly during the experiments. At higher pH starting values, the pH increases upon titrating a PAMA solution with a PAA solution. So, in order to form a complex at low pH, the pH becomes lower, whereas at higher pH, the pH increases even further. Only at pH = 9, complexation no longer takes place. The transition between these regimes, the so-called iso-protic point is found around pH = 6.7. Thus, starting the experiments around pH = 6.7 allows us to vary the composition of the system at a more or less constant pH. In Figure 3.9 we present data from the mole fraction titrations for 5, 10, 50 and 100 mM $NaNO_3$. In Table 3.3, we give the starting pH values for the polymer solutions. First we will discuss the scattering intensity (I) curves in Figure 3.9a. From the intensity peaks that appear around $f_{PAA} = 0.5$, we conclude that micellization occurs at all four ionic strengths. An overview of f_{PMC}, peak intensity values and corresponding micellar hydrodynamic radii is given in Table 3.4. For all $NaNO_3$ concentrations, a slow

[$NaNO_3$] (mM)	pH PAA	pH PAMA
5	6.73	6.75
10	6.76	6.66
50	6.75	6.75
100	6.72	6.63

TABLE 3.3. Starting pH values for the mole fraction titrations

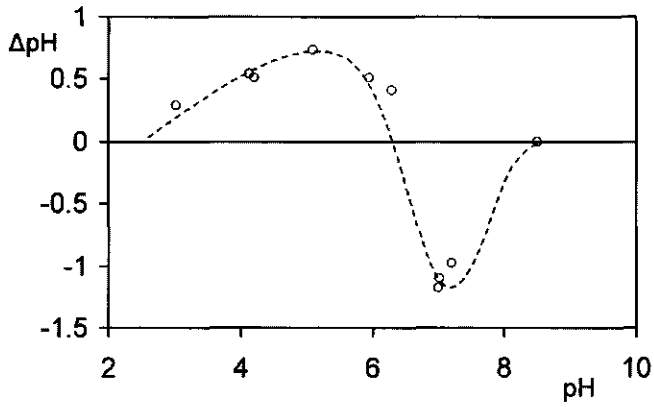

FIGURE 3.8. Maximum derivation of the pH from initial pH values, obtained by titrating a 6 mM PAMA solution with a 14 mM PAA solution solution in 100 mM NaCl. On the horizontal axis are the initial pH of both the solutions before mixing. On the vertical axis are the maximum changes in pH that occurred during the titrations, given as Δ pH = p$H_0 - pH_{max,min}$. Clearly, the iso-protic point is around pH 6.7. The dashed line is a guide to the eye.

[$NaNO_3$ (mM)	$f_{PAA,PMC}$	I_{max} (kHz)	pH_{PMC}	R_h (nm)
5	0.52	45.1	8.38	14.5
10	0.56	236	7.46	22.0
50	0.57	62.3	7.11	17.0
10	0.59	44.6	6.86	14.7

TABLE 3.4. Summary of relevant data from the mole fraction titrations

increase in intensity is seen from $f_{PAA} \approx 0$ to $f_{PAA} \approx 0.4$. We assume this represents the formation of very loose, low aggregation number complex particles. Aggregation into micelles is prevented by electrostatic repulsion, since these particles are positively charged by the excess PAMA. On the right hand side of the peak, PAA is present in excess, causing the micelles to fall apart into anionically charged, repelling particles. This is seen in the experimental data by a rapid decrease of I, giving a symmetrical

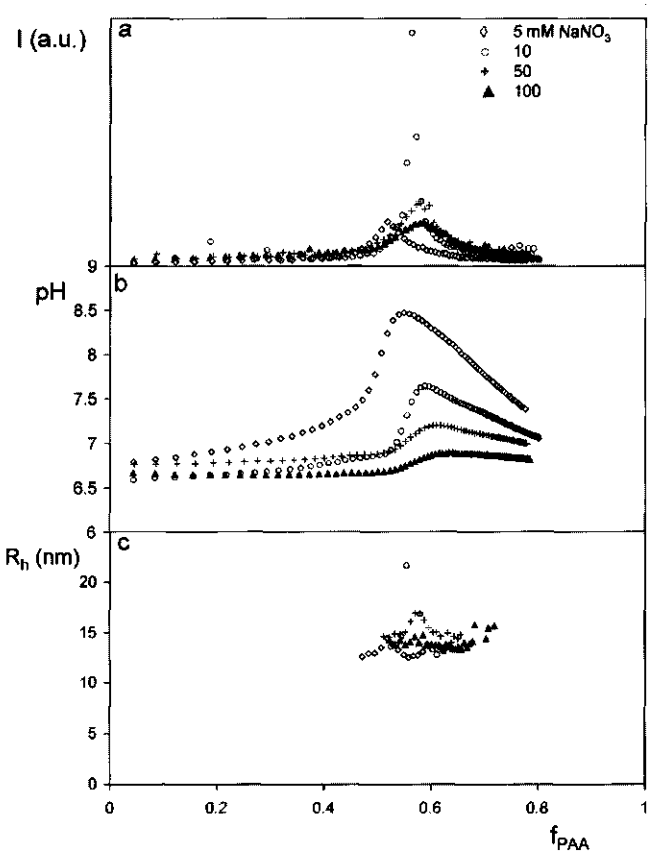

FIGURE 3.9. Experimental data from titrating a PAMA-PGMA solution with PAA solution at various [$NaNO_3$]. The concentration of PAMA groups was 1.6 mM. The inital pH of the PAMA-PGMA and PAA solutions were equal (around 6.7), as was the ionic strength for each experiment. In (a), the light scattering intensity is given in an arbitrary units. In (b), the pH is given and in (c) the micellar radii are given.

behavior around f_{PMC}. Only in the peak area, colloidal particles with a well-defined radius could be detected by dynamic light scattering. Hence, the micellar window covers only a small fraction part the f_{PAA} range. The I vs f_{PAA} data are in good agreement with the aggregation mechanism as discussed from light scattering intensity vs f curves in Chapters 1 and 2.

A second reason for identifying f_{PMC} at the chosen f_{PAA} values with peak intensity lies in the pH curve. At the PMC, nearly all polymer molecules will participate in the micellization, so there is almost no buffer in the bulk that can suppress the effect of proton uptake, i.e. the buffer capacity has a pronounced minimum. This is seen clearly

by the fact that $\partial pH/\partial f_{PAA}$ is at a maximum value around f_{PMC}. If we think of a relationship between f_{PMC} and pH_{PMC}, f_{PAA} is expected to increase if pH increases, resulting from the opposite direction of α_{PAA} and α_{PAMA} with respect to pH. This trend is indeed observed in the data in Table 3.4.

With increasing ionic strength, a lowering of I_{max} is expected, since the driving force for micellization decreases, leading to lower aggregation numbers and lower polymer volume fractions (ϕ) are expected in the micellar cores. This lower polymer volume fraction will lower the surface tension of the core/solvent interface, so that the aggregation number will decrease[14]. Both the radius and I_{max} are consistent with this idea for the 10, 50 and 100 mM experiments. With the 5 mM $NaNO_3$ experiment, however, the micelles at the PMC are smaller and I_{max} is much lower than with the other experiments.

We attribute this to the high pH_{PMC} for 5 mM $NaNO_3$. Figures 3.4 and 3.8 show that at pH values around 9 interaction between PAA and PAMA stops. We may conclude from this that at 5 mM the large shifts in pK generate large shifts in pH, such that the complexation process creates its own stop-mechanism.

In the set of pH curves shown in Figure 3.9b, two trends can be seen: (i.) The maximum pH values that are reached during the titrations decrease with increasing ionic strength, (ii.) The steepness of the $\partial pH/\partial f_{PAA}$ in the stoichiometric window decreases with increasing ionic strength. The pK shifts that the polyelectrolytes undergo upon complexation thus become smaller with increasing ionic strength. Therefore, the changes in bulk pH decrease with increasing $[NaNO_3]$, as the difference in screening environment between bulk solution and complex coacervate becomes less extreme with increasing ionic strength in the bulk.

From the pH data, we will now quantitatively check Equation 3.1. Since the initial pH values and the ionic strength of the solutions are matched, the pH changes during the titration experiments must result from complexation. At the PMC, the amount of protons in the system (micelles and bulk solvent) that is required to obtain electroneutrality in the micellar cores is given as

$$N_{total} = V_{PMC} f_{PAA,PMC} \left([PAA] + [PAMA]\right)_{PMC} \tag{3.8}$$

where the subscript PMC denotes the values of V, f_{PAA}, and [PAA] and [PAMA] at the PMC. If we neglect the very small contribution of protons in the bulk, then the number of protons that is bound to the polyelectrolytes at the PMC is given as

$$N_{system} = V_0 \left[PAMA\right]_0 \alpha_{PAMA,0} + \Delta V_{PMC} \left[PAA\right]_0 \left(1 - \alpha_{PAA,0}\right) \tag{3.9}$$

where the subscript PMC again denotes the value at the PMC and the subscript zero denotes the values in the PAA and PAMA-PGMA stock solutions and ΔV is the volume of added PAA stock solution, i.e. $V_{PMC} = V_0 + \Delta V_{PMC}$. The α values of PAA

and PAMA follow from the curves in Figure 3.2. A comparison of the values of N_{total} and N_{system} showed that $N_{total} >> N_{system}$ for all experiments, suggesting a significant excess of negative polyion charges in the micellar cores. In addition, $N_{total} - N_{system}$ increases with increasing [$NaNO_3$]. As the complexes must be electroneutral at the PMC, we must conclude that sodium ions also participate in the charge neutralization of the complex coacervate cores. In Table 5, f_{PAA}, PMC, N_{total}, N_{system}, and $N_{sodium}(N_{sodium} = N_{total} - N_{system})$ are given, normalized for the concentration of polyelectrolyte groups. It is quite remarkable that $n_{system} \approx 0.5$ for all experiments. We

[$NaNO_3$ (mM)	n_{total}	n_{system}	n_{sodium}
5	0.52	0.50	0.02
10	0.56	0.50	0.06
50	0.57	0.52	0.08
100	0.59	0.48	0.10

TABLE 3.5. n_{total}, n_{system} and n_{sodium} for all experiments. All values are normalized for the total number of polyelectrolyte groups, *i.e.* $n_i = N_i V_{PMC}^{-1} ([PAA]_{PMC} + [PAMA]_{PMC})^{-1}$

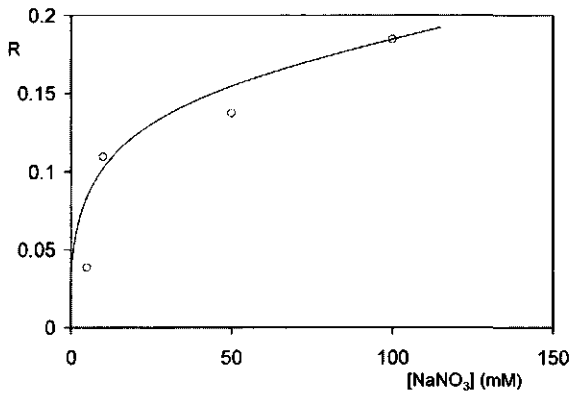

FIGURE 3.10. Fraction of sodium ions in the micellar cores at the PMC, vs. [$NaNO_3$]

then would expect to correspondingly find the PMC at $f_{PAA} = 0.5(= n_{system})$, so that the complex can form without participation of sodium ions. In the values in Table 3.5, we see that $n_{sodium} \approx f_{PAA,PMC} - 0.5$, i.e. the excess PAA that is incorporated in the complex is neutralized by sodium ions. There may be several reasons for participation of sodium ions in the complex, such as specific interaction between sodium ions and the polyelectrolytes, or the polyelectrolytes are geometrically limited in neutralizing all charges in the complex due to the restricted mobility of the PAMA chains that

are 'grafted' at the core-corona interface. With decreasing ionic strength the charge neutralization is in line with Equation 3.1. The fraction of sodium ions over the total number of small cations in the complex (R) is given as

$$R = \frac{n_{sodium}}{n_{sodium} + n_{system}} \tag{3.10}$$

In Figure 3.10, R is presented as a function of [$NaNO_3$]. With increasing ionic strength in the bulk, we see an increase in the participation of sodium ions in the complex. The value of R is clearly non-linear with [$NaNO_3$], and therefore the small ions are not only present due to diffusion into the complex. To further investigate the effect of $NaNO_3$ on the micelles, we titrated a micellar solution at its PMC with a 3 M $NaNO_3$ solution (data not shown). The initial ionic strength of the micellar solution was 10 mM $NaNO_3$. The pH of the solutions was not exactly matched: the $NaNO_3$ solution was neutral and the micellar solution around pH 7.5 as seen in Figure 3.9b. A strong decrease in pH was seen during the titration, that was far more than could be attributed to a difference in pH of the solutions alone. Hence, we must conclude that by introducing more sodium ions in the system, we displace protons from the complex, which leads to a decrease of the bulk pH. Around 0.3 M $NaNO_3$, the light scattering intensity became very low, indicating the absence of multimolecular aggregates. With increasing ionic strength, the monovalent (sodium and nitrate) ions will eventually provide a very efficient screening of the polyelectrolyte charges, so that for entropic reasons the micelles disintegrate.

3.5. Light Scattering Mass Analysis and core density

The curves in Figure 3.9a were analyzed with the light scattering mass analysis (LSMA) method, as described in Chapter 2. With this method, a rough estimate of the molar mass and aggregation number of the micelles can be calculated from the intensity curves. From the aggregation number, the micellar radius can be calculated as a function of the polymer volume fraction in the core, ϕ.

In Figure 3.11a, R_h at the PMC as determined from Figure 3.9c is plotted vs the ionic strength. In Figure 3.11b, the aggregation number, P (number of $PAMA_{35}PGMA_{105}$ molecules per micelle) is given and in Figure 3.11c, ϕ is given. The data in Figure 3.11c were determined by calculating R_{core}, using Equation 2.3 and by calculating H_{corona} using Equations 2.4 - 2.6. A theoretical micellar radius is now found from $R_{micel} = R_{core} + H_{corona}$. We minimized $|R_h - R_{micel}|$ in a fit procedure where ϕ was optimized. Before, we reasoned that the 5 mM experiment creates its own stop-mechanism by the large pH shifts that occur upon complexation. This is seen by the P value of the 5 mM $NaNO_3$ experiment in Figure 3.11b, that is in the same order as the 50 mM $NaNO_3$ and 100 mM $NaNO_3$ experiments. Yet, both P and R_h tend to increase with decreasing

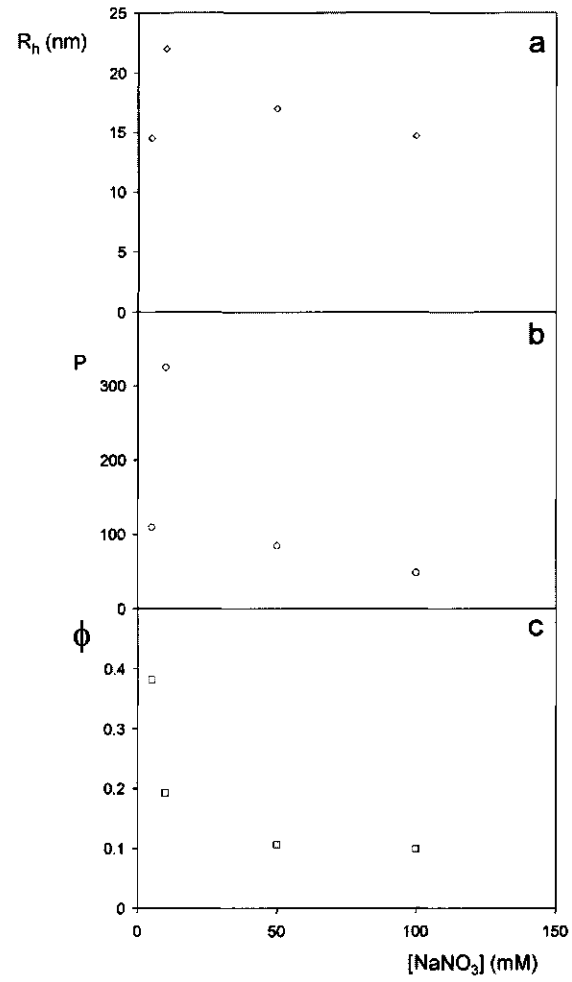

FIGURE 3.11. Hydrodynamic radius R_h (a), aggregation number P (b), and polymer volume fraction in the core ϕ (c). The data in (a) were taken from Figure 3.9c.

[$NaNO_3$], as is seen in Figure 3.11b by the 10, 50, and 100 mM $NaNO_3$ data. Upon minimizing $|R_h - R_{micel}|$, a monotonous trend is found for ϕ vs [$NaNO_3$], as is seen in Figure 3.11c. This decrease in ϕ with increasing [$NaNO_3$] is in line with expectations, as small ions tend to swell a complex coacervate. Despite the non-monotonous P and R_h, a monotonous trend in ϕ was found as a function of [$NaNO_3$]. In Figure 3.12, we plot R vs ϕ where R are the same data points as in Figure 3.10. In this Figure we see how ϕ changes as a function of the sodium ions content of the micellar core. If the experiment would be performed without any added $NaNO_3$, the micellar core would be free of sodium ions, i.e. the origin of Figure 3.10. Therefore, an extrapolation of the

data in Figure 3.12 to $R = 0$ corresponds to an extrapolation of the data in Figure 3.11c to $[NaNO_3] = 0$. Only in Figure 3.11c, the intersection point with the vertical axis is not easily determined, whereas in Figure 3.12, it is. The intersection point of the data with the vertical axis seems to be at $\phi = 0.5$. So, with the PAA/PAMA system, the polyelectrolytes will occupy at most half of the core volume.

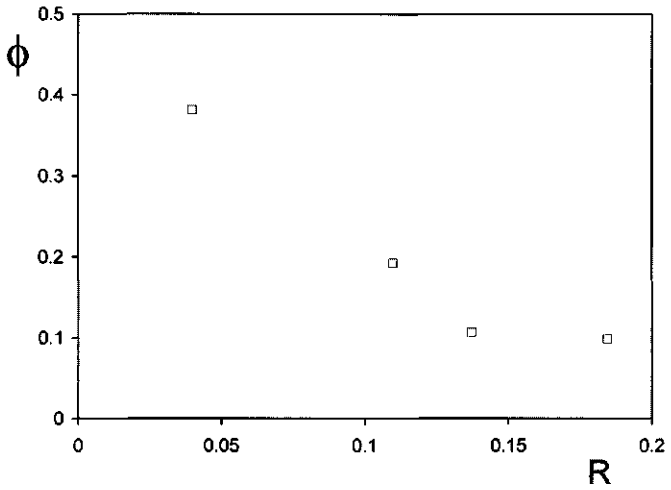

FIGURE 3.12. Polymer volume fraction in the micellar core vs fraction of sodium ions in the core.

3.6. The effect of total polymer concentration in mole fraction titrations

In Figure 3.13, we present data from mole fraction titrations at varying total concentrations. Again, we see for all experiments that a maximum in $\partial \mathrm{p}H/\partial f_{PAA}$ coincides with I_{max}, so that we determine the PMC for each experiment at I_{max}. With the 0.9, 1.8 and 6 mM PAMA experiments, the initial pH values are equal, around pH = 6.7. No difference is seen in the pH curves with these experiments. Both the changes in pH and the position of the PMC are highly similar. The similarity in pH curves demonstrates the buffering effect of the micelles. Although the buffering capacity has a pronounced minimum at the PMC, it is not zero. With the 2.7 mM PAMA experiment we demonstrate the relevance of the initial pH, which in this experiment is slightly higher than for the other experiments. Clearly, the pH deviates much more from the initial pH compared to the other experiments. With the 2.7 mM experiment, the solution was clear to the eye throughout the experiments. With the other experiments, however, a

macroscopic phase separation was seen at the PMC. The reason for this phase separation may be the position of the PMC: in Figure 4a we saw that increasing the fraction of PAA at charge stoichiometric conditions will lead to a precipitate. The PMC with the 0.9, 1.8 and 3.6 mM experiments is at $f_{PAA} \approx 0.55$, whereas the PMC with the 2.7 mM experiment is at $f_{PAA} \approx 0.52$. This slight difference, seems to be enough to prevent a macroscopic phase separation. The phase separation can also be seen in the hydrodynamic radii of the different experiments in Figure 3.13a. Just outside their PMC, all four experiments exhibit micellar radii around 15 nm. With the 2.7 mM experiment, the maximum R_h, exactly at the PMC is 18 nm. All other experiments show a radius around 30 nm exactly at the PMC. This radius is roughly equal to the contour length of the PAMA-PGMA block-copolymers.

$f_{PAA,PMC}$	$[NaNO_3]$ (mM)	pH	$C_{polymer}$ (g/l)	mixture(R_h(nm))
Premixed experiments with varying pH (Section 3.3.2)				
0.23	50	8.75	11.05	19.8
0.32	50	8.68	9.72	19.52
0.43	50	8.57	8.58	16.4
0.49	50	7.59	7.88	flocculation
0.62	50	6.70	6.28	flocculation
Mole fraction titrations at different $[NaNO_3]$ (Section 3.3.3)				
0.52	5	8.67	1.03	14.5
0.56	10	7.86	1.18	22.0
0.57	50	7.54	1.21	17.0
0.59	100	7.25	1.29	14.7
Mole fraction titrations with varying $C_{polymer}$ (Section 3.3.4)				
0.56	10	7.12	0.64	flocculation
0.55	10	7.44	1.24	flocculation
0.53	10	8.12	1.81	19.5
0.56	10	7.17	2.33	flocculation

TABLE 3.6. Colloidal stability of the micelles of all experiments performed in this study. If the mixture was colloidally stable, we give the radius of the micelles at the PMC. The polymer concentrations are expressed as the total polymer concentration at the PMC. The experimental series from which the data originate are indicated in the table.

3.7. Micellar Stability

In Table 3.6, we give an overview of the colloidal stability for all experiments. From the data we see that there are several conditions that promote flocculation. Most prominent

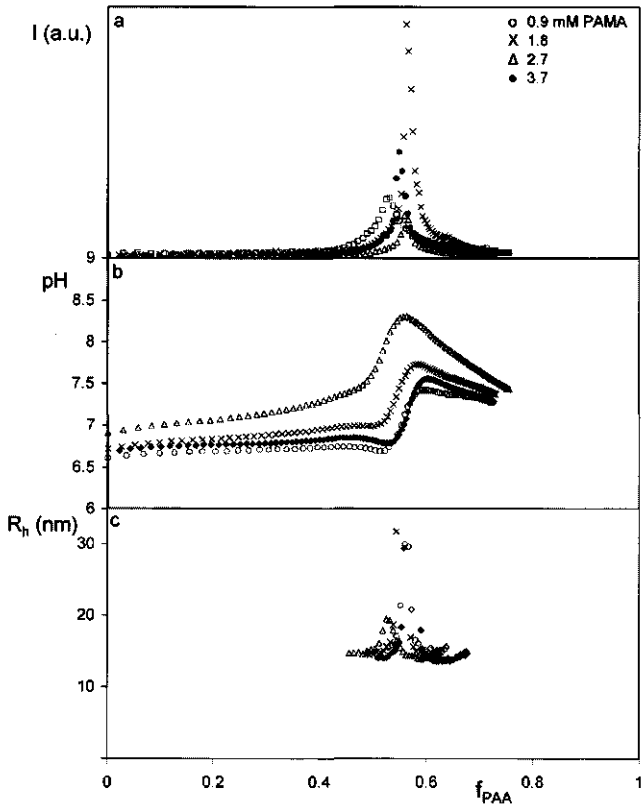

FIGURE 3.13. Light scattering titration data, obtained by titrating PAMA-PGMA solutions of various concentrations with a PAA solution. The ionic strength was 10 mM $NaNO_3$. The 0.9, 1.8 and 3.7 mM experiments were performed with initial pH 6.7. In (a), the light scattering intensity is given in arbitrary units. In (b), the pH is given and in (c) the micellar radii are given. With the 2.7 mM experiment, the initial pH was slightly higher, in order to demonstrate the influence of initial pH on the process.

is the value of f_{PAA} at the PMC. With increasing fractions of PAA in the micellar core, the grafting density of PGMA hairs on the core surface is decreased. The osmotic pressure that is generated in the corona is not sufficient and a macroscopic phase separation occurs. Several parameters are of influence on the position of the critical value of f_{PAA}. If we compare the second and third series, we see that at 10 mM $NaNO_3$, flocculation occurs at $f_{PAA} > 0.53$. At higher ionic strength, however, the micelles are stable and remain in solution, as can be seen from the 50 mM and 100 mM ionic strength experiments. With increasing ionic strength, the cores will increase their water fraction,

thereby lowering the surface tension between core and solvent. The surface tension is a key parameter in the driving force for phase separation. We therefore attribute the micellar stability at high ionic strength to the decrease of this driving force.
Another parameter that influences the micellar stability at a given f_{PAA} is the total polymer concentration. The $f_{PAA} = 0.49$ sample in the first series undergoes flocculation, whereas all experiments in the second series are colloidally stable with higher fractions of PAA in the core. We attribute this difference to the higher concentration of micelles in the first series of experiments.

3.8. Conclusions

From the experiments with fixed composition and varying pH, we conclude that micelles can be formed in a wide range of compositions. The position of pH_{max} depends on the composition of the system. With samples with composition $f_{PAA} > 0.5$, a macroscopic phase separation occurred at pH_{max}. At pH > 9.5, the micelles disintegrate. The micelles are (almost) fully pH reversible. The measured protonation behavior of the mixtures is different from the calculated protonation behavior of non-complexed mixtures, where the protonation behavior was calculated from the protonation behavior of the separate components in bulk solution. Upon varying the composition of the system at equal starting pH of the separate components in solution, a small micellar window was found, at compositions where the number of cationic and anionic polyelectrolyte groups are approximately matched. The quantitative analysis of the polyacid/polybase charge balance showed that with increasing ionic strength in the bulk, the small cations also increasingly participate in the charge neutralization. In addition, with increasing ionic strength, the polymer volume density in the core decreases. The total concentration of polymers did not influence the pH changes that occur upon changing the composition of the system. In our opinion this illustrates that the micelles are acting as a pH buffer. Despite the changes in pK and α, the polyelectrolytes still respond to changes in bulk pH.

3.9. References

1. J.Th.G. Overbeek and M.J. Voorn, Journal of Cellular and Comparative Physiology, 1957. **49**: p. 7-26.
2. S.T. Dubas and J.B. Schlenoff, Macromolecules, 2001. 34: p. 3736-3740.
3. D. Kovacevic, S. van der Burgh, A. de Keizer, and M. A. Cohen Stuart, Langmuir, 2002. **18**: p. 5607-5612.
4. D. Frugier and R. Audebert, eds. *Interaction between Oppositely Charged Low Ionic Density Polyelectrolytes: Complex Formation or Simple Mixture.* Macromolecular

Complexes in Chemistry and Biology, ed. P. Dubin, et al. 1994, Library of Congress Cataloging-in-Publication Data: Berlin. 135-149.

5. D. Kovacevic, S. van der Burgh, A. de Keizer, and M.A. Cohen Stuart, Journal of Physical Chemistry, 2003. **107** p. 7998-8002.
6. H. Dautzenberg, *Polyelectrolyte Complex Formation in Highly Aggregating Systems: Methodical Aspects and General Tendencies*, in Physical Chemistry of Polyelectrolytes, T. Radeva, Editor. 2001, Marcel Dekker, Inc.: New York. p. 743-792.
7. A.V. Kabanov, T. K. Bronich, V.A. Kabanov, K. Yu, and A. Eisenberg, Macromolecules, 1996. **29**: p. 6797-6802.
8. M.A. Cohen Stuart, N.A.M. Besseling, and R.G. Fokkink, Langmuir, 1998. **14**: p. 6946-6949.
9. A. Harada and K. Kataoka, Journal of American Chemical Society, 1999. **121**: p. 9241-9242.
10. M. Borkovec, B. Jnsson, and G.J.M. Koper, *Ionization Processes and Proton Binding in Polyprotic Systems: Small Molecules, Proteins, Interfaces, and Polyelectrolytes.* Surface and Colloid Science, ed. E. Matijevc. Vol. 16. 2001: Kluwer Academic, Plenum Press. 19-339.
11. A. E. Martell and R. M. Smith, *Critical Stability Constants, Volume 3: Other Organic Ligands. Critical Stability Constants.* 1977, New York: Plenum Press.
12. S.W. An and R.K. Thomas, Langmuir, 1997. **13**: p. 6881-6883.
13. N. G. Hoogeveen, M.A. CohenStuart, and G.J. Fleer, Faraday Discussions, 1994. **98**: p. 161-172.
14. O.V. Borisov and E.B. Zhulina, Macromolecules, 2002. **35**: p. 4472-4480.

CHAPTER 4

Characterization by Small Angle Neutron Scattering

ABSTRACT

Small angle neutron scattering experiments have been performed on complex coacervate core micelles. Variations in the experiments were the degree of polymerization of the corona block and overall concentration. As form factor for the micelles, an analytical approach was used, based on the Debye equation for particles consisting of spherical subunits. From the form factor, the aggregation numbers, molar mass, core radius, corona thickness, and core density of the micelles were determined. The values obtained agreed well with dynamic light scattering experiments.

Submitted to Macromolecules, 2004

4.1. Introduction

Small angle techniques using X-rays or neutrons are useful methods to characterize colloidal objects in terms of their overall radius, molar mass, internal structure and, in the case of concentrated systems, their interactions. One major advantage is the very small wavelength of the neutrons or electrons, that is in the order of 1 nm, whereas light scattering is done with a wavelength in the order of several hundreds of nanometers. As the wavelength is thus mostly (much) smaller than the colloidal particles, small angle neutron scattering (SANS) or small angle X-ray scattering (SAXS) are suitable techniques to study the internal structure of the particles at hand. This is in strong contrast to light scattering, which is restricted to determining the overall dimensions (and molar mass) of small colloidal particles, mostly at lower concentrations than the small angle techniques. In general, small-angle data are analyzed by comparing the experimental data with model scattering functions. These model scattering functions are based on assumptions with respect to the internal structure of the particles and, for concentrated systems, the particle-particle interactions. Given their dimensions and core-corona structure, SANS is an excellent tool for studying block-copolymer micelles, and numerous studies can be found in literature[1-10].

Although our data so far are consistent with the core-corona structure sketched in Figure 1.7, no direct structural information at nm level has been obtained, so that we do not know, e.g., the relative size of core and corona. In the present Chapter, we therefore apply small angle neutron scattering (SANS) to CCCM. The advantage of SANS with respect to SAXS is that the data can be analyzed on an absolute scale. This means that, starting from (i) the chemically determined neutron scattering contrast parameters, (ii) the so-called excess scattering lengths, (iii) the number density of scattering objects, and (iv) their wave-vector dependent scattering function, a very exact comparison between theory and experiment can be made. For these model scattering functions, we use an approach by Pedersen, that was developed especially for small angle scattering data from block-copolymer micelles[1, 3, 4, 11]. The aim of this SANS study is to determine the aggregation numbers, polymer density in the core and internal structure of the micelles, in terms of core radius and corona thickness.

To our knowledge this is the first SANS study of micelles with a polyelectrolyte coacervate core. Three excellent SANS articles were published on the system PAA-PAM diblock-copolymer with oppositely charged surfactant micelles. It was found that the aggregation number expressed as number of diblock-copolymer molecules per micelle was around 70, and that the surfactant micelles keep their micellar structure within the larger structure. So, the core exists of an ensemble of surfactant micelles, that are connected by the PAA blocks from the diblock-copolymer. The typical distance between the surfactant micelles showed up as a structure peak at high q values[12-14].

4.2. Model

In scattering studies, a central quantity is the momentum transfer or scattering wave vector q, given by

$$q = \frac{4\pi}{\lambda} sin\left(\frac{\theta}{2}\right) \tag{4.1}$$

where λ is the wavelength of the radiation and θ is the scattering angle. The q-dependent scattered intensity is a function of the excess scattering length of the particles, their number density and their radial distribution function, the Fourier transform of which yields the so-called form factor and interparticle structure factor. In the case of non-homogeneous particles, one can distinguish between the different excess scattering lengths of the different components of the particles. For the CCCM at hand, it is expedient to distinguish between the core and corona, having respective scattering lengths

$$\begin{aligned} \beta_{core} &= \left((b_{PAA} + b_{PVP}) - V_{PAM}\frac{b_{D_2O}}{V_{D_2O}}\right) N_{PAA} \\ \beta_{corona} &= \left(b_{PAM} - V_{PAM}\frac{b_{D_2O}}{V_{D_2O}}\right) N_{PAM} \end{aligned} \tag{4.2}$$

In Equation 4.2, the β values are thus calculated from the sum of the bound coherent scattering lengths of the separate atoms of the groups (b_i), and their molar volumes (V_i) that were taken from literature[10,15,16]. The block length of the corona block is given as N_{PAM}. In the case of β_{core}, we assume a 1:1 stoichiometry between PAA and PVP (the charged block from the diblock-copolymer (polyacrylic acid) and the oppositely charged homopolymer (poly *N*-ethyl-4-vinylpyridinium bromide) respectively) groups at the preferred micellar composition (PMC) and we assume that the excess scattering lengths of PAA and PVP in the core are homogeneously smeared out. This seems a reasonable assumption, as the smallest length scales that are probed in the experiment ($\approx q_{max}^{-1}$) are much larger than typical density fluctuations in the core. The "building blocks" of a CCCM are thought to consist of one corona block, one core block, and one equivalent of oppositely charged homopolymer, so that for the mass of such a unit for the system at hand we get $M_{bb} = M_{PAM} + N_{PAA}(m_{PAA} + m_{PVP})$ where M_i is the molar mass of a polymeric species and m_i is the molar mass of monomer i. In Table 4.1, values of β and M_{bb} for the system are given.

We see in Table 4.1, that the ratio between core and corona excess scattering length has a rather wide variation with N_{PAM}. This means that the scattering of the $PAA_{42}PAM_{97}$ sample has a large contribution from the core, whereas the scattering from the $PAA_{42}PAM_{417}$ samples will be mostly dominated by scattering from the corona blocks.

Sample	$\beta_{core}(10^{-12}m)$	$\beta_{corona}(10^{-12}m)$	$\beta_{core}/\beta_{corona}$	M_{bb} (g/mol)
$PAA_{42}PAM_{97}$	-6.11	-5.00	1.223	$2.08 * 10^4$
$PAA_{42}PAM_{208}$	-6.11	-10.71	0.571	$2.87 * 10^4$
$PAA_{42}PAM_{417}$	-6.11	-21.48	0.285	$4.35 * 10^4$

TABLE 4.1. Excess scattering lengths of diblock-copolymers and molar mass of building blocks

Calculated intensities that are to be compared with the experimental data follow from

$$I(q) = cF(q)_{micel} \qquad (a)$$

$$I(q) = c\left(F(q)_{micel} + A(q)^2_{micel}\left[S(q)_{hardsphere} - 1\right]\right) \qquad (b) \tag{4.3}$$

where Equation 4.3a is valid for low concentrations of scattering objects, and Equation 4.3b is valid for higher concentrations. The particle number density is denoted by c, and $F(q)_{micel}$ is the particle form factor. In Equation 4.3b $A(q)_{micel}$ is the scattering amplitude of the micelles, $S(q)_{hardsphere}$ is the hard-sphere structure factor, that takes into account the scattering contributions due to particle interaction. Note that this expression is somewhat more complicated than the more simple $I(q) = cF(q)S(q)$, that is often used. It was found by Pedersen et al.[3], that this simple approach is not suitable for block-copolymer micelles, and that Equation 4.3b, that is in a sense similar to the decoupling approximation, is a better way to describe micelle-micelle interactions. At the PMC, the number density of micelles c is given by

$$c = CP^{-1}M_{bb}^{-1}N_{AV}10^{-3} \tag{4.4}$$

where C is the polymer weight concentration, P is the aggregation number (expressed as the number of diblock-copolymers per micelle), and M_{bb} is the molar mass of a 'building block' (see also Table 4.1).

The form factor of a block-copolymer micelle with spherical core is given by[4]

$$F(q) = P^2\beta^2_{core}F_{core}(q, R_{core}) + P\beta^2_{corona}F_{corona}(q, N_{corona}, k) + \\ + P(P-1)\beta^2_{corona}S_{corona} + 2P^2\beta_{core}\beta_{corona}S_{core-corona} \tag{4.5}$$

In this equation, the first term denotes the form factor for the spherical core, the second term denotes the scattering from *Gaussian* corona chains, the third term is the scattering contribution due to interference between the closely packed corona chains, and the fourth term denotes the interference between the spherical core and corona chains. This form factor is based on the Debye equation[3], that gives the scattering function of particles consisting of subunits with spherical symmetry. Yet, this seems

an inappropriate approach for block-copolymer micelles, where the corona chains are not in a Gaussian conformation, but stretch away from the core-corona interface. This is corrected for by moving the starting point of the corona chains away from the core-corona interface, mostly this shift is in the order of R_{corona}[1,4] where R_{corona} is the dimension of the unperturbed corona chain in a good solvent. Below, we will give the expressions for the different terms in Equation 4.5. The core form factor is the well-know expression for a solid sphere:

$$F(q)_{core} = A(q)^2_{core}$$
$$A(q)_{core} = \frac{3[sin(qR_{core}) - qR_{core}cos(qR_{core}))}{(qR_{core})^3} \tag{4.6}$$

where R_{core} is given as

$$R_{core} = \left(\frac{3}{4\pi} P\phi^{-1} N_{core} N_{AV}^{-1} \left(V_{PAA} + V_{PVP}\right) 10^{21}\right)^{1/3} \tag{4.7}$$

with ϕ the polymer volume fraction of the core and $V_{PAA,PVP}$ the molar volumes. The scattering function of the corona is the Debye function for Gaussian chains

$$F_{corona} = \frac{2\left[exp\left(-q^2 R^2_{corona}\right) - 1 + q^2 R^2_{corona}\right]}{q^4 R^4_{corona}} \tag{4.8}$$

where R_{corona} is given by

$$R_{corona} = \sqrt{\frac{0.25 N_{corona} k}{6}} \tag{4.9}$$

with k the Kuhn length. We used $k = l_{PAM}6.25$ where l_{PAM} is the elementary 'step-length' of an PAM monomer, taken as 0.25 nm. The interference term for the corona chains is given as

$$S(q)_{corona} = A(q)^2_{corona} \left[\frac{sin\left(q\left[R_{core} + d\right]\right)}{q\left[R_{core} + d\right]}\right]^2 \tag{4.10}$$

where A_{corona} is given as

$$A(q)_{corona} = \frac{1 - exp\left(-q^2 R^2_{corona}\right)}{-q^2 R^2_{corona}} \tag{4.11}$$

Here d denotes the displacement of the starting point of the corona chains from the core-corona interface. As d always has a positive value, the starting point is shifted 'outwards', thereby mimicking the stretching of the corona chains. Finally, the core-corona cross-term is given as

$$S(q)_{core-corona} = A(q)_{core} A(q)_{corona} \frac{sin\left(q\left[R_{core} + d\right]\right)}{q\left[R_{core} + d\right]} \tag{4.12}$$

Equations 4.6 and 4.8 - 4.12 were taken from papers by Pedersen[2,4] that can be consulted for an extensive treatise of this model. The adjustable parameters in the

model are P and ϕ. Upon applying the model to the experimental data, the internal structure of the micelles in terms of corona thickness and core radius follows from

$$R_{micel} = R_{core} + H_{corona}$$
$$H_{corona} = d + 2R_{corona} \tag{4.13}$$

As $A(q)_{core}$ and $A(q)_{corona}$ are known, $A(q)_{micel}$ can be calculated by

$$A(q)_{micel} = P\left(\beta_{core}A_{core} + \beta_{corona}A_{corona}\frac{sin\left[q\left(R_{core}+d\right)\right]}{q\left(R_{core}+d\right)}\right) \tag{4.14}$$

and the hard-sphere structure factor $S(q)_{hardsphere}$ is given by

$$S(q)_{hardsphere} = \frac{1}{1 + 24\eta G\left(qR_{hs}\right)/\left(qR_{hs}\right)}$$
$$G(y) = \alpha\left(sin(y) - ycos(y)\right)/y^2 +$$
$$+\beta\left(2ysin(y) + (2 - y^(2))cos(y)02)/y^3\right) +$$
$$+\gamma\left[-y^4cos(y) + 4\{(3y^2 - 6)cos(y) + (y^3 - 6y)sin(y) + 6\}\right]/y^5 \tag{4.15}$$
$$\alpha = \frac{(1-2\eta)^2}{(1-\eta)^4}$$
$$\beta = \frac{-6\eta(1+0.5\eta)^2}{(1-\eta)^2}$$
$$\gamma = \frac{\eta\alpha}{2}$$

where η is the effective volume fraction of particles and R_{hs} is their hard-sphere radius. Equation 4.15 is based on the Percus-Yevick approximation[11].

Zero-angle scattering. Although the scattering at $q = 0$ cannot be determined experimentally, the $I(q), q$ data can be extrapolated to $q = 0$ for dilute systems, where the particle interactions are negligible. From $I(q = 0), P$ can be estimated by[4]

$$F(q=0) = P^2(\beta_{core} + \beta_{corona})^2$$
$$I(q=0) = cF(=0) \tag{4.16}$$

4.3. Materials and methods

Light scattering titrations. The initial PVP (38 gram/litre) and PAA-PAM (25 - 38 gram/litre) stock solutions were prepared in 50 mM $NaNO_3$ and pH was adjusted with 1 M NaOH or 1 M HNO_3 to obtain p$H = 7$ for both solutions. For the light scattering titrations, the stock solutions were diluted with $NaNO_3$ solution of equal ionic strength to obtain 0.5 - 1 gram/litre for the diblock-copolymers and 5 gram/litre for the PVP solution. The light scattering titration experiments were performed to determine the PMC. We assumed that the PMC is not sensitive to concentration, and we used the PMC that was found with the light scattering experiments to prepare the concentrated micellar solutions for the SANS experiments. With the light scattering titrations, the diblock-copolymer solutions were in the light scattering cell and these solutions were titrated with the PVP solution. The data were processed as described in Chapter 2. In addition, the light scattering data were also analyzed with the light scattering mass analysis (LSMA) method as described in Chapter 2.

SANS experiments. SANS experiments were performed with the D22 diffractometer at the Institut Max von Laue - Paul Langevin (ILL), Grenoble, France. Two detector distances were chosen, such that a q-range of 0.029 - 1.37 nm^{-1} was covered. The solvent was always pure D_2O. The temperature was kept constant at 293 K, and a wavelength of 0.8 nm was chosen. Radial averaging was done with software from the ILL. The scattering of pure solvent (D_2O) was substracted from the data.

Materials. As CCCM system we used the $PAA_{42}PAM_{97}$, $PAA_{42}PAM_{208}$, and $PAA_{42}PAM_{417}$ series with poly(N-methyl-4-vinylpyridinium iodide) (PVP) homopolymer with $M_w = 56000$ and chain length is 209. The PVP was received from Polymer Source Inc., Canada and was used as received. The PAA-PAM diblock-copolymers were the same samples as used in Chapter 2. All SANS experiments were done in D_2O, that was received from Isotec Inc., Miamisburg, USA, with 99.9 percent deuterated content.

4.4. Results and Discussion

4.4.1. Light scattering titrations

In Figure 4.1, light scattering titration data are shown for $PAA_{42}PAM_{97}$/PVP. In analogy to *e.g.* Figures 2.6, the PMC was found at the maximum in scattered intensity and the maximum in $|\partial p\mathrm{H}/\partial f_{PVP}|$, *i.e.* the PMC is at $f_{PVP} = 0.5$. Similar experiments were performed for $PAA_{42}PAM_{208}$ and $PAA_{42}PAM_{417}$ (data not shown), and the PMC was always found at $f_{PVP} = 0.5$. The data were also analysed with the light scattering mass analysis method, in Chapter 2. An overview of the DLS data and LSMA results is given in Table 4.2. It is seen in Table 4.2, that P decreases with increasing N_{PAM}, as was also found in Chapter 2 and this finding is in qualitative agreement with several theoretical studies on the effect of block lengths on aggregation numbers[17-19]. In

Table 4.3, concentrations and f_{PVP} values are shown for all SANS experiments in this study.

Sample	R_h	P (LSMA)	M_{micel} (LSMA)
$PAA_{42}PAM_{97}$	14.5	13.1	$2.7 * 10^5$
$PAA_{42}PAM_{208}$	20.2	9.0	$2.6 * 10^5$
$PAA_{42}PAM_{417}$	20.4	5.3	$2.2 * 10^5$

TABLE 4.2. Overview of results from light scattering titrations and LSMA

Total polymer concentration (g/l)	f_{PVP}
$PAA_{42}PAM_{97}$ (Figure 4.3)	
2.32	0.50
4.63	0.50
9.54	0.50
15.20	0.50
25.0	0.50
38.20	0.50
$PAA_{42}PAM_{97}$ (Figure 4.9)	
38.20	0.50
38.20	0.48
38.20	0.42
38.20	0.38
$PAA_{42}PAM_{208}$ (Figure 4.4)	
2.17	0.50
4.37	0.50
8.68	0.50
14.20	0.50
23.10	0.50
35.10	0.50
$PAA_{42}PAM_{417}$ (Figure 4.5)	
1.70	0.50
3.41	0.50
6.89	0.50
11.01	0.50
17.91	0.50
27.50	0.50

TABLE 4.3. Concentrations and compositions of the samples used for the SANS experiments

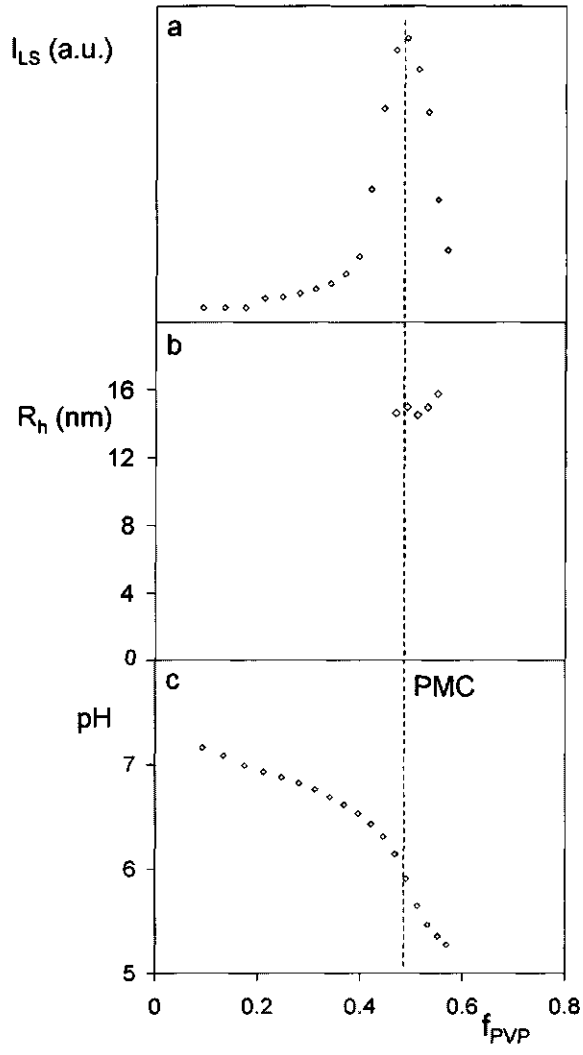

FIGURE 4.1. Light scattering titration data, performed with diluted stock solutions to determine the PMC for the SANS experiments. (a) laser light scattering intensity, (b) hydrodynamic radii, and (c) pH values. Stock concentrations were around 40 g/l, and dilution factor was 75 for the $PAA_{42}PAM_{97}$ solution and 5 for the PVP solution. The $PAA_{42}PAM_{97}$ sample was in the titration cell and was titrated with the PVP solution. The PMC was determined at the I_{max} and it was assumed that the PMC at this low concentration ($\approx$ 0.5 g/l) was equal to the PMC for the concentrated SANS samples. The initial pH values of the solutions were matched as was the ionic strength (50 mM $NaNO_3$). Similar experiments were performed with the $PAA_{42}PAM_{208}$ and $PAA_{42}PAM_{417}$ samples (data not shown).

4.4.2. Zero-angle scattering

In Figure 4.2, we show $I(q)$ vs q for the two lowest concentrations of each PAA-PAM sample. The intensities of the two series were averaged after normalization for concentration. In a rough approach to determine the molar mass of the micelles, the intercepts with the vertical axis were determined with linear regression. From these $q = 0$ values and the slopes, M_{micel} and P were determined using Equation 4.16. The results are given in Table 4.4. The P values that were determined with Equation 4.16 are generally 1.5 times higher than those found with the LSMA method. We attribute this difference to our light scattering setup where the non-correlated scattered intensity is discarded. This means that, when applying the LSMA method, the molar masses are systematically underestimated.

Sample	$P_{q=0}$	$M_{micel,q=0}$	$P_{LSMA}/P_{q=0}$
$PAA_{42}PAM_{97}$	23.1	4.8 * 10^5	0.57
$PAA_{42}PAM_{208}$	12.5	3.6 * 10^5	0.70
$PAA_{42}PAM_{417}$	8.9	3.9 * 10^5	0.60

TABLE 4.4. Micellar characteristics, as determined from Figure 4.2, using Equation 4.16

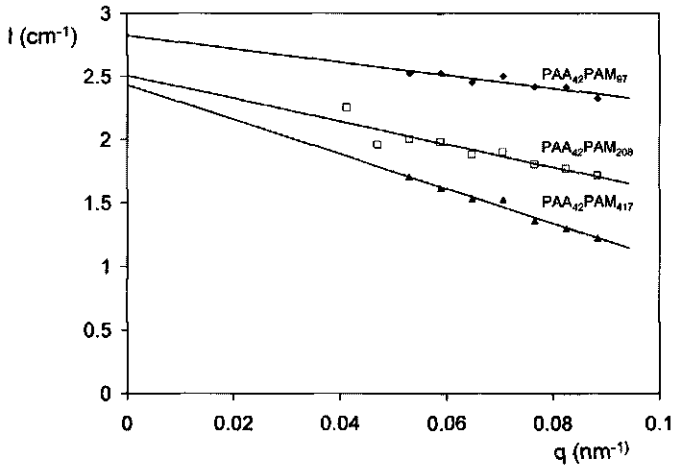

FIGURE 4.2. Linear regression of SANS data to q = 0 for the 2 lowest concentrations of $PAA_{42}PAM_{97}$, $PAA_{42}PAM_{208}$, and $PAA_{42}PAM_{417}$. See Table 4.3 for concentrations. The data of the two concentration series were averaged. The values that were determined for $q = 0$ were 2.82, 2.50,and 2.43 cm^{-1} respectively for $PAA_{42}PAM_{97}$, $PAA_{42}PAM_{208}$, and $PAA_{42}PAM_{417}$.

4.5. Form factor analysis

In Figures 4.3, 4.4 and 4.5, the SANS patterns for $PAA_{42}PAM_{97}$, $PAA_{42}PAM_{208}$, and $PAA_{42}PAM_{417}$ are shown on double logarithmic scales for the concentrations as denoted in Table 4.3. For each sample, the model as described in the theory section has been applied to the two lowest concentrations without the interparticle structure factors, thereby optimizing P and ϕ. Whether or not the interparticle structure factor has a significant effect on the scattered intensity, is mostly seen at the lower q limit. For all samples, we see that for the two lowest concentrations the model curve agrees nicely with the data points in the lower q ranges. To the model curves, a polydispersity in P was applied with a 20 percent spread. This was done in order to obtain smooth curves, without pronounced minima or maxima (compare *e.g.* Figure 2 of reference[4], that shows a monodisperse form factor of the model). The results for P and ϕ are given in Table 4.5. Note that the P values are in the same order as were found in Chapter 2, around several tens, and that ϕ also agrees nicely with the values that were deduced from Figure 2.9, where ϕ was found to be around 0.3.

For the higher concentrations, both Equations 4.3a and 4.3b were applied. In Figures 4.3 - 4.5 the model curves of Equations 4.3a and 4.3b are shown with the four highest concentrations. The highest model intensities are always Equation 4.3a. With increasing micellar concentration, an increased deviation of Equation 3a is seen for all samples. We assumed that P and ϕ are independent of concentration. The model curves that were obtained from Equations 4.3a and 4.3b were calculated with the model parameters as presented in Table 4.5, and, in the case of Equation 4.3b, only η and R_{hs} were optimized. The interparticle structure factor was calculated for a monodisperse system, and for R_{hs}, R_{micel} was chosen from the average P value as determined by Equation 4.13. With respect to the quality of the fits, we can say that the form factors of the

$PAA_{42}PAM_{97}$	P	M_{micel} (g/mol)	ϕ	R_{core} (nm)	H_{corona} (nm)	R_{micel} (nm)
$PAA_{42}PAM_{97}$	43.3	$9.0*10^5$	0.24	8.2	6.4	14.5
$PAA_{42}PAM_{208}$	21.7	$6.2*10^5$	0.13	7.9	9.3	17.3
$PAA_{42}PAM_{417}$	13.2	$5.7*10^5$	0.19	6.0	16.0	21.9

TABLE 4.5. Optimized values for P and ϕ, as determined by applying the model without interparticle structure factor to 2.32 g/l and 4.63 g/l for $PAA_{42}PAM_{97}$, 2.17 g/l and 4.37 g/l for $PAA_{42}PAM_{208}$, and 1.70 g/l and 3.41 g/l for $PAA_{42}PAM_{417}$.

samples are described reasonably well. At high q, the model intensities are somewhat too high, which is the most pronounced in Figure 4.3, with the shortest corona block where even the fluctuations from the core form factor are still clearly visible. Thus, the contribution of the core scattering at high q values is overestimated in the model form factor. One way to lower the contribution of $F(q)_{core}$ at higher q would be to write

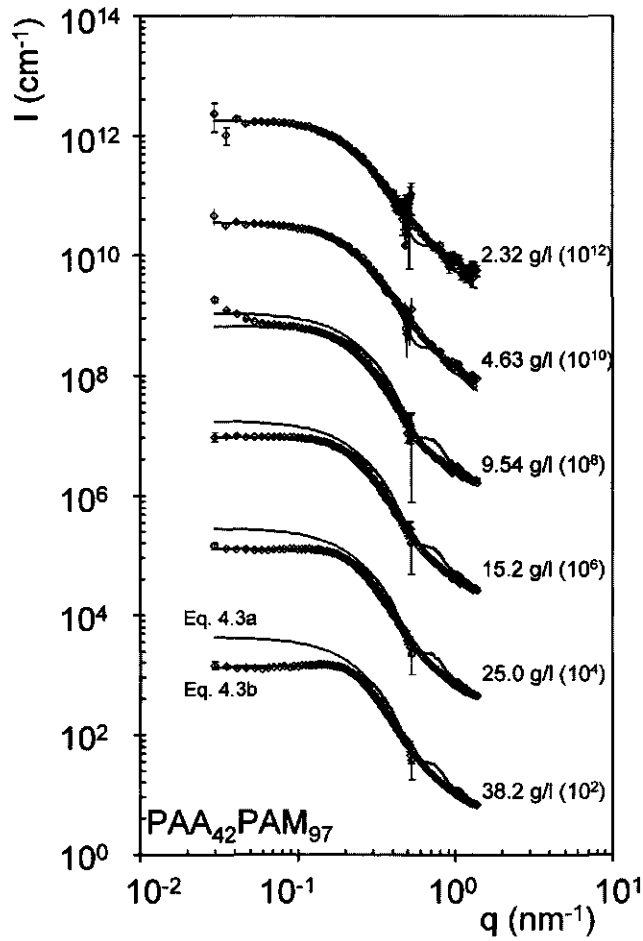

FIGURE 4.3. SANS data for the concentration series of $PAA_{42}PAM_{97}$. Concentrations are indicated in the figure, as is the off-set factor for better visibility of the separate curves. The open diamond symbols represent the experimental data. Except for the two lowest concentrations, there are two model lines per experiment. The lowest model values represent the model including the hard-sphere structure factor (Equation 4.3b), the upper solid lines represent Equation 4.3a. The two lowest concentrations were fitted with Equation 4.3a only. Fit parameters are given in Table 4.5.

$F(q)_{core}exp(-q^2s^2)$ that gives the scattering form factor for a core with a smoothly decaying scattering length density at the core-solvent interface[2]. The thickness of this interface is given by σ. The decay of the model core form factor as given in Equation

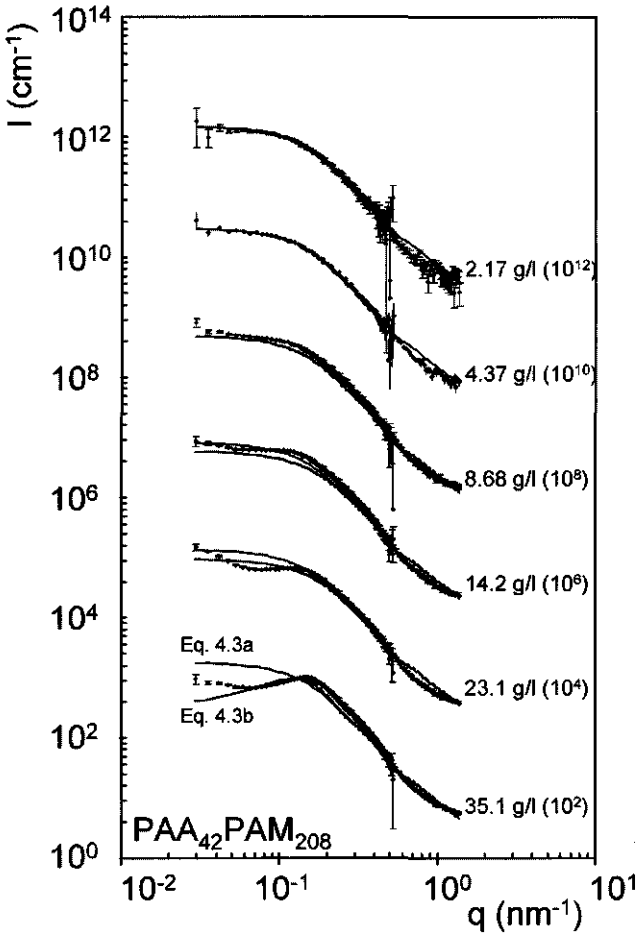

FIGURE 4.4. SANS data for the concentration series of $PAA_{42}PAM_{208}$. Concentrations are indicated in the figure, as is the off-set factor for better visibility of the separate curves. The open diamond symbols represent the experimental data. Except for the two lowest concentrations, there are two model lines per experiment. The lowest model values represent the model including the hard-sphere structure factor (Equation 4.3b), the upper solid lines represent Equation 4.3a. The two lowest concentrations were fitted with Equation 4.3a only. Fit parameters are given in Table 4.5.

4.6 follows a q^{-4} behavior at high q. Yet, with the smooth interface, a q^{-x} behavior is generated, with $x > 4$, depending on σ. Although this approach was successfully

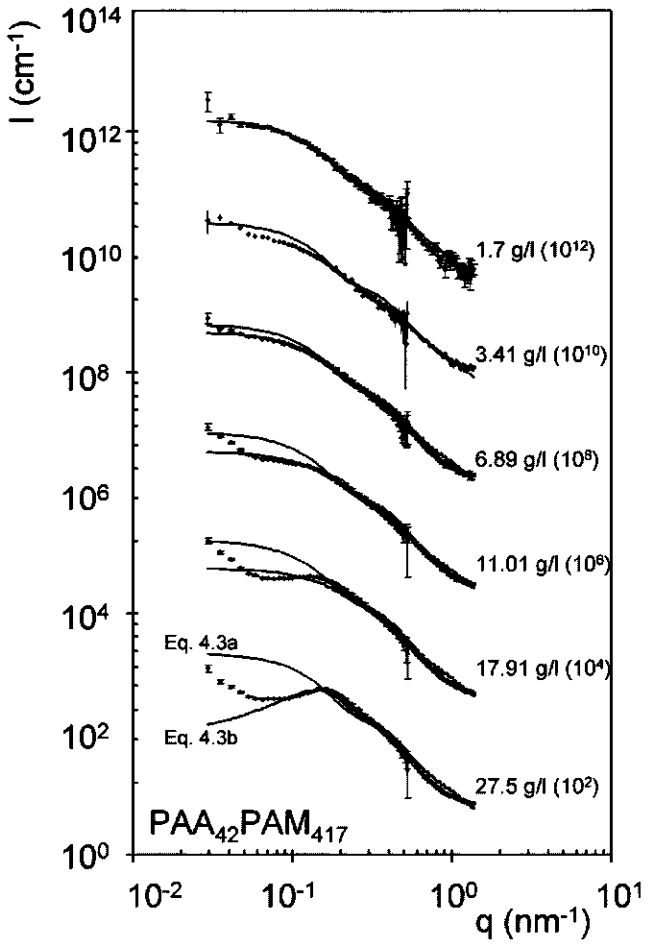

FIGURE 4.5. SANS data for the concentration series of $PAA_{42}PAM_{417}$. Concentrations are indicated in the figure, as is the off-set factor for better visibility of the separate curves. The open diamond symbols represent the experimental data. Except for the two lowest concentrations, there are two model lines per experiment. The lowest model values represent the model including the hard-sphere structure factor (Equation 4.3b), the upper solid lines represent Equation 4.3a. The two lowest concentrations were fitted with Equation 4.3a only. Fit parameters are given in Table 4.5.

applied in a study on hydrophobically associating block-copolymer micelles by Pedersen et al.[2], we decided to use the non-modified expression for the core form factor as given by Equation 4.6. In contrast to Pedersen et al.[2], we were not able to apply

contrast variation. Yet, a contrast-variation SANS study where the core and corona of the CCCM can be highlighted separately would give more insight into the structure of the core. However, with the present data, we believe that the use of $F(q)_{core}exp(-q^2s^2)$, even though it may improve the quality of the fits, would be somewhat arbitrary.
In addition, a more detailed form factor, taking into account core density fluctuations is desirable. Preferably, data obtained by a contrast matching of the PAM corona chains would allow for detailed analysis of the core structure. In such an approach, the number of adjustable core parameters (in the present study, this is only ϕ), would increase significantly. In analogy to the work of Pedersen et al.[2], form factors would be described as Gaussian blobs (in analogy to the second term in Equation 4.5). More over, such an approach requires also the introduction of several more scattering cross terms between the core blobs and corona chains, and between the PAA blocks and PVP homopolymers. We believe that such an approach, although physically correct, will not lead to an unambiguous interpretation of the present data. In addition, we assumed that the PMC is independent of polymer concentration and therefore we applied the experimentally determined polymer concentration of the SANS samples (see Table 4.3) in the fitting procedures. If the PMC *does* shift somewhat as a function of polymer concentration, a correction to the model data would have to be applied, taking into consideration the scattering contribution of the soluble complex particles as described in the speciation diagram in Chapters 1 and 2.
The hard-sphere structure factor gives a good description of the concentration variation of the $PAA_{42}PAM_{97}$ sample in Figure 4.3. Yet, with increasing corona block length in Figures 4.4 and 4.5, the lowest q values are not well described by Equation 4.3b. We attribute this to a change in micellar structure, that is becoming more starlike with increasing N_{PAM}, and therefore the micelles do not behave as hard spheres. One would expect that the micelle-micelle repulsion increases with increasing N_{PAM}. Yet, the $PAA_{42}PAM_{208}$ and $PAA_{42}PAM_{417}$ micelles seem to form clusters, as judged from the upswings at low q, whereas the data from the $PAA_{42}PAM_{97}$ sample, with a relatively low fraction of N_{PAM}, nicely follow Equation 4.15, which is based upon hard sphere repulsion. We explain the cluster formation that is seen at high concentrations with the $PAA_{42}PAM_{208}$ and $PAA_{42}PAM_{417}$ samples from intra-micellar 'entanglement' of the corona chains.
In Figure 4.6, an overview is given of P vs N_{PAM}, as determined by zero-angle scattering, the form factor analysis and the light scattering mass analysis. For all approaches, a decrease of P with increasing N_{PAM} is seen, as was found experimentally[17] and theoretically[18-20] in other studies.
In Figure 4.7, the micellar radii as determined by Equation 4.13 and dynamic light scattering are presented vs N_{PAM}. The dynamic light scattering data agree nicely with the SANS data on a quantitative and qualitative basis. The increase in overall radius

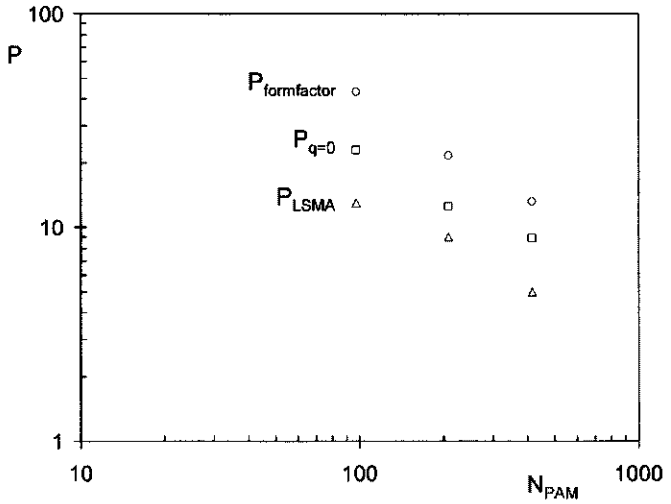

FIGURE 4.6. Aggregation numbers vs N_{PAM}, as determined from the micellar form factor, $q = 0$ (Equation4.16) and the LSMA method. The scaling exponents that were determined for these approaches are -0.82, -0.53, and -0.65 respectively.

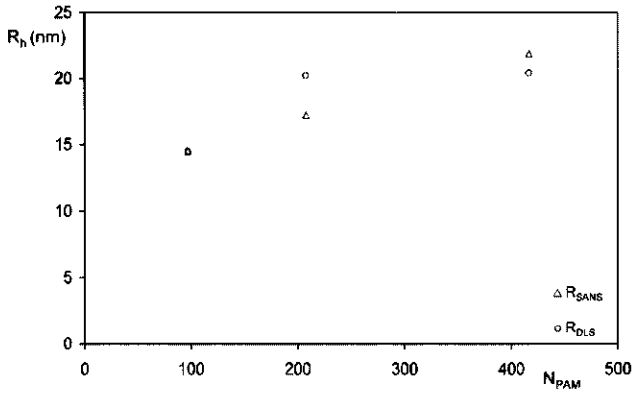

FIGURE 4.7. Micellar radii vs N_{PAM}, determined by dynamic light scattering and the form factor fit parameters (Equation 4.14).

with increasing corona block was also reported by Willner et al.[17]. In Figure 4.8, we present R_{core} and H_{corona} vs N_{PAM}. A decrease of R_{core} with increasing N_{PAM} is seen as expected. The decrease in R_{core} is highly overcompensated by the increase of H_{corona}, thereby increasing R_{micel} with increasing N_{PAM} as was seen in Figure 4.7. In

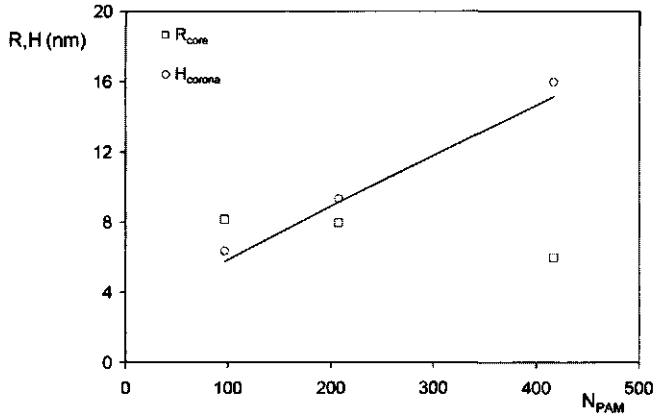

FIGURE 4.8. Radius of core R and thickness of corona H , as determined from the form factor fit parameters. The solid curve (H_{corona}) is calculated from Equations 2.6 and 2.7, with $l = 0.25$, and $\upsilon = 0.8$.

Figure 4.8, we compare the experimental corona thickness with the analytical model by Wijmans and Zhulina[21], who presented analytical expressions for H_{corona} (see Chapter 2, Equations 2.6 and 2.7), that predict the thickness of a polymer layer grafted unto a curved surface. The model calculations are denoted by the solid curve, that agrees nicely with the experimental data points. The mimicking of the stretching of the corona chains by an outward displacement of the starting point of the chains thus gives a good quantitative description of the dimensions of the corona.

4.6. SANS data with various f_{PVP}

In Figure 4.9, SANS data are presented that were obtained with the $PAA_{42}PAM_{97}$ system for $f_{PVP} = 0.38$, 0.42, 0.48, and 0.50. As can be seen in Figure 4.1a, these f_{PVP} values start just beyond the critical excess anionic charge (CEAC) ($f_{PVP} = 0.38$) and end just at the PMC ($f_{PVP} = 0.50$). In Figure 1.8, we plotted a schematic view of the concentrations of the separate components, soluble complex particles (SCP), and micelles as a function of composition of the system. Going from $f_{PVP} = 0.38$ to 0.50, we thus expect a decrease of the concentration of SCP and an increase of the micellar concentration. Moreover, we stated that at the PMC, $C_{SCP} = 0$ and $C_{micelles}$ is at a maximum. The experimental curves in Figure 4.9 were fitted using the $PAA_{42}PAM_{97}$ fit parameters as presented in Table 4.5, and the micellar concentration, R_{hs} and η were optimized. The micellar concentrations that were obtained were 17.6, 22.4, 29.5, and 38.2 gram/litre were found for $f_{PVP} = 0.38$, 0.42, 0.48, and 0.50 respectively. An increase in the micellar concentration is thus seen, going from the CEAC to the PMC, thereby confirming the speciation diagram. Yet, going from $f_{PVP} = 0.50$ to 0.38, a

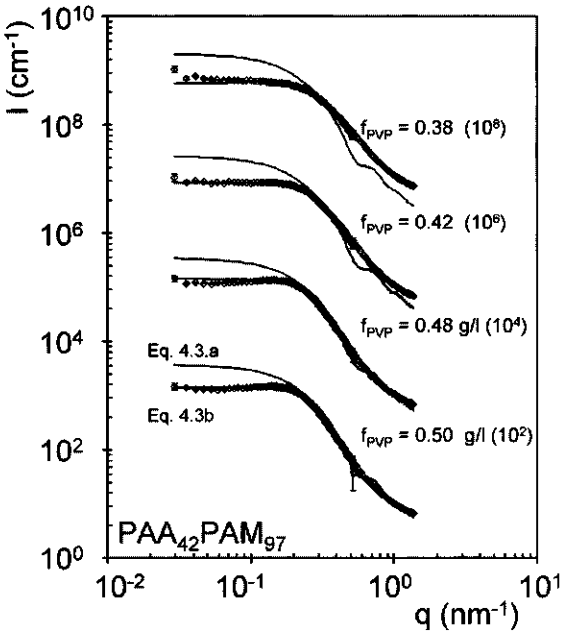

FIGURE 4.9. SANS data for the $PAA_{42}PAM_{97}$ sample with various f_{PVP}. Total concentration in all experiments was around 38.2 g/l. The offset factors of the data are given in the figure. As in Figures 4.3 - 4.5, there are two model curves per experiment, where the upper solid lines represent Equation 4.3a, and the lower solid lines represent Equation 4.3b.

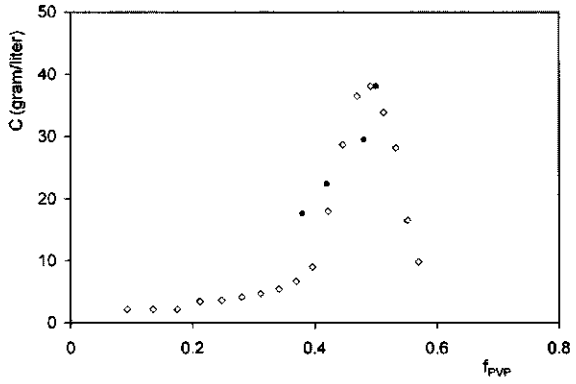

FIGURE 4.10. The same I_{LS} data as in Figure 4.1a only now normalized for the polymer concentration of the SANS sample at the PMC such that $I_{LS,max}$ corresponds to 38.1 gram/litre, together with the weight concentrations of $PAA_{42}PAM_{97}$ micelles for various f_{PVP}, as determined from Figure 4.9.

decrease is seen in the quality of the description of the experimental curves by the model. We attribute this to increasing concentrations of SCP, that are not taken into consideration in the model. Therefore, the concentrations that were found may not be too exact, yet, the trend is clear. As the overall polymer concentration is roughly constant for the experiments shown in Figure 4.9, this means that for $f_{PVP} = 0.38$, the SCP concentration is around 20 g/l, and a proper fit of the experimental data cannot be expected from a micellar form factor only. In Figure 4.10, we present the concentrations that were found vs. f_{PVP}, and the light scattering data from Figure 4.1a. The light scattering data are normalized to the polymer concentration at the PMC, as $I \propto c$ where c is the number density of micelles in solution. Clearly, $\partial C/\partial f_{PVP}$ are different for the two data-sets, with the light scattering data probably being the most reliable. Yet, the increase of c, upon going from the CEAC to the PMC is very well illustrated by these experiments.

4.7. Conclusions

We conclude that the model is suitable for obtaining P and ϕ from the SANS data, as the values are in agreement with those found in earlier studies. The complex coacervate core micelles show a pronounced concentration effect in the scattering data. With a relatively large core, this concentration effect can be described by a hard-sphere structure factor. If the length of the corona block is much longer than the core block, the micelles form clusters at high concentration, and this effect cannot be described by the hard-sphere structure factor. The concentration of micelles in the system is a function of the composition. At the PMC, the micellar concentration is at a maximum. Recommendations for future SANS experiments on complex coacervate core micelles include the use of (partially) deuterated diblock-copolymers, so that the corona excess scattering length can be matched to that of the solvent. This would allow for a detailed analysis of the core internal structure. At this moment, the interference between PAA and PVP and the nature of the core-solvent interface are still unknown. In addition, SANS experiments in a wider range of compositions than the present study may shed some more light on the speciation of the mixture into free molecules, soluble complex particles, and complex coacervate core micelles.

Acknowledgement We thank Dr. B. Farago from the Institut Laue Langevin, Grenoble, France for assistance during the experiments and data handling. We thank the Institut Laue Langevin for providing beam time.

4.8. References

1. J.S. Pedersen, I.W. Hamley, C.Y. Ryu, and T.P. Lodge, Macromolecules, 2000. 33: p. 542-550.
2. J.S. Pedersen, C. Svaneborg, K. Almdal, I. W. Hamley, and R. N. Young, Macromolecules, 2003. 36: p. 416-433.
3. J. S. Pedersen, Journal of Chemical Physics, 2001. 114: p. 2839-2846.
4. J.S. Pedersen and M.C. Gerstenberg, Macromolecules, 1996. 29: p. 1363-1365.
5. L. Willner, A. Poppe, J. Allgaier, M. Monkenbusch, P. Linder, and D. Richter, Europhysics Letters, 2000. 51: p. 628-634.
6. L. Willner, J. Allgaier, M. Monkenbusch, and D. Richter, Europhysics Letters, 2001. 55: p. 667-673.
7. Y-Y Won, H.T. Davis, and F.S. Bates, Journal of Physical Chemistry B, 2000. 104: p. 7134-7143.
8. V. Castelletto, I.W. Hamley, and J.S. Pedersen, Journal of Chemical Physics, 2002. 117: p. 8124-8129.
9. W. Groenewegen, A. Lapp, S.U. Egelhaaf, and J.R.C. van der Maarel, Macromolecules, 2000. 33: p. 4080-4086.
10. W. Groenewegen, S.U. Egelhaaf, A. Lapp, and J.R.C. van der Maarel, Macromolecules, 2000. 33: p. 3283-3293.
11. J.S. Pedersen, Advances in Colloid and Interface Science, 1997. 70: p. 171-210.
12. P. Hervé, M. Destarac, J.-F. Berret, J. Lal, J. Oberdisse, and I. Grillo, Europhysics Letters, 2002. 58: p. 912-918.
13. J-F. Berret, P. Hervé, O. Aguerre-Chariol, and J. Oberdisse, Journal of Physical Chemistry B, 2003. 107: p. 8111-8118.
14. J.-F. Berret, G. Cristobal, P. Hervé, J. Oberdisse, and I. Grillo, The European Physical Journal E, 2002. 9: p. 301-311.
15. C. Wandrey, A. Bartkowiak, and D. Hunkeler, Langmuir, 1999. 15: p. 4062-4068.
16. J. Brandrup and E.H Immergut, Polymer Handbook. 3rd. ed, ed. J. Brandrup and E.H. Immergut. 1989: John Wiley and Sons: Chichester.
17. S. Forster, M. Zisenis, E. Wenz, and M. Antonietti, Journal of Chemical Physics, 1996. 104: p. 9956-9970.
18. R. Nagarajan and K. Ganesh, Journal of Chemical Physics, 1989. 90: p. 5843-5855.
19. O.V. Borisov and E.B. Zhulina, Macromolecules, 2002. 35: p. 4472-4480.
20. C. M. Wijmans and E.B. Zhulina, Macromolecules, 1993. 26: p. 7214-7224.

CHAPTER 5

Complex Coacervate Micro-emulsions

ABSTRACT

Electrostatically driven self assembly was studied with a three-component system: annealed polybase, annealed polyacid, and a double hydrophilic diblock-copolymer, consisting of an annealed polyacid block and a water-soluble neutral block of varying block length. The main parameter investigated was the mixing ratio of polyacid homopolymers and diblock-copolymer. Without the homopolymer, complex coacervate core micelles are formed. The radius of the micelles, determined with dynamic light scattering, was very sensitive to the fraction of homopolymer, and increased from 25 to 150 nm, when the fraction of homopolymer was increased from 0 to 0.6. Preferably, the micelles formed at compositions where the total number of cationic groups slightly exceeded the number of anionic groups. The mixing ratio polyacid and diblock-copolymer did not affect the preferred composition of the micelles. With increasing amounts of polyacid, the micellar window in the compositional diagram became wider. A semi-quantitative comparison of aggregation numbers with the fraction of polyacid, showed that there are two regimes for the sensitivity of the aggregation number to this polyacid fraction. At low fractions of polyacid, the change in aggregation number is rather sensitive to the polyacid fraction.

Submitted to Langmuir, 2004

5.1. Introduction

Interaction between oppositely charged polyelectrolytes in aqueous solution may result in phase separation when the excess charge sign of the macroscopic mixture is (close to) zero. This phase separation is called complex coacervation. If one of the polyelectrolytes is linked to a water-soluble neutral block, the phase separation can be restricted to colloidal dimensions and complex coacervate core micelles may be formed[1-5]. Upon titrating one of the components with the other component, a so-called preferred micellar composition (PMC) is found, where only complex coacervation core micelles (CCCM's) exist[6, 7].

In Chapter 2 - 4 we have characterized these two-component micelles in bulk solution. In this Chapter, we extend the two-component system to a three-component system, where the third component is a homopolymer with charge sign equal to that of the diblock-copolymer. We show that the micelles can solubilize both cationic and anionic macromolecules, and that the size of the micelles will increase even with small amounts of the third component.

5.2. Materials and methods

The PAA-PAM diblock-copolymers are the same as described in Figure 2.2 and Table 2.2. The PAA-PAM samples were synthesized from the PAA homopolymers that were used in this study, so that the chain length of PAA_{PAA} is the same as the PAA block in the PAA-PAM diblock-copolymers. The PAMA homopolymer was also described in Table 2.2 and Figure 2.2. All other chemicals were of analytical grade.

As our experimental method, we used the light scattering titration that was described in Chapter 2. With this method, a solution of (di-block)-copolymer is titrated with a solution containing an oppositely charged homopolymer. After each dosage, light scattering intensity, pH, and, if possible, radius of the objects was measured. The laser wavelength was 514 nm and all experiments were done at 90°. The scattered intensity is detected with an optical fibre, that discriminates between correlated and non-correlated scattering. The non-correlated scattered intensity is discarded. The composition of the system during these experiments is expressed as f_{PAMA}, defined as

$$f_{PAMA} = \frac{[PAMA]}{[PAMA] + [PAA]} \tag{5.1}$$

where [i] denotes the total molar concentration of chargeable groups of species i in the system. The concentration [PAA] is the sum of the contributions from the PAA-PAM diblock-copolymer PAA-PAM and the PAA homopolymer. The fraction of homopolymer in the system, Λ, is given as

$$\Lambda = \frac{[PAA]_{PAA}}{[PAA]_{PAA} + [PAA]_{PAA-PAM}} \tag{5.2}$$

where $[PAA]_{PAA}$ denotes the PAA homopolymers and $[PAA]_{PAA-PAM}$ denotes the PAA groups from the PAA-PAM diblock-copolymer. All concentrations in Equation 5.2 are expressed in terms of ionizable groups.

All experiments were performed at a starting pH of 6.7 for the bulk solutions (PAMA, PAA and PAA-PAM), T = 293 K, and ionic strength of 30 mM $NaNO_3$. The starting pH was obtained by adding acid or base to the polymer solutions. Polymer concentrations were 1 gram/litre for the PAA-PAM solutions, corresponding to around 2 mM chargeable groups, 0.3 gram/litre for the PAA solutions, and 6 grams/litre for the PAMA solution. The volume changes during the titrations were in the order of 5 percent. The solutions of PAA-PAM diblock-copolymers (and PAA homopolymers) were in the titration cell, and these solutions were titrated with the PAMA solution.

5.3. Results and Discussion

In Figures 5.1, 5.2 and 5.3 we show data from dynamic light scattering titration experiments for $PAA_{42}PAM_{97}$ with $\Lambda = 0$, 0.10 and 0.37, for $PAA_{42}PAM_{208}$ with $\Lambda = 0$, 0.10 and 0.19, and for $PAA_{42}PAM_{417}$ with $\Lambda = 0$, 0.13 and 0.43, respectively. In Figures 5.1a, 5.2a and 5.3a the 90° light scattering intensities (I) are plotted vs. f_{PAMA}. The pattern of the data clearly follows that of the light scattering diagram in Figure 1.9. With increasing Λ, we observe an increase of the width of the micellar window (the range where the peak occurs) covers larger parts of f_{PAMA} than with $\Lambda = 0$. In addition, the I values at the PMC are much higher with $\Lambda > 0$. Despite these high I values, the solutions were still optically clear. In Figures 5.1b, 5.2b, and 5.3b the pH data are shown. As the pH of all stock solutions was set at pH = 6.7, changes in pH result from changes in pK and charge density that the polyelectrolytes undergo upon complexation. From the pH data and the I data, the PMC can be found. In Chapters 2 and 3 we have shown that at the PMC, both I and $\partial pH/\partial f_{PAMA}$ are at a maximum. In Figure 5.1, we see that this situation is found at $f_{PAMA} \approx 0.4$. This slight excess of $f_{PAA}(f_{PAA} = 1 - f_{PAMA})$ at the PMC has been observed before with PAA and PAMA as polyelectrolytes[7]. The PMC is not sensitive to Λ and was always found at $f_{PAMA} \approx 0.4$. In addition, an experiment with $\Lambda = 1$ has been performed, and a macroscopic phase separation was observed between $f_{PAMA} = 0.2$ and $f_{PAMA} = 0.6$.

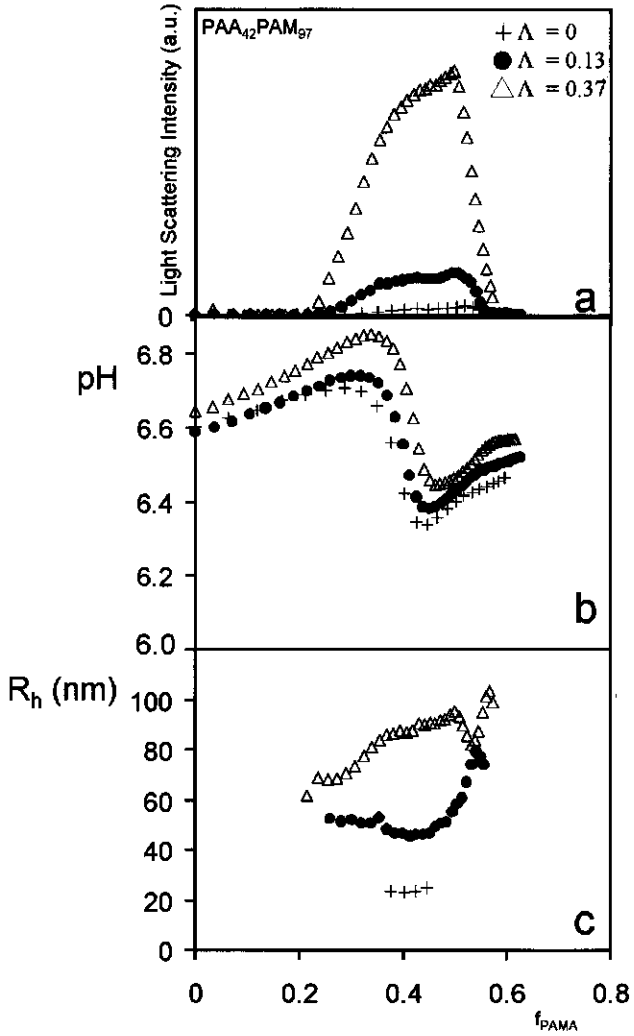

FIGURE 5.1. Experimental data from light scattering titration experiments for $PAA_{42}PAM_{97}$ with $\Lambda = 0$, 0.13 and 0.37. (a) Light scattering intensity, (b) pH, (c) Hydrodynamic radii.

In Figures 5.1c, 5.2c and 5.3c we show the hydrodynamic radii R_h of the micelles. For the $\Lambda = 0$ experiments, the R_h values agree with those found in Chapter 2, and are around 20 - 30 nm. For $\Lambda > 0$, the particles are (much) larger than with $\Lambda = 0$.
We have seen that with the two-component PAA-PAM/PAMA system, CCCM's are formed with a core-shell structure. In addition, with the two-component PAA/PAMA

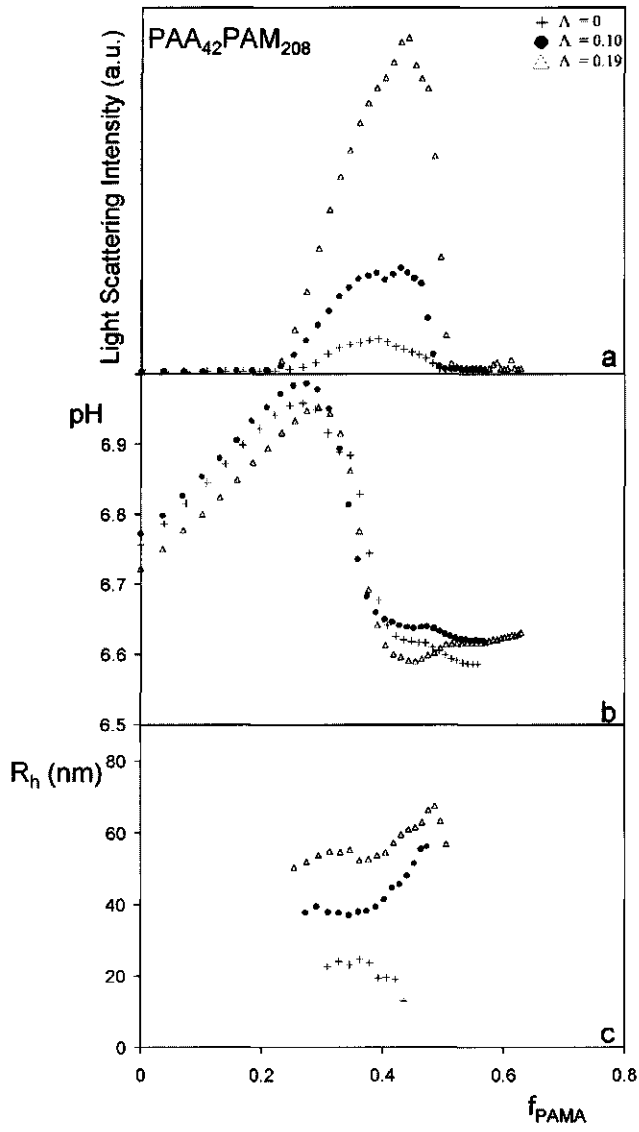

FIGURE 5.2. Experimental data from light scattering titration experiments for $PAA_{42}PAM_{208}$ with $\Lambda = 0$, 0.10 and 0.19. (a) Light scattering intensity, (b) pH, (c) Hydrodynamic radii.

system, a macroscopic phase separation was observed. When these two two-component systems are combined into the three component PAA/PAA-PAM/PAMA system, colloidal objects are formed, that are much larger than the two-component CCCM's, but

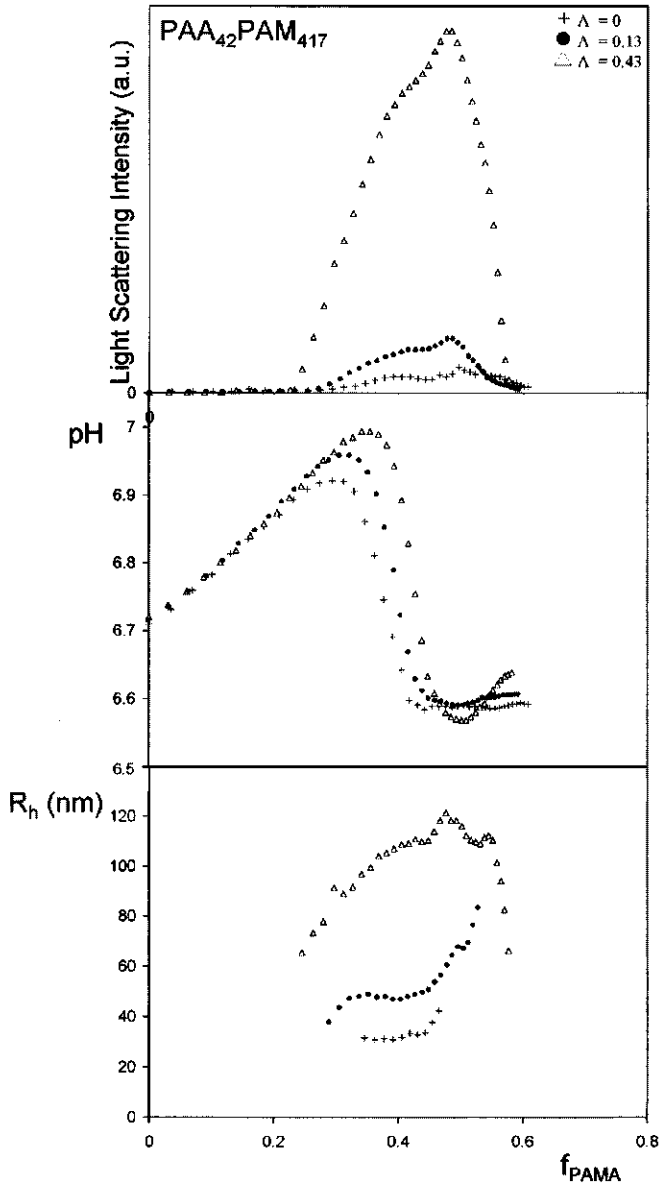

FIGURE 5.3. Experimental data from light scattering titration experiments for $PAA_{42}PAM_{417}$ with $\Lambda = 0$, 0.13 and 0.43. (a) Light scattering intensity, (b) pH, (c) Hydrodynamic radii.

no phase separation was seen. So, apparantly, a coexistence of the two-components results, CCCM and a macroscopic phase separation, is unfavorable as it is not observed. As these larger particles are still colloidally stable, we believe that they have the same core-shell structure as the CCCM with PAM chains in contact with the solvent, only now the core has more internal structure. The interior of the core is formed by the PAA chains and part of the PAMA chains, whereas the exterior of the core is formed from the other part of the PAMA chains and the PAA blocks from the PAA-PAM diblock-copolymers. In Figure 5.4, we show a sketch of these particles, and we will call them complex coacervate core particles (CCCP). In contrast to the aggregation shown in Figure 1.7, we see that the interior of the core is formed by a neutral complex coacervate of the two oppositely charged homopolymers. The micelle has now become an emulsified droplet of complex coacervate, that is colloidally stabilized by the PAA-PAM diblock-copolymers. The CCCP that are formed with $\Lambda > 0$ thus have a significantly

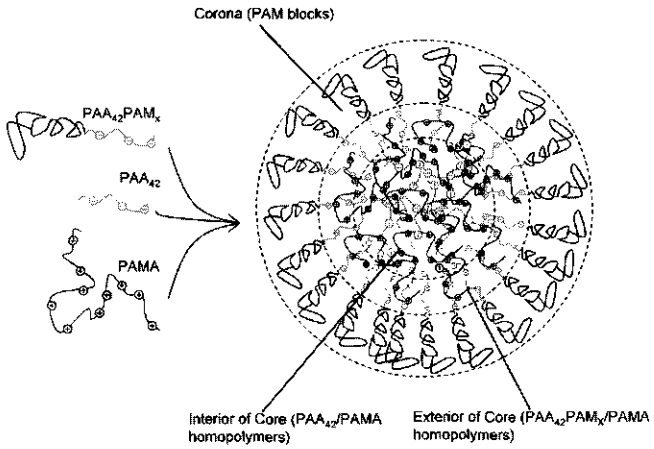

FIGURE 5.4. Sketch of the formation of CCCP.

higher molar mass, which explains the higher I values for the $\Lambda = 0.10$ experiment in Figures 5.1c, 5.2c, and 5.3c as $I \propto CM$ (C is the weight concentration of and M is the molar mass). Yet, an analysis of the absolute I values (light scattering mass analysis method), as described in Chapter 2) gave a poor agreement with the experimentally determined radii and it turned out that the measured intensities were (greatly) underestimated. We attribute this to form factor effects due to the large size of the CCCP, that causes a lowering of $P(q)$ in Equation 1.10a., as $P(q) < 1$ if $R_h * 20 > \lambda$.
In Figure 5.5, the radii of the CCCP at the PMC are plotted vs. for $PAA_{42}PAM_{97}$, $PAA_{42}PAM_{208}$, and $PAA_{42}PAM_{417}$. A linear increase of R_h is observed for all PAA-PAM samples. At $\Lambda = 0$, the sizes of the CCCM agree with those found in Chapter

2 with the same polymer samples. It is easily understood that at $\Lambda = 1$, R_h goes to infinity because there is no stabilizng PAM block. In this study, we focus on objects in solution and do not consider the so-called 'emulsification failure' which would be the value of where the PAA-PAM diblock-copolymers can no longer stabilize the system and a phase separation is expected. It is seen from the data in Figure 5.3 that large droplets of complex coacervate can be stabilized. If we assume that the contribution of the thickness of the PAM corona to the radius of the objects is independent of Λ, the largest droplets of coacervate that are solubilized are over 100 nm in radius. The increase in molar mass of the CCCP can, in a rough approach, be estimated from $(R_{\Lambda=0.6}/R_{\Lambda=0})^3$ and is around 2 orders of magnitude for the highest values of Λ. In

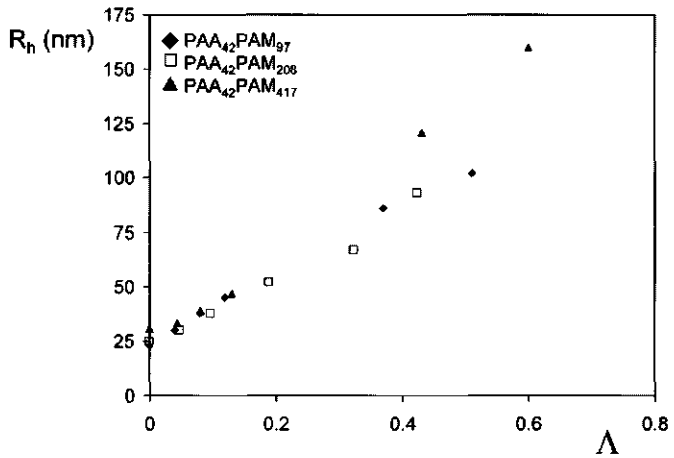

FIGURE 5.5. Hydrodynamic radii R_h of the CCCM and CCCP at the PMC (f_{PAMA} = 0.4) vs λ for $PAA_{42}PAM_{97}$, $PAA_{42}PAM_{208}$, and $PAA_{42}PAM_{417}$.

Figure 5.6, we show the experimentally determined aggregation diagram of the system, now given as Λ vs. f_{PAMA} instead of I vs. f_{PAMA}. This diagram was constructed from all I vs. f_{PAMA} curves, by taking all f_{PAMA} values where a sharp change in $\partial I/\partial f_{PAMA}$ was observed. In Figure 1.9, we have called these points critical excess cationic charge (CECC) and critical excess anionic charge (CEAC). In Figure 5.1c these points are found at $f_{PAMA} \approx 0.2$ (CECC) and $f_{PAMA} \approx 0.5$ (CEAC). The solid black lines are linear fits through the data points. We see that the micellar window widens a bit if Λ is increased. This can be understood if the different contributions to the free energy balance of micellization are considered. The driving force for phase separation for both the CCCM and the CCCP are (i) the entropy gain of the system that is generated from the release of the counterions from the polyelectrolyte double layers and (ii) the decrease of electrostatic energy, that arises from the enhanced screening of the charges

in the coacervate phase, compared to the bulk solution. The equilibrium aggregation number is then determined by (a) the surface free energy, i.e. the area of core/solvent interface per chain. This contribution favors high aggregation numbers, so that the core/solvent contact area per molecule is low. The steric and excluded volume effects of core and corona block, respectively, favor low aggregation numbers, as (b) high aggregation numbers lower the conformational entropy of the core block by strong stretching and (c) minimization of the core/solvent contact area generates a high grafting density of corona chains on the core/solvent interface, which is unfavorable. With the CCCP,

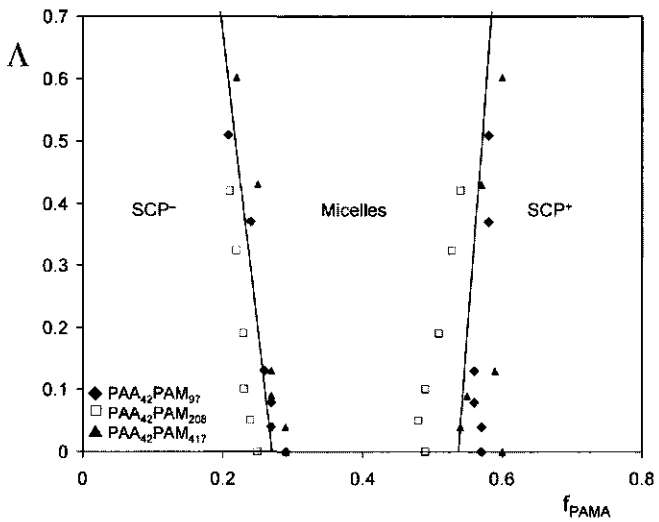

FIGURE 5.6. Speciation diagram of the CCCM, CCCP and $SCP^{+,-}$ (soluble complex particles). The data points were obtained by taking the upper and lower f_{PAMA} values of the micellar peak boundaries in the I vs f_{PAMA} data. Solid lines are linear fits through all data points.

satisfying condition (a) is less accompanied by a strong stretching of the core block (b) and high osmotic pressure in the corona (c). The interior of the core is formed from the PAA/PAMA homopolymers, thereby relaxing condition (b) as the core block does not need to stretch from core/corona interface to the centre of the core and condition (c) as the number of PAM chains per unit core material decreases (and thus also the grafting density of PAM chains at the core/corona interface) with increasing Λ. Apparently, this leads to the wider micellar range with increasing Λ.

Although the PAA homopolymers are not chemically linked to the PAA-PAM molecules, one could consider their presence as an increase of N_{core}. An increase of Λ thus can be

seen as an increase of the fictive length of the core block, N'_{core} given as

$$N'_{core} = N_{core}\frac{1}{1-\Lambda} \tag{5.3}$$

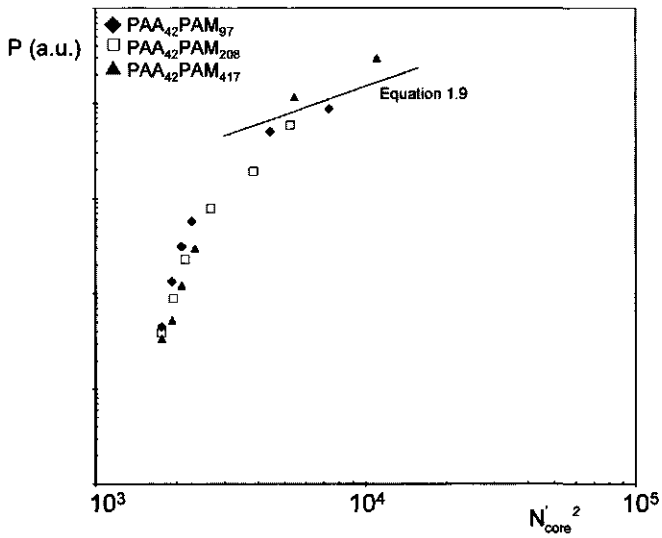

FIGURE 5.7. Dependence of P on ${N'_{core}}^2$. Experimental data were obtained by Equations 5.3 and 5.4, the solid line is the crew-cut limit scaling law from Borisov and Zhulina[10]

By introducing N'_{core}, the aggregation number of the micelles can be expressed as the number of PAM chains per micelle. The thickness of the micellar coronas for the PAA-PAM samples was estimated by SANS described in Chapter 4, where it was found that the corona thickness is 6.4, 9.3, and 16 nm for $PAA_{42}PAM_{97}$, $PAA_{42}PAM_{208}$, and $PAA_{42}PAM_{417}$ respectively. Let us simplify the physical picture a bit and assume that this corona thickness is independent of R_{CCCP}, and thus independent of Λ. Assuming a constant core density, the aggregation number can then be estimated as

$$P \propto (R_{CCCP} - H_{corona})^3 \tag{5.4}$$

Borisov and Zhulina[9] found that for the crew-cut limit in block-copolymer micelles the following scaling relation ship is valid: $P \propto N^2_{core}$. In Figure 5.7, P is plotted in arbitrary units vs ${N'_{core}}^2$ to see the dependence of P on ${N'_{core}}^2$ on double logarithmic scales. In Figure 5.7, we also show this scaling prediction. Firstly, we see that the dependence of P on ${N'_{core}}^2$ clearly has two regimes. At low values for ${N'_{core}}^2$, P is very sensitive to variations in ${N'_{core}}^2$, whereas at higher values for N'_{core} the aggregation number is much less sensitive. We think that for $N'_{core} >> N_{core}$, we are in the crew-cut

regime, as $R_{core} >> H_{corona}$. At these higher N'_{core} values, the scaling exponent of the experimental data seems not too different from the Borisov and Zhulina model. Yet, the number of data points is somewhat too low to determine whether or not the model and experiment are in good agreement.

5.4. Conclusions

We have studied three-component electrostatically associating colloidal objects. The components were PAMA and PAA homopolymer, and PAA-PAM diblock-copolymer. The block length of the PAA block in the diblock-copolymer was equal to the chain length of the PAA homopolymer. Dilute solutions of PAA and PAA-PAM were premixed, and titrated with the PAMA solution. The main parameter investigated was the PAA/PAA-PAM mixing ratio. This mixing ratio did not influence the PMC, that was always found around $f_{PAMA} = 0.4$. The radius of the particles, however, was very sensitive to the mixing ratio of PAA and PAA-PAM. Without PAA, the particle hydrodynamic radius was around 25 nm, and when half of the PAA groups in the mixture originated from the PAA homopolymer, the CCCPs were over a 100 nm hydrodynamic radius. These particles may also be considered complex coacervate micro-emulsions.

From the data, we deduced that the interior of the particle core consists of both homopolymers, and that the exterior of the core is formed from the PAMA homopolymers and the PAA block from the diblock-copolymer. By this finding, the concept of 'encapsulating' homopolymers *oppositely* charged to the diblock-copolymer only, as shown in Figure 1.7 is extended. The results in this paper show that both anionic and cationic polyelectrolytes can be encapsulated in a complex coacervate core micelle. From an applied point of view, one can say that this three component approach dramatically lowers the amount of (expensive) diblock-copolymer that is required to emulsify complex coacervate material. From simple analysis we found that the molar mass of a CCCP may be two orders of magnitude larger than the molar mass of a CCCM. A comparison with scaling models for relations between aggregation numbers and block lengths for hydrophobically associating systems, showed that the crew-cut regime seemed to apply for the largest particles, where the radius of the core is much larger than the thickness of the corona.

5.5. References

1. A. Harada and K. Kataoka, Macromolecules, 1998. 31: p. 288-294.
2. A. Harada and K. Kataoka, Langmuir, 1999. 15: p. 4208-4212.
3. A. Harada and K. Kataoka, Macromolecules, 1995. 28: p. 5294-5299.

4. A.V. Kabanov, T. K. Bronich, V.A. Kabanov, K. Yu, and A. Eisenberg, Macromolecules, 1996. 29: p. 6797-6802.
5. M.A. Cohen Stuart, N.A.M. Besseling, and R.G. Fokkink, Langmuir, 1998. 14: p. 6946-6849.
6. S. van der Burgh, A. de Keizer, and M.A. Cohen Stuart, Langmuir, 2004, 20, pp 1073 - 1084(Chapter 2 of this thesis)
7. S. van der Burgh, A. de Keizer, and M.A. Cohen Stuart, Submitted to Macromolecules, 2003. (Chapter 3 of this thesis)
8. N. Hoogeveen, M.A. Cohen Stuart, and G. J. Fleer, Macromolecular Chemical Physics, 1996. 197: p. 2553-2564.
9. O.V. Borisov and E.B. Zhulina, Macromolecules, 2002. 35: p. 4472-4480.

CHAPTER 6

Complex Coacervation Core Micelles on Silica and Polystyrene Surfaces

ABSTRACT

The adsorption of mixtures of a diblock-co-polymer with a negatively charged block and a neutral, hydrophilic block and an oppositely charged homopolymer on anionic and hydrophobic surfaces was studied with reflectometry. It turned out that the adsorbed mass is at a maximum when the number of cationic and anionic polyelectrolyte groups is equal. In bulk solution, the components form micelles at this composition. The thickness of the layers was in the order of the micellar radius in bulk solution, i.e. 25 nm. The adsorption kinetics are sensitive to block lengths of the diblock-copolymer. The adsorbed layers were stable with respect to solvent exposure and even 1 M ionic strength could not completely erode the layers. The layers dramatically influenced the functionality of the surface, as they acted as excellent anti-fouling agents versus protein adsorption.

6.1. Introduction

The formation of multilayers from oppositely charged polyelectrolytes on charged surfaces is an area of growing interest[1-5]. For applied aspects, one can think of e.g. surface modification[5] or enzyme immobilization[6]. Another method to modify surface functionality is by adsorbing a *grafted* polymer layer unto a surface[7].
In Chaptes 2 - 4, the aggregation mechanism, colloidal stability, and charge neutralization of complex coacervation core micelles (CCCM) has been studied. Here, we present results on adsorption of oppositely charged components on various surfaces. However, we do not feed the components to the surface in an alternating fashion, as is the common practice in multilayering[8, 9]. The components are premixed first and these mixtures are flown along the surface.
Firstly, we characterize the layers that are formed upon exposing various surfaces to a wide range of mixing ratio's of the CCCM components. The results are discussed in terms of adsorption kinetics, adsorbed mass plateau values, and reversibility of the layer formation. Secondly, changes in surface functionality upon adsorption are demonstrated.

6.2. Materials and methods

Materials. Light scattering (titration) experiments were described in Chapter 2. For reflectometry experiments, we used silica in the form of silicon wafers (Aurel GmbH, Germany) carrying an oxide layer of about 73 nm as determined by ellipsometry. The polystyrene coated wafers carried an oxide layer of about 41 nm, on top of which was a 66 nm polystyrene layer. A colloidal solution of silica particles with a radius of 95 nm was prepared in our own Laboratory according to the Stöber method[10]. Before use, this silica solution was diluted to the appropriate concentrations with 10 mM $NaNO_3$ solution and treated ultrasonically during an hour. Lysozyme was obtained from Sigma, L6876, lot.nr. 51K7028 and was used as received. At pH = 7, a silica surface is negatively charged, as its iso-electric point is at p$H \approx 2$[11]. The poly(acrylic acid)-co-poly(acryl amide) (PAA-PAM) and poly(*N*-ethyl-4-vinylpyridiniumbromide) were described in Table 2.2. and Figure 2.2. All other chemicals were of analytical grade.
All experiments were performed at pH = 7 and ionic strength of 10 mM $NaNO_3$. Typical polymer concentrations were 0.2 - 0.5 g/l for PAA-PAM and 0.1 g/l for PVP, corresponding to approximately 0.4 mM PAA and PVP monomeric units. In our experiments, the composition of the PAA-PAM/PVP mixtures was expressed as f_{PAA}, given as

$$f_{PAA} = \frac{[PAA]}{[PAA] + [PVP]} \tag{6.1}$$

where [PAA] and [PVP] denote overall concentrations, expressed in terms of the monomeric groups.

Reflectometry. The amount of adsorbed polymer per unit area deposited on substrates during exposure to various solutions was monitored by reflectometry. The solutions were supplied to the substrate by means of an impinging-jet flow cell, as described extensively elsewhere[12, 13]. In this technique, raw reflectometry data appears in the form of real time changes in the signal ΔS, that can be converted into an absolute adsorbed mass per unit area, Γ (mg/m^2), by

$$\Gamma = \frac{1}{A_s}\frac{\Delta S}{S_0} \tag{6.2}$$

where S_0 is the signal from the bare surface and A_s is a sensitivity factor. The latter is proportional to the $\partial n/\partial c$ value of the solution containing the adsorbate, and also depends on other parameters, such as the thickness of the oxide layer, wavelength of the laser beam, and angle of incidence. As our layers are not homogeneous, the $\partial n/\partial c$ of the adsorbed layer cannot be calculated straightforwardly. At this moment, the composition of our adsorbed layers is not known precisely and therefore we will only present the ΔS data, with respect to the value of S_0 just before addition of the adsorbate, i.e. $\Delta S/S_0$ vs. time(s). Semiquantitatively, however, ΔS is linear with the adsorbed mass per unit area, with 0.1 unit of $\Delta S/S_0$ corresponding to roughly 2 mg/m^2 on the silica surfaces and to 4 mg/m^2 on the polystyrene surfaces respectively. The reflectometry experiments were performed as follows. Firstly, a 10 mM $NaNO_3$ solution was flushed through the cell, until a stable baseline was reached. At that point, we switched to a solution containing the adsorbates, and we recorded $\Delta S/S_0$.

The reflectometry data can be analysed by using the following kinetic equations. Firstly, the flux of micelles to the surface is given by

$$J = kv^{1/3}D^{2/3}(c_b - c_s) \tag{6.3}$$

where k is an experimental set-up parameter, v is the kinematic viscosity of the solution, D is the diffusion coefficient of the adsorbing particles and c_b and c_s are the weight concentrations of adsorbate in the bulk and close to the surface, respectively[12]. The flux J can be linked to the time derivative of the reflectometry data, $\partial(\Delta S/S_0)/\partial t$ data as follows:

$$\left(\frac{\partial\frac{\Delta S}{S_0}}{\partial t}\right)_0 = \beta J \tag{6.4}$$

where the subscript zero denotes the initial adsorption rate. At this initial stage, c_s in Equation 6.4 is essentially zero. The value of β distinguishes between the transport-limited case ($\beta = 1$) and the attachment-limited case ($\beta < 1$)[11, 14].

6.3. Results and Discussion

6.3.1. Characterization of the layers

In Figure 6.1, we show plateau adsorption values as well as light scattering intensity data vs. f_{PAA}, for mixtures of PVP with $PAA_{42}PAM_{97}$ and $PAA_{42}PAM_{417}$ respectively, on a silica surface. We see that at $f_{PAA} = 0.5$, the intensity and adsorption are both at a maximum for both samples. For the light scattering intensity, this is in agreement with the results in Chapters 2 and 4, where we have shown that for PAA/PVP the preferred micellar composition (PMC) is reached at roughly equal amounts of PAA and PVP groups. For both $PAA_{42}PAM_{97}$ and $PAA_{42}PAM_{417}$, we see that the plateau adsorption values are also at a maximum at the PMC. Thus with a micellar system, the highest adsorbed mass is found at the PMC. The maximum values for both samples are roughly equal, around $\Delta S/S_0 \approx 0.09$ for $f_{PAA} = 0.5$, corresponding to around 3 mg/m^2.

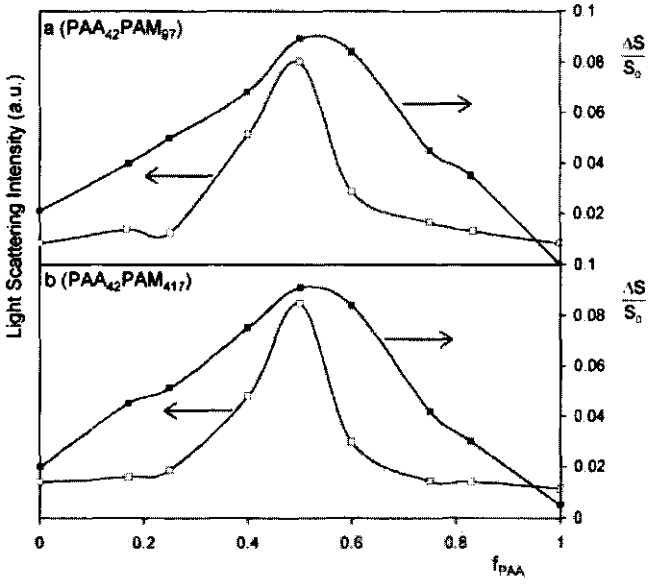

FIGURE 6.1. Reflectometry plateau values (filled squares, right hand side vertical axis) and light scattering intensity data (open squares, left hand side vertical axis) for $PAA_{42}PAM_{97}$ and $PAA_{42}PAM_{417}$ on silica surface at pH = 7 and 10 mM $NaNO_3$.

In Figure 6.1, it is clear that the pure components $PAA_{42}PAM_{97}$ and $PAA_{42}PAM_{417}$ barely adsorb on the silica surface. This is relevant information, and may shed some light on the adsorption process. The corona blocks thus have no affinity for the surface, so that the driving force for micellar adsorption must come from the core material. In

order to study the adsorption process in more detail, we show for $f_{PAA} = 0$, 0.25, 0.5, and 0.83 the raw reflectometry data in Figure 6.2. The silica surface was exposed to polymer solutions after a stable baseline was reached. The moments where the flow was switched from solvent (10 mM $NaNO_3$ solution) to polymer solution corresponds to the abrupt rise of the signal. The positions of the moments of addition on the horizontal axis are fully arbitrary. In this figure, there is a quite a lot of information with respect to kinetics. Although the adsorption plateau levels are roughly equal for the $PAA_{42}PAM_{97}$ and $PAA_{42}PAM_{417}$ micelles ($f_{PAA} = 0.5$), the times needed to reach the plateau are quite different. The $PAA_{42}PAM_{97}$ sample reaches the maximum about three times faster than the $PAA_{42}PAM_{417}$ sample. In order to get insight in these kinetic differences, we recall the results of Chapters 2 and 4, where we showed that the aggregation number of $PAA_{42}PAM_{97}$ is higher than that of the $PAA_{42}PAM_{417}$ sample, which qualitatively agrees with theoretical models for varying corona block lengths[15]. It was found experimentally in Chapter 4, that for the PAA-PAM samples used in this study in combination with PVP, there is a power law dependence of the aggregation number (the number of diblock-copolymers per micelle), P, on the corona chain length with scaling exponent -0.82, i.e. $P \propto M_{PAM}^{-0.82}$. The hydrodynamic radii of the micelles are roughly equal, around 25-35 nm, with the $PAA_{42}PAM_{417}$ sample being somewhat larger than the $PAA_{42}PAM_{97}$ sample. As [PAA] + [PVP] is equal for both samples, the number concentration of micelles is thus roughly a factor four higher for the $PAA_{42}PAM_{417}$ sample, as the aggregation number is four times lower. By simplifying Equations 6.2 and 6.3, we can make a semi-quantitative comparison of the value of β for $PAA_{42}PAM_{97}$ and $PAA_{42}PAM_{417}$. The $\Delta S/S_0$ values can be converted to a number density of micelles on the surface, ρ:

$$\rho \propto \frac{\Delta S}{S_0} \left(\frac{\partial n}{\partial c}\right) M_{micelle}^{-1} \tag{6.5}$$

The $\partial n/\partial c$ values were calculated according to $\partial n/\partial c = \Sigma W_i(\partial n/\partial c)_i$, where W_i is the weight fraction of component i[16], and were almost equal for $PAA_{42}PAM_{97}$ and $PAA_{42}PAM_{417}$. The molar mass of a micelle followed from the molar mass of the components and the aggregation numbers. We assume that k and η are equal for both samples. Furthermore, we assume that (i) D is equal for both samples as R_h is roughly the same as we have seen in Chapters 2 and 4, (ii) that the micelles are spherical: $D \propto R_h^{-1}$, (iii) that [PAA]+[PVP] is equal for both samples, and (iv) c_b can be related the aggregation number by $c_b \propto P^{-1}$. From the above assumptions and Equations 6.3 and 6.4, we now have the following scaling relationship:

$$\frac{\beta_{PAA_{42}PAM_{97}}}{\beta_{PAA_{42}PAM_{417}}} \propto \frac{\left(\left(\frac{\partial \rho}{\partial t} P^{-1}\right)_0\right)_{PAA_{42}PAM_{97}}}{\left(\left(\frac{\partial \rho}{\partial t} P^{-1}\right)_0\right)_{PAA_{42}PAM_{417}}} \tag{6.6}$$

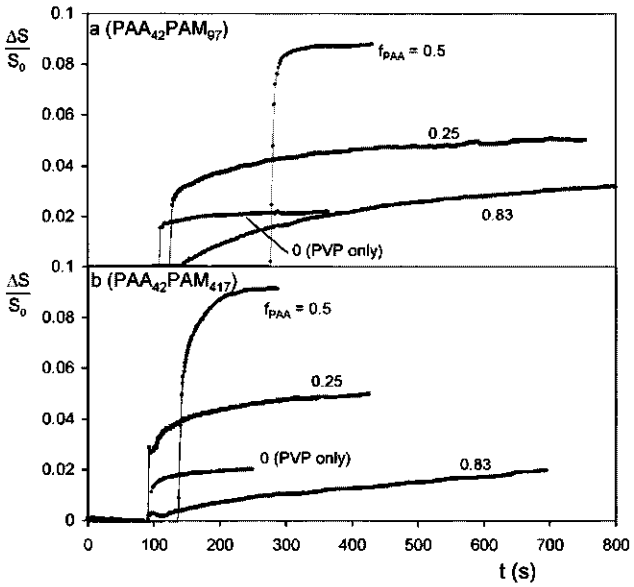

FIGURE 6.2. Reflectometry data for $PAA_{42}PAM_{97}$ and $PAA_{42}PAM_{417}$ for f_{PAA} = 0, 0.25, 0.5, and 0.83 on silica. The moments of sample exposure correspond to the abrupt increments of the signals. Experimental conditions: pH = 7, 10 mM $NaNO_3$, polymer concentration around 0.1 gram/litre.

In our data, the $(\partial\rho/\partial t)_{PAA_{42}PAM_{97}}/(\partial\rho/\partial t)_{PAA_{42}PAM_{417}}$ value were determined to be 0.40 for $f_{PAA} = 0.5$, which corresponds to $\beta_{PAA_{42}PAM_{97}}/\beta_{PAA_{42}PAM_{417}} = 1.6$. A high value of β corresponds to a transport-limited adsorption regime, whereas a low value of β corresponds to attachment-limited regime. Although we have no values of β on an absolute scale, we can say from the β-ratio that the adsorption of the $PAA_{42}PAM_{417}$ sample is somewhat more attachment-limited, and thus slower in kinetics.

The differences in kinetics shed some light on the way the micelles are oriented on the surface. In Figure 6.1, we saw that the pure PAA-PAM does not adsorb on the silica surface. From that we must conclude that the affinity of the micelles for the silica comes from the core material. So, in order to adsorb, the micelles must 'unfold' their core-corona structure to allow for contact between core and surface. It is easily understood from Figure 1.6, that this unfolding process is much easier for the $PAA_{42}PAM_{97}$ sample than for the $PAA_{42}PAM_{417}$ sample, where the thick corona hinders a fast rearrangement of the micellar structure. This is confirmed by the β-ratio between the two samples, that illustrates the difference in kinetics for the initial adsorption stages. Another kinetic difference was seen in the way the curves reach their plateau value, *i.e.* in the way the layer is filled out. It is very likely, that in analogy to Figure 1.6, the

core material makes up a larger part of the layer with the $PAA_{42}PAM_{97}$ sample than with the $PAA_{42}PAM_{417}$ layer, which will be PAM dominated. For a micelle, it thus takes more time to diffuse through the thick brush that is formed by the $PAA_{42}PAM_{417}$ sample, than through the relatively thin brush of the $PAA_{42}PAM_{97}$ sample.
In Figure 6.2 we do not only see kinetic differences with different M_{PAM}, but also with different f_{PAA}. With the $f_{PAA} = 0.83$ samples, we can hardly speak of a plateau, even after 700 seconds, whereas with the $f_{PAA} = 0.25$ kinetics are much faster. As the silica surface is anionic, these kinetic differences can be explained from the excess charge sign of the PAA-PAM/PVP mixture, that is zero at the PMC, cationic below the PMC, and anionic above the PMC. So, with $f_{PAA} > 0.5$, the barriers are not only steric, but electrostatic as well. The repulsion slows down the kinetics to a large extent. This trend was seen for all other raw $\Delta S/S_0$ vs t curves (data not shown).

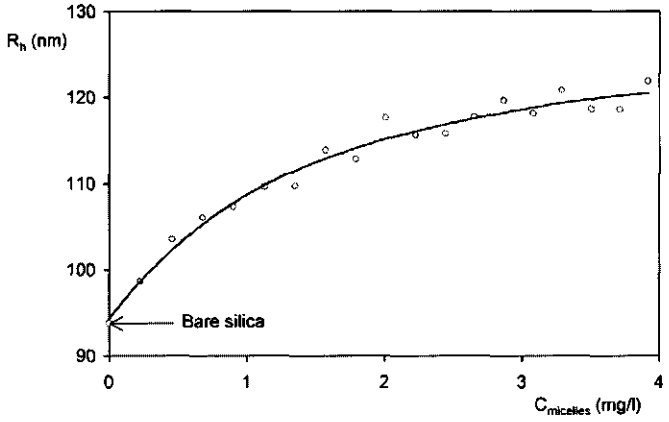

FIGURE 6.3. Overall hydrodynamic radius R_h of silica particles with initial radius 95 nm, covered with $PAA_{42}PAM_{417}$/PVP micelles. Concentration of micelles is given on the horizontal axis.

It is generally known, that adsorption of polymers or polyelectrolytes on colloidal particles may affect their colloidal stability. We have adsorbed the micelles at $f_{PAA} = 0.5$ ($PAA_{42}PAM_{97}$, $PAA_{42}PAM_{208}$, and $PAA_{42}PAM_{417}$) on colloidal Stöber silica particles with radius $R_h = 95$ nm. A solution containing the silica particles was titrated in a light scattering cell with micellar solutions ($f_{PAA} = 0.5$, p$H = 7$). Micellar stock concentration was the same as used with the reflectometry experiments. After every dosage of micellar solution, the light scattering intensity and particle radius were recorded. In Figure 6.3, we show the results for $PAA_{42}PAM_{417}$. Clearly, the overall radius levels off at 120 nm, i.e. the micelles form a layer of 25 nm thickness. This thickness corresponds to the hydrodynamic radius of the micelles, as was determined in Chapter 4 for the $PAA_{42}PAM_{417}$/PVP system. We conclude from this that the micelles do indeed unfold,

so that the core material adsorbs on the surface, and the corona forms a brush on top of the core material, in contact with the solvent. In future work we will present AFM images, to check whether the micelles form patches or a homogeneous layer. Although the concentration of silica in the concentrated stock solutions was not known exactly, an estimate can be made of the adsorbed amount of micelles on the silica particles, if we assume that all micelles are adsorbed on the silica. Here we found that the surface coverage was approximately 1.8 mg/m^2 at the plateau value R_h = 120 nm, which is not too different from the 3 mg/m^2 that was estimated above. Similar titration experiments were performed with micelles formed from PVP and the $PAA_{42}PAM_{97}$ and $PAA_{42}PAM_{208}$ samples, but these micelles did not stabilize the silica particles. Even low micellar concentrations led to precipitates. Apparently, only very long PAM hairs are able to prevent the core material from acting act as a flocculant between the silica particles.

6.3.2. Robustness of the layers vs solvent and high ionic strength

Another interesting phenomenon is the stability of the micellar layers on the silica surfaces. With $f_{PAA} = 0.5$, we have exposed the adsorbed layers to solvent (10 mM $NaNO_3$ solution) and 1 M $NaNO_3$ solution. In Figure 6.4, we again show $\Delta S/S_0$ curves with $f_{PAA} = 0.5$ for $PAA_{42}PAM_{97}$ and $PAA_{42}PAM_{417}$ on silica. After the plateau value was reached, we exposed the layers to the background solvent, i.e. a 10 mM $NaNO_3$ solution. It is clearly seen, that only a few percent of the adsorbed mass is 'rinsed' from the surface. After this quick desorption step, a stable plateau value is again obtained. The layers are thus quite robust when exposed to solvent, and will not spontaneously redistribute over a bulk phase. When the layers were again exposed to the micellar solutions, the adsorbed mass returned to its initial plateau value. Upon exposure to 1 M $NaNO_3$ solution, the adsorbed mass decreased to approximately 80 percent of the original plateau value. In Figure 6.5, we show reflectometry data of adsorption of $PAA_{42}PAM_{97}$ and $PAA_{42}PAM_{417}$ with composition $f_{PAA} = 0.5$ on a polystyrene surface. Clearly, the micelles also adsorb on a hydrophobic surface. The $\Delta S/S_0$ values are somewhat lower than with the silica surface (0.06 vs. 0.09). However, the sensitivity is different, as 0.1 unit $\Delta S/S_0$ corresponds to 2 mg/m^2 for silica and 4 mg/m^2 for polystyrene coated silica. The differences in adsorption kinetics between $PAA_{42}PAM_{97}$ and $PAA_{42}PAM_{417}$ that were observed in Figure 6.3 for adsorption on silica, are also seen with the polystyrene surface. The driving force, however, must be completely different, as the polystyrene surface is uncharged, so that counterion release is not a relevant process. With a hydrophobic surface, the water molecules are 'released' from the polystyrene surface, on which they are trapped in a so-called 'iceberg structure', which is the same driving force for micellization of amphiphilic molecules. The system as a whole thus gains entropy by minimizing the contact area between polystyrene and

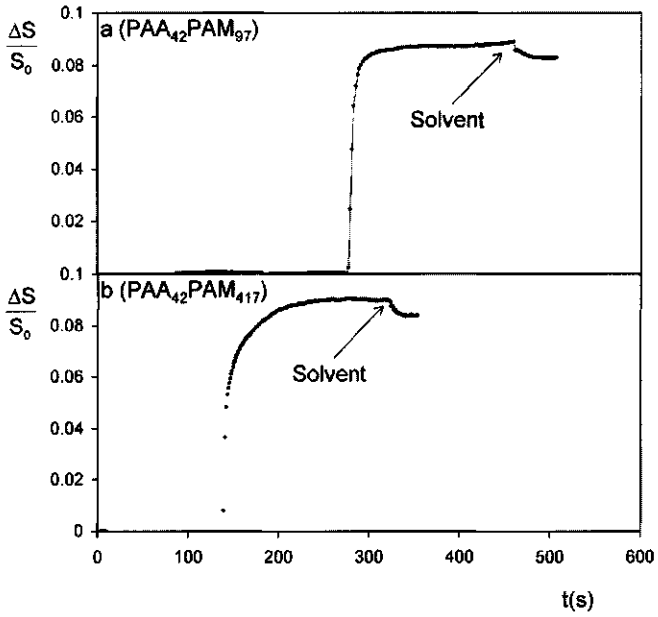

FIGURE 6.4. Effect of exposure of $PAA_{42}PAM_{97}$ and $PAA_{42}PAM_{417}$ with $f_{PAA} = 0.5$ on silica to solvent. Experimental conditions: pH = 7, 10 mM $NaNO_3$

solvent. Also with the micelles on polystyrene, we have tested the robustness of the layers by exposure to solvent and 1 M $NaNO_3$. The results are also given in Figure 6.5. The moments of exposure to solvent are indicated by arrows in the figure. We see that for both $PAA_{42}PAM_{208}$ and $PAA_{42}PAM_{417}$, the exposure to solvent erodes the layers to a somewhat larger extent than with the silica surface. The $PAA_{42}PAM_{97}$ sample was also exposed to 1 M $NaNO_3$ (after the solvent exposure) to check whether the layer could be eroded any further. The exposure to 1 M $NaNO_3$ is indicated in the figure. The large fluctuations in the signal result from large differences in refractive index between 10 mM and 1 M $NaNO_3$, that create a lot of scattering when the liquids are mixed in the reflectometry cell. After a short time, however, we have again a steady signal. We then end up with very low $\Delta S/S_0$ values, which is again due to the difference in refractive index, that leads to a shift of the baseline. In order to have a correct comparison of the plateau value after exposure to 1 M $NaNO_3$, we again changed to 10 mM $NaNO_3$ solution, *i.e.* the initial solvent. Now, when we finally reach a plateau value, we see that roughly one third of the primary adsorption plateau value is left. So, neither the pure solvent nor 1 M $NaNO_3$ solution are able to erode the layer completely.

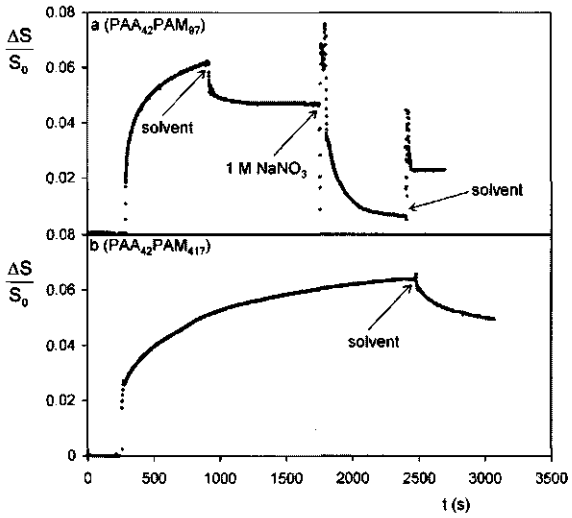

FIGURE 6.5. Adsorption of $PAA_{42}PAM_{97}$ and $PAA_{42}PAM_{417}$ with $f_{PAA} = 0.5$ on polystyrene surfaces. After adsorption,both samples have been exposed to solvent and 1 M $NaNO_3$ solution ($PAA_{42}PAM_{97}$), as indicated by the arrows.

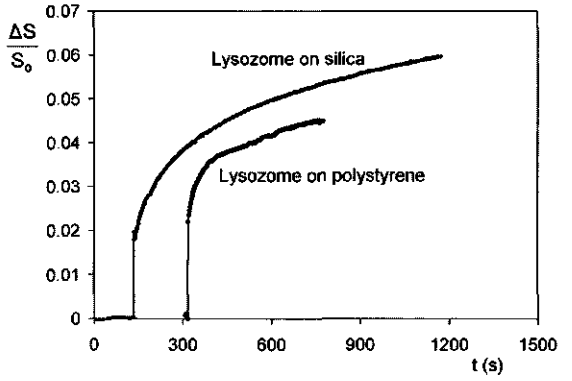

FIGURE 6.6. Adsorption of lysozyme on silica and polystyrene surfaces in 10 mM $NaNO_3$ solution, pH = 7. Lysozyme concentration was 100 ppm.

6.3.3. Functionality of micelle-covered surfaces

We now have studied the adsorption of micelles on two different surfaces, as well as the stability of the layers. A next step was to see if these micellar layers also change the functionality of the surfaces. In order to do so, we have exposed the layers to a lysozyme solution. In Figure 6.6, we show the adsorption of lysozyme (100 ppm) on bare silica and polystyrene surfaces surface at pH = 7 in 10 mM $NaNO_3$. Clearly, the lysozyme

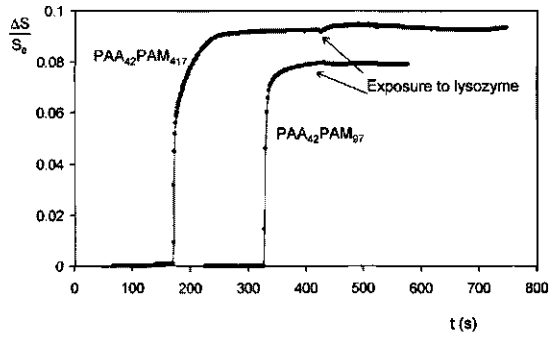

FIGURE 6.7. Exposure of $PAA_{42}PAM_{97}$ and $PAA_{42}PAM_{417}$ layers with $f_{PAA} = 0.5$ to lysozyme solution, as indicated by arrows in the figure. Experimental conditions: pH = 7, 10 mM $NaNO_3$

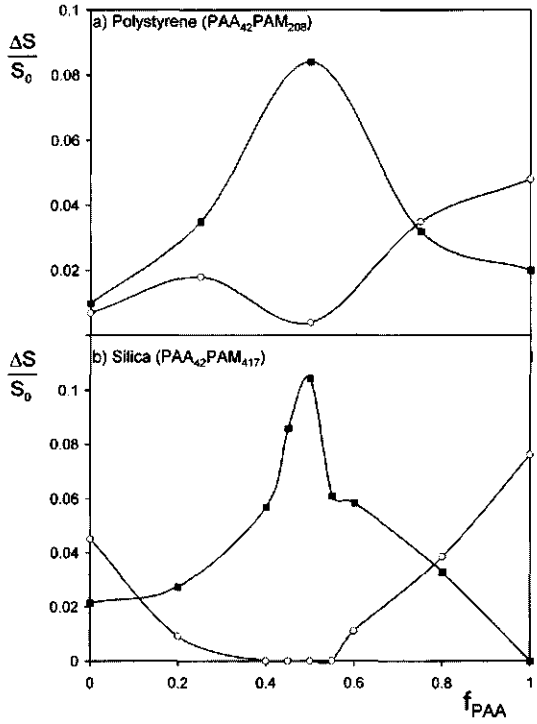

FIGURE 6.8. Adsorption of $PAA_{42}PAM_{208}$ on polystyrene (a) and $PAA_{42}PAM_{417}$ on silica (b) at pH = 7 in 10 mM $NaNO_3$, indicated by the closed symbols. The open symbols represent the increase in $\Delta S/S_0$ after exposure of the micellar layers to lysozyme solution. The lines are a guide to the eye.

forms a rather thick layer on both surfaces. One could compare this adsorption process to fouling of surfaces in e.g. industrial or medical equipment. We will now show that the adsorbed micelles as discussed in the previous sections, can prevent such fouling. In Figure 6.7, we show results from exposing silica surfaces covered with $PAA_{42}PAM_{97}$ and $PAA_{42}PAM_{417}$ micelles to the same lysozyme solution as in Figure 6.6, again at pH = 7 and 10 mM $NaNO_3$. The lysozyme exposure is indicated in the figure by arrows. Upon exposure to the lysozyme solution, the adsorbed mass does not change, i.e. the micellar layer is not desorbed and no lysozyme adsorbs onto the micellar layer or the silica surface. The micelles thus act as an anti-fouling agent. In future research we will present data on anti-fouling of various surfaces and different proteins. In Figure 6.8, we give an overview for polystyrene (a) and silica (b) surfaces, where we plot the $\Delta S/S_0$ plateau levels of micellar adsorption (closed symbols) and the excess $\Delta S/S_0$ after lysozyme exposure after the first micellar adsorption step. Note that the shape of the $\Delta S/S_0$ vs f_{PAA} curve in Figure 6.8b is somewhat different from Figure 6.1b, as the peak is somewhat more pronounced. We attribute this to the use of a different silicium wafer, that may have slightly different surface properties. The absolute values of adsorption around the PMC are comparable, though with Figure 6.1b. Clearly, the excess protein adsorption shows a pronounced minimum around the PMC for both systems. Note that Figure 6.8b confirms the aggregation diagram as presented in Chapter 1 and 2, as the protein adsorption is zero in a small f_{PAA} window around the PMC, and not just exclusively at the PMC.

6.4. Conclusions

We have studied adsorption of complex coacervation core micelles on hydrophilic anionic surfaces (silica) and hydrophobic surfaces (polystyrene) with reflectometry and dynamic light scattering. The layer thickness on silica particles amounted to 25 nm, which is in line with the hydrodynamic radius of the micelles in bulk solution. The kinetics of adsorption were sensitive to variations in internal structure of the micelles. Micelles with a large core and thin corona adsorb much faster than micelles with a small core and large corona. From these observations, and from the lack of affinity of the corona blocks for the surface, we conclude that the micelles unfold their core-corona structure and that the core material is adsorbing on the surface. The corona chains form a brush on top of the core material. Variation of the corona block length in the light scattering experiments showed that the silica beads are only colloidally stable when the corona block is at least 400 units. With shorter corona blocks, the silica particles formed a precipitate with the micelles. We have exposed silica strips with the adsorbed micelles to solvent and 1 M $NaNO_3$. The solvent was able to desorb several percents of the adsorbed mass from the silica surface and about one fifth from the polystyrene surfaces. With 1 M $NaNO_3$, some more of the layers could be eroded. In total one

fifth was eroded from the silica surface with respect to the initial plateau values and around two third from the polystyrene surface. We have studied the functionality of the micellar layers as anti-fouling agents. It turned out that the micellar layers were very well able to protect both silica and polystyrene surfaces against protein adsorption.

6.5. References

1. F. Caruso, R.A. Caruso, and H. Moehwald, Science, 1998. **282**: p. 1111-1114.
2. P.T. Hammond, Current Opinion in Colloid and Interface Science, 2000. 4: p. 430-442.
3. P. Bertrand, A. Jonas, A. Laschewsky, and R. Legras, Macromolecules Rapid Communication, 2000. **21**: p. 319-348.
4. A. Baba, F. Kaneko, and R.C. Advincula, Colloids and Surfaces A, **173**: p. 39-49.
5. T.W. Graul and J.B. Schlenoff, Analytical Chemistry, 1999, **71**: p 4007-4013.
6. F. Caruso and C. Schueler, Langmuir 2000, **16**: p. 9595-9603.
7. C.G.P.H. Schröen, M.A. Cohen Stuart, K. van der Voort Maarschalk, A. van der Padt, and K. van 't Riet, Langmuir, 1995, **11**: p. 3068.
8. D. Kovacevic, S. van der Burgh, A. de Keizer, and M. A. Cohen Stuart, Langmuir, 2002, **18**: p. 5607-5612.
9. D. Kovacevic, S. van der Burgh, A. de Keizer, and M. A. Cohen Stuart, Journal of Physical Chemistry, 2003, **107**: p. 7998-8002.
10. A. de Keizer, E.M. van der Ent, and L.K. Koopal, Coloids and Surfaces A: Physicochemical and Engineering Aspects, 1998, **142**: p. 303-313.
11. N.G. Hoogeveen, M.A. Cohen Stuart, and G.J. Fleer, Journal of Colloid and Interface Science, 1996, **182**: p. 133-145.
12. J.C. Dijt, M.A. Cohen Stuart, and G.J. Fleer, Advances in Colloid and Interface Science, 1994, **50**: p. 79-101
13. E.P.K. Currie, A.B. Sieval, M. Avena, H. Zuilhof, E.J.R. Sudhölter, and M.A. Cohen Stuart, Langmuir, 1999. **15**: p. 7116-7118
14. M.A. Cohen Stuart and A. de Keizer, textitAdsorption Kinetics of Polymeric Molecules, in *Oxide Surfaces*, J. Wingrave, Editor. 2001, Marcel Dekker: New York. p. 157-199.
15. O.V. Borisov and E.B. Zhulina, Macromolecules, 2002. **35**: p. 4472-4480.
16. A. Harada and K. Kataoka, Macromolecules, 1998. **31**: p. 288-294

Summary

Self-assembly is an important phenomenon in biology as well as in man-made applications. This process occurs with molecules that consist of parts with different affinity for a solvent in which they are immersed. A classical example is soap, and the different affinity for water is called amphiphilicity, as one part of the soap molecules is hydrophilic and the other part is hydrophobic. For small soap molecules or surfactants, the self-assembly occurs above a certain concentration, the so-called CMC (critical micelle concentration). Above this CMC, it is favorable for the hydrophobic parts of the surfactants to form small colloidal domains, that form the micellar core. The micellar exterior or corona is formed by the hydrophilic parts of the surfactants. When the amphiphilic molecules are of a polymeric nature, the CMC is lowered considerably, and may not even be experimentally accessible. Although self-assembly is mostly associated with hydrophobic phase separation, another possibility to induce phase separation is by bringing together oppositely charged macromolecules in aqueous solution. In this thesis, self-assembly between charged diblock-copolymers and oppositely charged homopolymers was studied. Under the appropriate choice of experimental conditions and diblock-copolymer design, small colloidal objects may be formed, which we call complex coacervate core micelles (CCCM). One of the most relevant parameters is the mixing ratio of the components. We call the composition where CCCM's are found the preferred micellar composition (PMC). The CCCM's are relatively novel particles in the field of self-assembly, and can be applied to solubilize charged species, whereas the hydrophobically associating systems are well known to solubilize hydrophobic molecules.

In *Chapter 1*, a general introduction to the subject is given. The relevant physical chemical disciplines in order to understand CCCM's are briefly discussed. In addition, the experimental approach is elaborated. Briefly, a dilute solution containing one of the components is titrated with a concentrated solution, containing the oppositely charged component. The experiment is performed in a light scattering cell. The solutions start out with equal ionic strength and pH and after each dosage, the pH and 90° laser light scattering intensity was recorded.

In *Chapter 2*, we study the effect of variations in the design parameters of the diblock-copolymer and homopolymer on the colloidal stability and aggregation mechanism. Design parameters are *e.g.* the block lengths of the diblock-copolymer, chain

length of the homopolymer, and chemical structure of these components. It was found that the block length ratio of the core and corona blocks in the diblock-copolymer must meet the minimum requirement $N_{corona}/N_{core} > 3$. In addition, it is demonstrated that increasing hydrophobicity of the corona blocks promotes the colloidal stability of a CCCM system. The hydrodynamic radii of colloidally stable CCCM was in the order of several tens of nanometers. Furthermore, the aggregation mechanism of the CCCM's is discussed in detail using a simple light scattering vs composition speciation diagram. From an experimental light scattering vs composition diagram, the molar mass (and thus the aggregation number) of the CCCM can be estimated using the so-called light scattering mass analysis (LSMA). By calculating the micellar radius of a CCCM from the aggregation number as determined by the LSMA, the core polymer density could be fitted to the experimental radii, and it was found that the core polymer volume density is in the order of 30 percent. For one series of diblock-copolymers with constant N_{core} and varying N_{corona}, it was found that the aggregation number decreases with increasing N_{corona}. This finding is qualitatively in line with theoretical predictions for similar systems. Despite the decrease in aggregation number, the micellar radius increases with increasing N_{corona}.

The charge neutralization process is analyzed in *Chapter 3* at different mixing ratio's and ionic strength. Two experimental approaches were applied. In the series of experiments that is described first, the pH was varied between 3 and 10 for several mixtures of diblock-copolymer and homopolymer, with varying composition. It was found that the pH where micelles were formed decreased with increasing amounts of poly acid in the mixture. In the second series of experiments that is described, the composition is varied at equal starting pH for the diblock-copolymer solution and homopolymer solution. The experiments were performed by titrating the diblock-copolymer solutions with the homopolymer solutions at 5, 10, 50 and 100 mM $NaNO_3$. During the titrations, the bulk pH changed and a maximum was found in $|\partial pH/\partial f|$ corresponding to the PMC. The pH changes that were seen during the titrations decreased with increasing $NaNO_3$ concentration. Also proton titrations were performed with the components at 5, 10, 50, and 100 mM $NaNO_3$, which gives insight in the charge density of the free components. From the pH changes and the charge densities of the separate components and applying electroneutrality to the CCCM at the PMC, it was found that with increasing background electrolyte concentration, more sodium ions reside in the complex. Application of LSMA showed that the core polymer volume density decreases in this window of ionic strength from 30 percent to around 15 percent.

Small angle neutron scattering experiments are presented in *Chapter 4*. The samples were the same as in the series used in Chapter 2, namely a diblock-copolymer

with constant N_{core} and increasing N_{corona}. We applied a model that allows us to deduce the aggregation number, core radius, corona thickness, and polymer volume density in the micellar corona. Again, a decreasing aggregation number was found with increasing N_{corona}, similar to the findings in Chapter 2. The core radius decreased slightly with increasing N_{corona}, and this was overcompensated by an increase of the corona thickness. The micellar radius thus increases with increasing N_{corona}, as was also found in Chapter 2. The core polymer density was found to be around 20 percent, which is 10 percent lower as was found from the LSMA.

In *Chapter 5*, a three-component system was described, consisting of anionic homopolymers, anionic-neutral diblock-copolymers, and cationic homopolymers. This is a variation of the two-component system, that consists of *e.g.* cationic homopolymers and anionic-neutral diblock-copolymers. The main focus of this chapter is on the amount of anionic homopolymers. It was found that even small amounts of these polyanions strongly increase the aggregation number, and when the number of polyanion groups from the homopolymer roughly equals the number of polyanion groups from the diblock-copolymer, the aggregation number has increased around a factor of hundred. For the two-component system, the radii are around 20 - 30 nm, whereas with the three-component system, the particles may increase their radius up to 150 nm. We propose to consider these three component particles as a complex coacervate micro emulsion.

In *Chapter 6*, the interaction between CCCM and various surfaces is studied. It was found that the micelles have favorable interactions with polystyrene and silica surfaces, and that a maximum in adsorbed amount is found at the PMC. The affinity of the CCCM for the surfaces is thus higher than that of the separate components. From the adsorption data, we propose that in order to adsorb on a surface, a CCCM must unfold it's core-corona structure, and that the affinity for the surface comes from the complex coacervate core. Thus, directly on the surface, a film of complex coacervate is formed; on top of this film, the corona chains form a planar polymer brush. The length of the corona block N_{corona} was of little influence on the adsorption process. The micelles also adsorb on colloidal silica particles, and only with very long corona blocks were the silica particles colloidally stabilized. Furthermore, we show that a layer of CCCM can protect surfaces from protein adsorption, *i.e.* CCCM show great potential for use as anti-fouling agents in *e.g.* biomedical devices, contact lenses, and membrane surfaces.

Samenvatting

Polymeren zijn lange moleculen, die bestaan uit chemisch aan elkaar gebonden subeenheden. Deze subeenheden noemt men ook wel monomeren. Indien een polymeer volledig uit n type monomeer bestaat, noemt men dit een homopolymeer. Een diblok-copolymeer is een polymeer dat bestaat uit twee chemisch aan elkaar gelinkte polymeren met verschillende typen monomeren. De eigenschappen van een polymeer worden bepaald door het totale aantal monomeren - de ketenlengte - en de chemische samenstelling van de monomeren. De chemische samenstelling van de monomeren bepaalt of het polymeer oplosbaar is in water, of juist onoplosbaar. Tevens kan een monomeer - afhankelijk van zijn chemische samenstelling - een proton opnemen of juist afstaan aan de oplossing en zodoende geladen worden. Geladen groepen zijn altijd oplosbaar in water. Polymeren bestaande uit geladen groepen noemt men ook wel polyelectrolieten. Een belangrijk verschijnsel bij polyelectrolieten is de afstoting tussen groepen op dezelfde keten. Deze afstoting wordt veroorzaakt door de korte afstand tussen de gelijkgeladen groepen op de keten. De chemische samenstelling van de monomeren bepaalt dus of de interactie tussen polymeren onderling en tussen polymeren en oplosmiddel attractief of repulsief is.

Met diblok-copolymeren kan het dus het geval zijn dat het ene deel van het molecuul oplosbaar is in water en het andere deel onoplosbaar. Deze tweeslachtigheid binnen n molecuul leidt ertoe dat boven een specifieke concentratie in water deze moleculen spontaan colloïdale deeltjes zullen vormen zoals wordt getoond in Figuur 1.1. Deze deeltjes heten micellen. De kern van de micellen bestaat uit de onoplosbare delen van de moleculen en de mantel wordt gevormd door de oplosbare delen van de moleculen. De aanleiding voor het vormen van deze micellen is de *repulsie* tussen de onoplosbare delen van de diblok-copolymeren en de watermoleculen.

In dit proefschrift worden micellen beschreven die niet gebaseerd zijn op repulsie, maar op *attractie*. In Figuur 1.4 wordt het verschijnsel complex coacervatie getoond. Dit fenomeen is gebaseerd op de attractie tussen polymeren met tegengestelde lading. Beide polymeren zijn individueel goed oplosbaar in water, echter wanneer ze samen worden gebracht, wordt een onoplosbaar complex gevormd. Indien het aantal geladen groepen van de positief en negatief geladen polymeren ongeveer gelijk is, zal complex coacervatie resulteren in een coexistentie van twee fasen; de ene fase is een geconcentreerde oplossing van beide polymeren, de andere fase bestaat (bijna) alleen uit water. Dit verschijnsel is ook mogelijk met geladen biopolymeren zoals bijvoorbeeld eiwitten

en DNA. De complexvorming tussen de tegengesteld geladen polymeren kan worden tegengegaan door het toevoegen van oplosbaar zout aan de oplossing. Oplosbaar zout splitst in water in negatief en positief geladen ionen. Deze ladingen gaan een competitie aan met de ladingsattractie tussen de polymeren. Bij voldoende hoge zoutconcentratie zal het complex coacervaat oplossen, doordat de zoutionen de competitie winnen.
Complex coacervatie is niet alleen mogelijk met homopolymeren, maar ook met diblok-copolymeren. Dit biedt de mogelijkheid om de afmetingen van de complex coacervaat fase te beperken tot colloidale dimensies. In Figuur 1.7 wordt de vorming van deze deeeltjes getoond. Deze deeltjes heten complexcoacervaatkern micellen en dit proefschrift behandelt de karakterisering van deze deeltjes in oplossing alsook een toepassing van deze deeltjes aan oppervlakken.
Er zijn vele parameters van belang voor de vorming en stabiliteit van deze micellen. Zoals blijkt uit Figuur 1.7, hebben, kunnen er drie verschillende ketenlengtes en chemische eigenschappen gevarieerd worden. Respectievelijk kunnen onderscheiden worden het homopolymeer, het kernblok van de diblok-copolymeer en het mantelblok van de diblok-copolymeer. Tevens is de mengverhouding van de homopolymeren en diblok-copolymeren te variren. De mate van oplading van de monomeren die gebruikt zijn bij de beschreven experimenten in dit proefschrift is vaak afhankelijk van de pH. Bij negatieve monomeren betekent dit dat hoe hoger de pH, hoe hoger de oplading. Bij positieve monomeren is dit andersom, hoe lager de pH, hoe loger de oplading. De precieze mate van oplading hangt af van de dissociatie constante van een gegeven monomeer. Bij een polyelectroliet is de dissociatie 'constante' een functie van de mate van oplading, omdat door de ladingsrepulsie het steeds moeilijker wordt om meer gelijkgeladen groepen te introduceren op de keten. De attractie tussen de tegengesteld geladen monomeren is voor een belangrijk deel afhankelijk van de mate van oplading, zodat de pH eveneens een belangrijke parameter is. Als laatste is de concentratie van zout-ionen van belang; de reden hiervoor is hierboven beschreven.
In *Hoofdstuk 2* wordt de rol van de ketenlengtes en chemische samenstelling van de monomeren besproken. Het blijkt dat de lengte verhouding van het kernblok en mantel zeer relevant is. Als het kernblok te lang is, dan zijn de gevormde micellen niet stabiel; als het mantelblok te lang is, is er te weinig attractie en worden er geen micellen gevormd. Bij een constante lengte voor het kernblok en toenemende lengte van het mantelblok, neemt het aggregatiegetal (het aantal diblok-copolymeren per micel) af, hetgeen in overeenstemming is met theoretische voorspellingen. De ketenlengte van het homopolymeer is alleen van belang indien dit zeer kort of zeer lang is. Bij zeer korte homopolymeren zullen er geen micellen gevormd worden. Bij zeer lange homopolymeren bepaalt de lengte van het homopolymeer de afmetingen van de micellen. Tussen deze extremen is de ketenlengte van het homopolymeer over een zeer breed gebied niet relevant voor vorming en eigenschappen van de micellen.

Het is gebleken dat de micellen slechts gevormd worden in een smal gebied van mengverhouding tussen homopolymeer en diblok-copolymeer, namelijk als het aantal negatieve en positieve monomeren ongeveer gelijk is aan elkaar. Dit betekent ook dat de micellen ladingsneutrale objecten zijn. Rondom deze samenstelling is de concentratie van micellen een functie van de macroscopische verhouding tussen de polymeren. De grootte van de micellen varieert ongeveer tussen 12 en 40 nm hydrodynamische straal en de aggregatiegetallen varieren van enkele tientallen tot enkele honderden.
In *Hoofdstuk 3* wordt de rol van zoutconcentratie nader bekeken. Van de individuele componenten wordt de pH-afhankelijke oplading bekeken bij verschillende zoutconcentraties. Er is gebleken dat bij oplopende zoutconcentratie de polymeren een hogere ladingsdichtheid hebben. Dit is te wijten aan de afscherming van de ladingsrepulsie van geladen groepen op de keten door de geladen zout ionen in oplossing. In een complex coacervaat - waar de positieve en negatieve polyelectroliet ketens elkaar dicht hebben genaderd - is de afstoting tussen gelijkgeladen groepen veel minder dan in oplossing. Hierdoor zal de dissociatieconstante veranderen en ook de ladingsevenwichten. Experimenteel is dit gemeten door de pH te meten van de oplossingen. Hoe hoger de zoutconcentratie waarin de micellen gevormd worden, hoe minder de ladingsevenwichten verschuiven. Tevens bevat de kern van de micellen met toenemende zoutconcentratie meer water en is het aggregatiegetal lager. Tevens is in dit hoofdstuk de rol van de pH onderzocht. Het blijkt dat er over een breed pH gebied deeltjes gevormd worden, maar dat er een voorkeur is voor een bepaalde pH, afhankelijk van de samenstelling van het polymeermengsel.
In *Hoofdstuk 4* worden resultaten besproken van neutronenverstrooïng. Er is gebleken dat bij toenemende lengte van het mantel blok van de diblok-copolymeer een afname optreedt van het aggregatiegetal. De interactie tussen de micellen is onderzocht door verschillende concentraties te meten. Er is gebleken dat micellen met korte ketens voor het mantelblok onderling afstoten, en deze afstoting kan goed beschreven worden met een model voor afstotende bollen. Wanneer echter het mantelblok veel langer is dan het kernblok, kan de interactie tussen de micellen niet beschreven worden met dit model voor afstotende bollen. Waarschijnlijk vormen deze micellen clusters als gevolg van mantel-mantel verwikkeling.

In *Hoofdstuk 5* wordt een driecomponenten systeem onderzocht, bestaande uit een positief polyelectroliet, een negatief polyelectroliet, en een negatief-neutraal diblok-copolymeer. Met dit systeem worden deeltjes gevormd, die vergelijkbaar zijn met emulsiedruppels. Het binnenste van de deeltjes bestaat uit onoplosbaar complex, gevormd uit de twee polyelectrolieten. De mantel van de deeltjes bestaat wederom uit de diblok-copolymeren.

De adsorptie van complexcoacvervaatkern micellen aan diverse oppervlakken wordt besproken in *Hoofdstuk 6*. Gebleken is dat de micellen zowel aan silica als polystyreen kunnen adsorberen. De aard van deze oppervlakken is respectievelijk negatief geladen, dus hydrofiel en hydrofoob. Uit de adsorptie data is afgeleid dat de micellen ontvouwen bij adsorptie, zodat het complexcoacervaat aan het oppervlak adsorpbeert en de mantels van de micellen en zogeheten polymeerborstel vormen aan het oppervlak. Deze polymeerborstel kan tevens deze oppervlakken beschermen tegen eiwitadsorptie.

Dankwoord

Het dankwoord van een proefschrift is bij uitstek geschikt om iedereen die heeft bijgedragen aan dit project te bedanken. Tijdens het uitvoeren van het onderzoek zijn er drie mensen van de vakgroep die aan alle hoofdstukken hebben bijgedragen. Als eerste wil ik mijn promotor Martien Cohen Stuart bedanken voor het bieden van de gelegenheid om dit project uit te voeren op de vakgroep. Martien, die tevens vaak zeer creatieve ideeën had voor experimenten en een zeer heldere kijk op interpretatie van de data. Als co-promotor mag ook zeker Arie de Keizer niet onvermeld blijven. Arie heeft zich vaak met chirurgische precisie gebogen over mijn schrijfsels en berekeningen. Hoewel dit nogal eens wat extra werk voor mij opleverde, heeft dit absoluut een positieve invloed op het proefschrift gehad. Arie, bedankt. Als laatste, Remco Fokkink dankzij wiens inspanningen de lichtverstrooïer en reflectometers altijd operationeel waren, voor het meedenken met het ontwerp van de titratie-opstelling. Alledrie hebben tevens tijd gemaakt om af te reizen naar Grenoble en daar bij nacht en ontij neutronen verstrooïng en röngten verstrooing experimenten uit te voeren. Tijdens een terugreis van deze expedities heeft ook nog eens de vorige auto van Remco dankzij een Franse vrachtwagenchauffeur stevig kennis gemaakt met de vangrail met ondergetekende achter het stuur met nog 800 km voor de boeg. Nogmaals, alle drie ontzettend bedankt!

Tijdens dit onderzoek heb ik twee studenten mogen begeleiden, Bram Sperber en Wiebe de Vos. Beiden hebben zeer uitstekend werk geleverd en dit waren zeer nuttige en leerzame perioden voor mij. Ten tijde van Bram's afstudeervak moest het onderwerp eigenlijk nog van de grond komen en jouw data waren de eerste succesvolle lichtverstrooïngstitraties. Een aantal hiervan is dan ook terug te vinden in Hoofdstuk 2. Bram, nog veel succes gewenst met het afronden van je eigen promotie. Ten tijde van Wiebe's afstudeervak waren de inzichten zoals beschreven in dit boekje bijna allemaal al bekend. Mede hierdoor en ook zeker dankzij Wiebe's stevige aanpak zijn er zeer veel resultaten behaald. Een aantal hiervan staat in Hoofdstuk 6. Wiebe, veel succes gewenst met het afronden van je studie.

Op een zijspoor van het onderzoek dat beschreven staat in dit boekje heeft Davor Kovacevic van University of Zagreb zeer mooie resultaten behaald op het vlak van multilagen gevormd uit zwakke polyelektrolieten. Davor, bedankt, ik vond onze samenwerking zeer prettig.

De theoretische modellering van complex coacervatie tussen zwakke polyelectrolieten is

zeer grondig aangepakt door Maartien Biesheuvel. Hoewel de resultaten hiervan niet in dit proefschrift terug te vinden zijn, hebben de vele en zeer nuttige discussie's die gevoerd zijn absoluut een positieve weerslag gehad op dit boekje.
Verder wil ik de overige collega's van FysKo bedanken voor de gezelligheid op de vakgroep, zoals de enthousiaste deelname aan de bierbrouwcursussen, de (soms felle) discussie's aan de lunchtafel, de vele uitjes, etc... Iedereen bedankt!
De samenwerking met de opdrachtgever, Rhodia uit Aubervilliers, Frankrijk was zeer prettig. Tijdens de bezoeken over en weer was men altijd enthousiast over behaalde resultaten. De wetenschappelijke inbreng gecombineerd met 'wat kunnen we ermee doen' vond ik zelf altijd een prettig uitgangspunt voor overleg. Je voudrais bien vous remercier de la part de l'Université de Wageningen, pour la collaberation pendant les derniers cinq ans. La support financielle, les samples de rhodibloc, et la liberté scientifique nous a fait énormément plaisir. J'espère qu'il y aura plus de collaberation dans la future entre Wageningen et Aubervilliers.
Buiten het werk om was er altijd voldoende afleiding met de vrienden/vriendinnen groep, middels de vele verjaardagen, de computerweekenden en de jaarlijkse oud en nieuw viering. Ik hoop dat dit nog vele jaren zo voort blijft duren.
Mijn ouders wil ik bedanken voor het feit dat het voor mij mogelijk gemaakt hebben om te studeren. Tijdens de studie hebben zij mij ook altijd gesteund.
De laatste woorden zijn voor Ingrid en Lianne. In de laatste vijf jaar is er veel gebeurd. Grote vreugde vanwege de geboorte van Lianne en alle dagen sindsdien, groot verdriet vanwege het veel te vroeg overlijden van jouw vader. Zeer tegenstrijdige emoties op onze bruiloft drie weken na deze droevige gebeurtenis. Het is me duidelijk geworden dat we samen kunnen feesten, maar ook elkaar kunnen steunen als er weinig te feesten valt. Met deze basis kunnen we alles aan wat de toekomst brengt.

Laten we nu een biertje gaan pakken,
Stefan

Levensloop

Stefan van der Burgh werd geboren op 28 april 1973 te Dordrecht. In 1992 behaalde hij het VWO diploma aan scholengemeenschap De Lage Waard te Papendrecht. Van 1992 tot 1998 studeerde hij Levensmiddelentechnologie aan de Wageningen Universiteit te Wageningen met afstudeervakken bij de vakgroepen Informatica, Fysische Chemie en Kolloïdkunde en Proceskunde. Het afstudeervak bij Proceskunde is uitgevoerd bij AVEBE Process Research te Veendam. Van januari 1999 tot oktober 2003 is de auteur in dienst geweest als onderzoeker in opleiding bij de vakgroep Fysische Chemie en Kolloïdkunde van de Wageningen Universiteit te Wageningen. Gedurende deze periode werd het in dit proefschrift beschreven onderzoek uitgevoerd. Vanaf oktober 2003 is de auteur werkzaam als post-doctoraal onderzoeker bij deze vakgroep.